คุณสมบัติเชิงเคมี เชิงกายภาพและเชิงกลของมอร์ตาร์อบแห้งหลังการสัมผัสเพลิงไหม้

นางสาวอรณิชา รองวิริยะพานิช

วิทยานิพนธ์นี้เป็นส่วนหนึ่งของการศึกษาตามหลักสูตรปริญญาวิศวกรรมศาสตรมหาบัณฑิต
สาขาวิชาวิศวกรรมโยธา ภาควิชาวิศวกรรมโยธา
คณะวิศวกรรมศาสตร์ จุฬาลงกรณ์มหาวิทยาลัย
ปีการศึกษา 2555

CHEMICAL PHYSICAL AND MECHANICAL PROPERTIES OF OVEN – DRIED MORTAR AFTER FIRE EXPOSURE

Ms. Onnicha Rongviriyapanich

A Thesis Submitted in Partial Fulfillment of the Requirements

for the Degree of Master of Engineering Program in Civil Engineering

Department of Civil Engineering

Faculty of Engineering

Chulalongkorn University

Academic Year 2012

หัวข้อวิทยานิพนธ์	คุณสมบัติเชิงเคมี เชิงกายภาพและเชิงกลของมอร์ตาร์อบแห้งหลังการสัมผัสเพลิงไหม้
โดย	นางสาวอรณิชา รองวิริยะพานิช
สาขาวิชา	วิศวกรรมโครงสร้าง
อาจารย์ที่ปรึกษาวิทยานิพนธ์หลัก	ผู้ช่วยศาสตราจารย์ ดร. วิทิต ปานสุข
อาจารย์ที่ปรึกษาวิทยานิพนธ์ร่วม	ผู้ช่วยศาสตราจารย์ ดร. จรูญ รุ่งอมรรัตน์

คณะวิศวกรรมศาสตร์ จุฬาลงกรณ์มหาวิทยาลัย อนุมัติให้นับวิทยานิพนธ์ฉบับนี้เป็นส่วนหนึ่งของการศึกษาตามหลักสูตรปริญญามหาบัณฑิต

…….. คณบดีคณะวิศวกรรมศาสตร์
(รองศาสตราจารย์ ดร. บุญสม เลิศหิรัญวงศ์)

คณะกรรมการสอบวิทยานิพนธ์

……. ประธานกรรมการ
(ศาสตราจารย์ ดร. ธีรพงศ์ เสนจันทร์ฒิไชย)

…….. อาจารย์ที่ปรึกษาวิทยานิพนธ์หลัก
(ผู้ช่วยศาสตราจารย์ ดร. วิทิต ปานสุข)

……. อาจารย์ที่ปรึกษาวิทยานิพนธ์ร่วม
(ผู้ช่วยศาสตราจารย์ ดร. จรูญ รุ่งอมรรัตน์)

……. กรรมการ
(รองศาสตราจารย์ ดร. ธัญวัฒน์ โพธิศิริ)

……. กรรมการภายนอกมหาวิทยาลัย
(ผู้ช่วยศาสตราจารย์ ดร. วรพงศ์ ศรีโสพัส)

อรณิชา รองวิริยะพานิช : คุณสมบัติเชิงเคมี เชิงกายภาพและเชิงกลของมอร์ตาร์อบแห้งหลังการสัมผัสเพลิงไหม้. (CHEMICAL PHYSICAL AND MECHANICAL PROPERTIES OF OVEN – DRIED MORTAR AFTER FIRE EXPOSURE) อ. ที่ปรึกษาวิทยานิพนธ์หลัก : ผศ. ดร. วิทิต ปานสุข,อ. ที่ปรึกษาวิทยานิพนธ์ร่วม : ผศ. ดร. จรูญ รุ่งอมรรัตน์, 119 หน้า.

วัสดุก่อสร้างประเภทคอนกรีตยังคงเป็นวัสดุที่ได้รับความนิยมอย่างแพร่หลายในงานวิศวกรรมโยธาเนื่องจากเป็นวัสดุที่สามารถเทหล่อในที่ได้หลายขนาดและรูปร่างของชิ้นงาน อย่างไรก็ตาม วัสดุประเภทคอนกรีตก็มีข้อจำกัดในการใช้งานเช่นเดียวกัน ในปัจจุบันเหตุการณ์เพลิงไหม้สามารถเกิดขึ้นได้โดยทั่วไป จากเหตุการณ์เพลิงไหม้ในประเทศไทย พ.ศ. 2553 ได้ส่งผลกระทบต่อพฤติกรรมทางกลศาสตร์ของโครงสร้างคอนกรีตอย่างมาก ทั้งนี้เป็นผลมาจากผลกระทบของเหตุเพลิงไหม้ต่อคุณสมบัติทางเคมีและคุณสมบัติทางกายภาพที่เปลี่ยนไปหลังการสัมผัสเพลิงไหม้

การศึกษานี้ได้ทำการจำลองเหตุการเพลิงไหม้ของชิ้นตัวอย่างมอร์ตาร์ที่มีความหนา 20 มม. และ 40 มม. ภายใต้กราฟไฟมาตรฐานการทดสอบวัสดุ ASTM E119 เป็นระยะเวลา 60 นาทีและ 120 นาที การทดสอบคุณสมบัติทางเคมี ทางกายภาพและทางกลของวัสดุจะกระทำบนชิ้นตัวอย่างที่แตกต่างกันออกไป ได้แก่ ผงตัวอย่างมอร์ตาร์ขนาดเส้นผ่านศูนย์กลางไม่เกิน 0.15 มม. ชิ้นตัวอย่างทรงลูกบาศก์ขนาด 5.0 มม. และชิ้นตัวอย่างรูปคานขนาดเล็ก โดยเปรียบเทียบผลการทดสอบในรูปของความสัมพันธ์ระหว่างระยะเวลาที่สัมผัสเพลิงไหม้กับคุณสมบัติต่าง ๆที่เปลี่ยนไป ซึ่งผลการทดสอบคุณสมบัติทั้งสามคุณสมบัตินั้นสอดคล้องซึ่งกันและกัน นอกจากนี้การศึกษานี้ยังได้ศึกษาถึงความสัมพันธ์ระหว่างคุณสมบัติทางเคมีและกายภาพ และความสัมพันธ์ระหว่างคุณสมบัติทางกายภาพและทางกล

ผลการศึกษานี้แสดงให้เห็นว่าแบบจำลองที่นำเสนอนั้นสามารถใช้ในการทำนายคุณสมบัติทางกายภาพและทางกลของวัสดุที่เปลี่ยนไปโดยอาศัยปริมาณสารประกอบเคมีที่คงค้างในชิ้นตัวอย่างมอร์ตาร์หลังการสัมผัสเพลิงไหม้ได้

ภาควิชา วิศวกรรมโยธา ลายมือชื่อนิสิต.....

สาขาวิชา วิศวกรรมโครงสร้าง ลายมือชื่อ อ.ที่ปรึกษาวิทยานิพนธ์หลัก.....

ปีการศึกษา 2555 ลายมือชื่อ อ.ที่ปรึกษาวิทยานิพนธ์ร่วม .....

5470454521 : MAJOR CIVIL ENGINEERING

KEYWORDS : FIRE EXPOSURE / FIRE DETERIORATION / RIGID BODY SPRING MODEL / RBSM / MORTAR

ONNICHA RONGVIRIYAPANICH : CHEMICAL PHYSICAL AND MECHANICAL PROPERTIES OF OVEN – DRIED MORTAR AFTER FIRE EXPOSURE. ADVISOR : ASST. PROF. WITHIT PANSUK, Ph.D., CO-ADVISOR : ASST. PROF. JAROON RUNGAMORNRAT, Dr., 119 pp.

Even though concrete is one of the most popular construction materials; however, it also has many cons in use at the same time such as a severe deterioration after subjected to fire exposure. Nowadays, fire accidents occur easily in all over the world including Thailand and almost of structural concrete under fire incidents were diminished, i.e. the mechanical properties caused by a decomposition of chemical compound and changes in physical structure.

A series of experiment is conducted for macroscopic specimens in burning process conforming to standard temperature – time curve of ASTM E119, then they are cut in order to investigate the attenuation of chemical properties on less than 0.15 mm diameter powder sample, physical properties on 5 mm cubic and mesoscopic samples for mechanical properties test. The relationships between chemical – physical and physical – mechanical properties are compared with numerical simulation considering the effect of chemical and physical properties on mechanical properties.

Based on the results of the current study, the proposed numerical simulation can be used to assess the changes of material model as a function of the residual chemical compound content of mortar samples after high temperature treatment.

Department : Civil Engineering	Student's Signature .....
Field of Study : Civil Engineering	Advisor's Signature .....
Academic Year : 2012	Co-advisor's Signature .....

ACKNOWLEDGEMENTS

No different task can be completed successfully without the collaborative effort of many persons, and this study is no exception.

First of all, the author wishes to express her deep appreciation and sincerely gratitude to her thesis advisor, co – advisor and Japanese supervisor from Hokkaido University, Assistant Professor Withit Pansuk, Dr., Assistant Professor Jaroon Rungamornrat, Dr., Associate Professor Yasuhiko Sato, Dr., for their guidance, assistance and constant support throughout her study in Chulalongkorn University and her short – term internship program at Hokkaido University, Sapporo, Japan.

Sincerely words of thanks must also go to the members of her supervising committee: Professor Teerapong Senjuntichai, Dr., Associate Professor Thanyawat Pothisiri, Dr., Worapong Srisoros, Dr., for their invaluable suggestions and critical comments that helped to refine the scope and content of this work.

To all students and staff of Department of Civil Engineering, Chulalongkorn University and the Laboratory of Engineering for Maintenance Systems, Hokkaido University, the author wishes to express her sincere appreciation for friendly and supportive atmosphere that certainly helped her to carry out this study in a pleasant working environment.

I am grateful for the scholarship granted to me by the Faculty of Engineering and Department of Civil Engineering, Chulalongkorn University during the course of this study.

Last but not least, sincere appreciation is extended to the author's family, whose love, support, and sacrifices have encouraged and guided the author in all of her pursuits in life and enable her to stand where she is now.

CONTENT

Page

Page

Page

LIST OF TABLES

Page

LIST OF FIGURES

Page

LIST OF FIGURES

Page

LIST OF FIGURES

Page

LIST OF FIGURES

Page

CHAPTER 1

INTRODUCTION

1.1 General background

Even though concrete is one of the most popular construction materials because it can be casted in place in various shape or size, there are many disadvantages in use at the same time. Structural concrete is probably deteriorated owing to many conditions such as low quality control during construction, disaster or subjecting to an aggressive environment especially exposing to fire; for example, the severe fire accidents in Thailand in May 2010 had impacts to many people who live in that zone. For deteriorated structure after exposing to fire, visual inspection and non – destructive testing are the basic methods which can be brought to evaluate a remaining performance of structural concrete. In case of concrete exposing to a short time fire, spalling may occur in the depth which is less than reinforcement covering but the strength of structure is rapidly reduced and collapse in the final when concrete is exposed to fire for a long time and reinforcement is exposed to fire directly. Therefore, it must bring about greatly impacts to the safety of live, properties, and domestic economy. However, visual inspection may not proper and adequate because it depends on an inspector's experience, a few numbers of experienced inspectors, cost increasing and danger. Therefore, a computer simulation should be developed in order to clarify both invisible and visible damages before making some decisions about repairing, strengthening or demolition.

Nowadays, a simulation may not represent burnt concrete behavior correctly due to many factors affected deteriorations which cannot explain effect of each factor on deterioration clearly, and lack of experimental result. For example, the molecular structure of cement hydrated products such as calcium silicate hydrate (CSH) and calcium hydroxide (CH), underlying parameter of strength and durability, are disturbed. In fire exposed concrete or elevated temperature, the rearrangement of microstucture induces the decomposition of cement hydrated products which is the change in molecular structure to non – strength compounds. Because of the significantly change in molecular structure of mortar exposing to fire on material performance, this research focuses on experimental results involved constitutive law and the deterioration of mortar under standard curve of ASTM E119 – 00a: Standard Test Methods for Fire Tests of Building Construction and Materials [1]. To accomplish this, the constitutive relation and the deteriorated effect of mortar were gathered from experiments in which one parameter varied, e.g. exposure time. Beam shape specimens with dimension of 50 x 400 x 20 and 50 x 400 x 40 mm, Ø150 x 300 mm cylinder and cylinder recommended by RILEM TC 129 – MHT: 'Test methods for mechanical properties of concrete at high temperatures', Modulus of elasticity for service and accident conditions [2], 25 mm briquette and 50 mm cubic samples were burnt with two different times exposure to clarify the relationship between a reduced performance and elapse exposure time. Then, 3 – point flexural test was done on mesoscopic prismatic specimen; and tensile softening branch was obtained by using finite element analysis. Finally, the material model for relating each property was proposed and verified by macroscopic experimental data.

1.2 Literature review

This literature review covered the relevant background information to this thesis. After providing more depth and insight into fire incidents and its severity on cementitious material after high temperature condition, an experiment of material properties in terms of residual chemical compounds, changed physical properties and mechanical properties affected by those two properties is presented. Following that, relevant research and information regarding the changed material properties of cementitious material is discussed. Finally, the numerical approach to simulate the behavior of mortar is reviewed with focus on Rigid Body Spring Model (RBSM).

1.3 Objectives

1. To study the effect of fire deterioration causes the reduced material performance and let failure criteria change.
2. To propose the constitutive law as a function of time exposure for discrete analysis of mortar exposed to fire incident.
3. To develop a suitable numerical simulation of mortar that is verified by experiment.

1.4 Scope of Research

For the current study, the samples were made with the Portland cement of Type 1 and the siliceous fine aggregate commonly used in Thailand, i.e. river sand. The prismatic mortar samples were cured in the saturated condition at least 28 days. At the age of 28 – day old, all specimens were dried in the oven at 105 °C for a day in order to eliminate remaining free water. Then, oven – dried specimens were kept in a sealed box until test; therefore, the moisture content of samples was kept constant by atmospheric humidity.

There were three test programs of oven – dried specimens consisting of control specimens, an hour and two hours exposed to fire. The thermal loading was applied on all faces of prismatic specimen for simulating an unsealed condition in which similar to the actual fire accidents. Heating process was conforming to the standard temperature – time curve of ASTM E119 [1]. According to the unsealed condition and very small thickness of those samples, a difference of temperature history in each layer along cross section was negligible; therefore, fire deterioration was assumed to be uniform. After 24 - hour of naturally cooled down in the furnace, specimens have been removed and always kept in vacuum desiccators in order to prevent effects of external moisture and carbonation reaction.

For both control and damaged specimens, cement hydrated products which were experimentally determined were limited only calcium silicate hydrate (CSH) and calcium hydroxide (CH) because of their importance for material strength and durability.

Finally, a numerical simulation was performed on non – linear analysis discrete model namely Rigid Body Spring Model (RBSM) which was able to prevent the bias of failure direction by using randomized geometry of elements (Voronoi diagram).

1.5 Expected Results

1. To understand the effect of deterioration on reduced material performance and failure criteria.
2. To understand the constitutive law as a function of time exposure for discrete analysis of mortar exposed to fire incident.
3. To proposed a suitable numerical discrete simulation of mortar that is verified by experiment.

CHAPTER 2

LITERATURE REVIEW

2.1 Introduction

As shown in some of previous study, material properties of cementitious material likely concrete, mortar or hardened cement paste are significantly diminished after exposed to high temperature treatment. Hydration products, i.e. calcium silicate hydrate (CSH) and calcium hydroxide (CH), were generated and expanded to the free space [3], it can be reasonably said that the pore connectivity was gradually diminished during the course of hydration. After subjected to high temperature, the decomposition of cement hydrated products was easily initiated at 530 °C [4, 5] because the molecular of water had been liberated from cement paste [6, 7]. Therefore, it is not only the total pore space increased due to coarsening effect [5, 8], the mechanical properties of cementitious material is porosity dependent [9].

2.2 Fire severity

2.2.1 Fire load concept

An American researcher, Ingberg [10], proposed the fire load concept for establishing the standard fire curve with the two main assumptions as follows;

1. Fire resistance of structural concrete is depended on only fire severity which can be determined from the area under temperature – time curve.
2. Fire severity is relied on only the intensity of fire

However, these two assumptions do not consider the open area of structure, type and weight of fuel, rate of ignition, and thermal conductivity which also affect the fire severity during fire incidents.

2.2.2 Chemical and physical properties of concrete at eleavated temperature

Compound, a stable mass, is not easy to decompose without any severe conditions. After hydration between cement powder and water, cement hydrated products namely calcium silicate hydrate (CSH) and calcium hydroxide (CH), main parameters of material strength and durability, were produced. However, there are not only CSH and CH, hydration products also extend to calcium aluminate hydrate (CAH), calcium sulfoaluminate hydrate (Ettringite), and heat. For heat, it was rapidly generated when cement powder has mixed with water during the first fifteen minutes and concrete becomes fresh state. In dormant period, concrete contains fresh and be plastic state for a few hours as the designed workability; therefore, the heat production is stopped in this period. Closed to final setting time, hydration reaction starts proceeding again to make hardened concrete and maximum heat is generated in four to eight hours after the first hydration [11].

In mix proportion, water should be free of impurities or potable water because water contaminants may have an effect on long term durability of concrete. When cement powder was hydrated by water in mix proportion, state of water has become which can be divided into two types as shown followings [11]:

1. Evaporable water or free water

   Water in capillary pores or gel pores can be easily boiled and vaporized at 105 °C in oven.

2. Non – evaporable water or fraction water

This kind of water is a part of molecular structure of cement hydrated product likely CSH or CH and it cannot evaporate or liberate in general condition. However, non – evaporable water starts escaping when concrete is burnt at 1,000 °C but it start significantly being affected when temperature reaches 110 °C corresponding to totally evaporate for another one [4]. Normally, the average amount of this water is approximately 23 percent by weight of cement powder.

To see that when concrete or cement paste is exposed to fire incidents, even though evaporable water is easier to eliminate from material rather than non – evaporable one, but if temperature still increase, molecular structure of hydration products is probably disturbed because of the vaporization of non – evaporable water.

As mentioned before, CSH and CH are the main compounds of cement hydration products; therefore, they should be an underlying parameter of material properties such as material strength, permeability or durability of hardened concrete. After subjected to high temperature, free moisture is firstly vaporized at around 100 °C [7], then CH and partial CSH is initiated to decompose at further than 430 °C and 500 °C, respectively [5, 7] starting with boiling and volatization. For further 600 °C of ignition, the dehydration rate is substantially increased which plays the important role on change of material properties. Although the dissociation of chemical compound after fire causes significantly changes to molecular structure of cement paste.

Chinese researchers, Gai – Fei Peng and Zhi – Shan Huang [5], proposed the non – linear numerical model for determining the residual CSH content in samples for

600 °C, 700 °C and **800 °C** constant temperature in furnace as shown in Eq. (2.1), Eq. (2.2) and Eq. (2.3), respectively

$$\frac{\Delta y}{y_0} = -1.0\times10^{-6}t^3 + 0.0013t^2 - 0.36t + 97.72 \quad (2.1)$$

$$\frac{\Delta y}{y_0} = -2.0\times10^{-6}t^3 + 0.002t^2 - 0.67t + 100.61 \quad (2.2)$$

$$\frac{\Delta y}{y_0} = -2.0\times10^{-8}t^5 + 8.0\times10^{-6}t^4 - 0.0015t^3 + 0.13t^2 - 5.47t + 99.82 \quad (2.3)$$

Where Δy = residual CSH content after high temperature treatment

y_0 = CSH content in control samples

t = duration of high temperature treatment (min)

It can be seen that the residual CSH decrease with the increment of duration. The reason is, molecular of water in CSH boiled and liberated after heating leads to the decomposition and reduction of total CSH content in whole sample.

In case of CH, chemical compounds, lime and water, is newly formed after exposed to high as shown in Eq. (2.4).

$$Ca(OH)_2 \rightarrow CaO + H_2O \quad (2.4)$$

The decomposition as expressed in Eq. (2.4) is not so significant on strength loss due to expansion and shrinkage of new compound during the formation process [7, 12]; therefore, it is one possibility to say that the surface cracks of cementitious material after subjected to fire exposure caused by the phenomenon in Eq. (2.4).

Surface cracking and spalling can be observed easily when concrete subjected to high temperature. There are various forms of deterioration when concrete is subjected to fire or heat depending on the fire severity, e.g. aesthetic and serviceability

deteriorations. Although aesthetic deterioration is not significantly considered for load bearing capacity of structural concrete, surface cracking is not desirable. In addition, the serviceability of structural concrete must be decreased after the high temperature treatment.

Omer Arioz [4] proposed the deterioration of concrete exposed to fire at different temperatures by using Ordinary Portland cement in mix proportion. Microcrackings start introducing at around 300 °C due to the increasing of internal stress caused thermal expansion and surface cracks can be visualized at around 600 °C. The development of surface cracks is a function of elevated temperature means higher temperature made cracks are obviously visible. After temperature reaches 1200 °C, surface spalling may occur because of completely decomposed specimens. The increment of surface cracks is shown in Fig. 2 – 1.

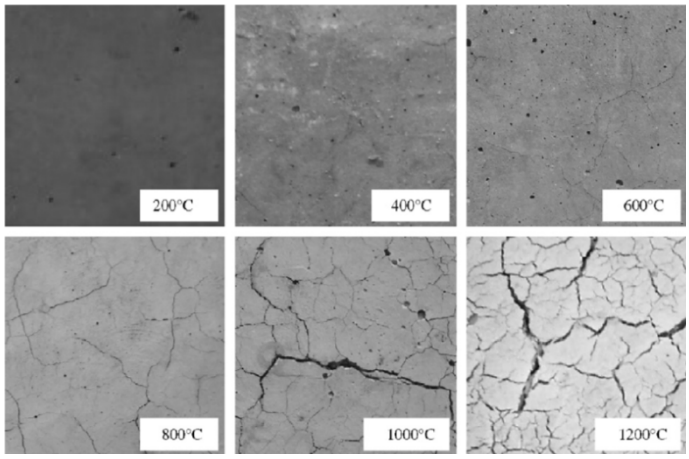

Fig. 2 – 1 The increment of surface cracks [4]

In previous studies, many researchers [5, 6, 8] have encountered the effect of high temperature treatment in term of changed chemical properties on microstructure of cementitious material. After heating, the pore – structure coarsening is mainly caused by the decomposition of CSH and CH because they are generated and expanded to the

free space after course of hydration [3]. There are several techniques to evaluate the changes in physical appearance of fire – damaged concrete; the commonly used methods are to measure the total pore space of samples which can be quantitatively examined by using Archimedean or mercury porosimetry intrusion (MIP) technique and to visualize the pore – structure coarsening by scanning electron microscope (SEM) observation. The quantitative result of MIP and qualitative result of SEM can confirm that the microstructure of cementitious material have been disturbed by high temperature. Generally, the changes in physical structure of fire – damaged concrete is caused by chemical compound reduction for both CSH and CH but rehydration process of CH is rather complicated and highly random in nature [7]. Therefore, the porosity of fire – deteriorated concrete may not differ from control samples significantly. Furthermore, for post – fired concrete, mechanical behavior of cement – based material is also disturbed. When concrete is heated, chemo – physical relation affecting its mechanical behavior bring the failure of structural concrete for both visible and invisible damages [13]. Several investigators [5, 6, 8, 9, 13] have also discovered the effect of additional space and temperature on mechanical properties which will be described how changed physical properties affect mechanical behavior later.

2.2.3 Mechanical properties of concrete at elevated temperature

As previously discussed, mechanical behavior of post – fired concrete is diminished by the effect of loss of bonded moisture and chemical compound reduction. Several mechanical properties such as compressive strength, indirect tensile strength, modulus of elasticity have been changed against temperature for post – cooling concrete.

Taiwanese researchers, Y. F. Chang, Y. H. Chen, M. S. Sheu and G. C. Yao [13], have studied on heated cylindrical shape concrete samples and proposed the numerical model for mechanical properties of unheated and heated concrete at each of different temperatures. Three samples were heated and naturally cooled down to room temperature in the oven after 18 – month old in order to prevent surface spalling; after that, each sample has been tested. Equations as expressed in Eq. (2.5), Eq. (2.6) and Eq. (2.7) are for normalized compressive strength, indirect tensile strength and modulus of elasticity, respectively.

$$\frac{f_{cr}'}{f_c'} = \begin{cases} 1.01 - 0.00055T & 20°C < T \le 200°C \\ 1.15 - 0.00125T & 200°C \le T \le 800°C \end{cases} \quad (2.5)$$

$$\frac{f_{tr}'}{f_t'} = \begin{cases} 1.05 - 0.0025T & 20°C < T \le 100°C \\ 0.80 & 100°C < T \le 200°C \\ 1.02 - 0.0011T & 200°C < T \le 800°C \end{cases} \quad (2.6)$$

$$\frac{E_{cr}}{E_c} = \begin{cases} -0.00165T + 1.033 & 20°C < T \le 125°C \\ \dfrac{1}{1.2 + 18 \times (0.0015T)^{4.5}} & 125°C < T \le 800°C \end{cases} \quad (2.7)$$

Where f_{cr}' = compressive strength of heated specimens (MPa)

f_c' = compressive strength of original specimens (MPa)

f_{tr}' = splitting tensile strength of heated specimens (MPa)

f_t' = splitting tensile strength of original specimens (MPa)

E_{cr} = modulus of elasticity of heated specimens (MPa)

E_c = modulus of elasticity of original specimens (MPa)

T = average temperature between surface and center of samples (°C)

For the same heat treatment, the mechanical capacity of fire – damaged concrete as shown in three equations above is reduced in this order: modulus of elasticity, splitting tensile strength and compressive strength.

In fire incident, both physical and mechanical properties of concrete will be changed relating to weight loss of water. As a result of free water boiled and dehydration, material strength also decreases compared with the reference specimens at different temperature. The weight loss of water and the percent retained of material strength are shown in Fig. 2 – 2.

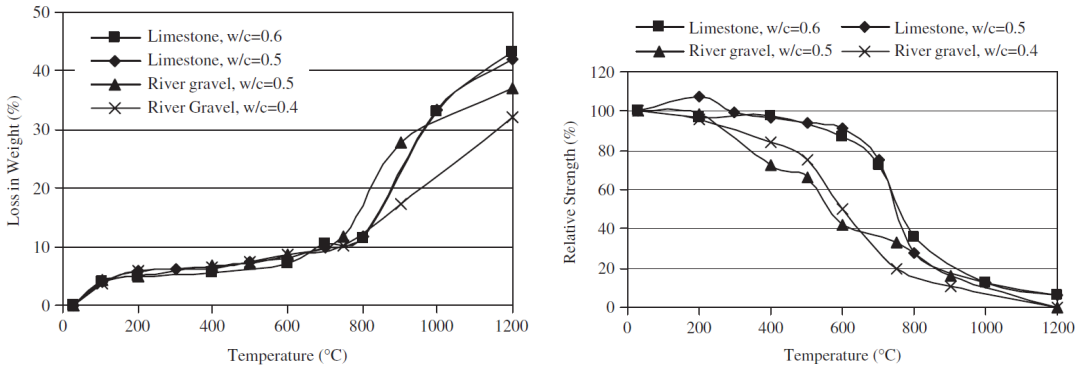

Fig. 2 – 2 Weight loss of water and residual strength for post – fire concrete [4]

To summarize an effect of water content of type of aggregate in mix proportion from two figures above, both of them were not found to be significant affected on the amount of water loss related to strength reduced after exposing to elevated temperature. In spite of all of different mix proportions in his study, it can be showed that the results have similar trend; therefore, it can be concluded that the reduction of compressive strength caused by a release of free water and dehydration due to high temperature. The relationship between weight loss of water and material strength loss is shown in Fig. 2 – 3.

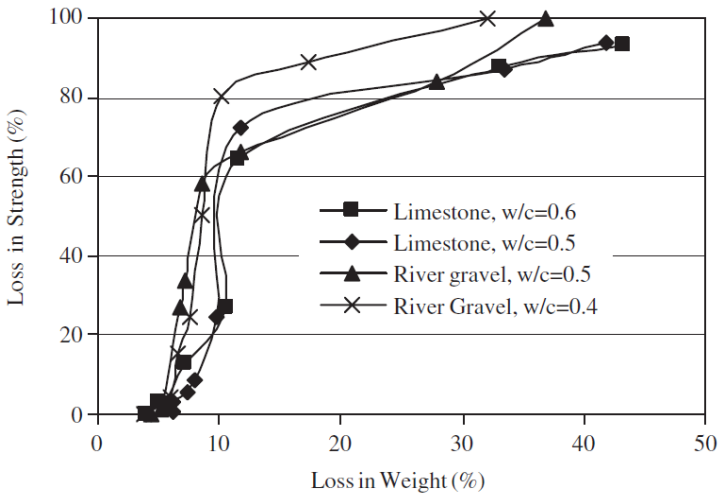

Fig. 2 – 3 Relationship between weight loss of water and strength lost [4]

However, type of aggregate also has an effect on concrete deterioration due to thermal expansion. Hertz [14] said a concrete made from limestone has a less risk to be damaged than siliceous type because of lower thermal expansion.

Generally, original mechanical properties of concrete can be investigated by some traditional methods but they may not suitable for suddenly damaged likely fire deterioration on concrete because of character and causes of changes with respect to temperature [6]. For example:

RILEM has introduced the RILEM TC 129 – MHT: Test methods for mechanical properties of concrete at high temperatures “Modulus of elasticity for service and accident conditions” [2]. Secant modulus of heated concrete has been done on at least 90 – day old the cylindrical specimens in the range of 3 to 4 slenderness ratio with three of thermocouples embedded at the surface of samples as shown in Fig. 2 – 4 to ensure the uniformity of fire.

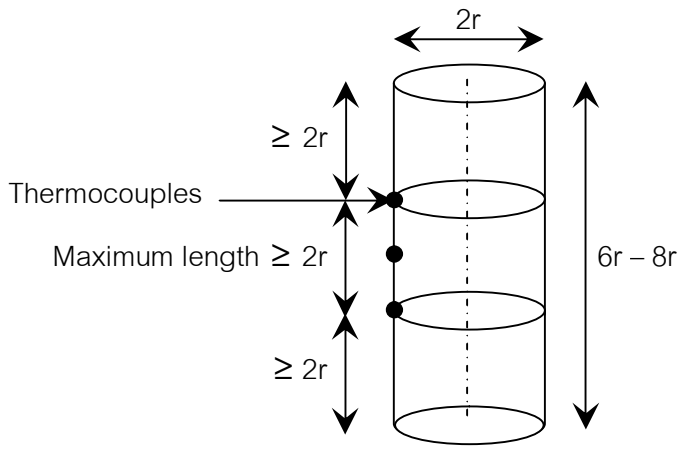

Fig. 2 – 4 Specimen recommended by RILEM TC 129 – MHT

Before burning process, samples are applied a small compressive stress at the end point of both central axes called pre – loaded level. Then after burning and cooling down to room temperature, the cyclic load as shown in Fig. 2 – 5 applies to determine the hot modulus of elasticity

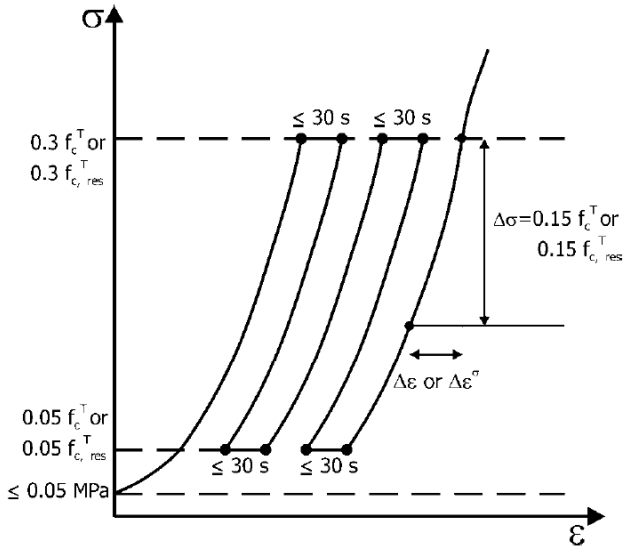

Fig. 2 – 5 Determination of modulus of elasticity by cyclic loading [2]

The determination of modulus of elasticity is similar to Young's modulus law which is the slope of stress – strain components at 30% and 15% of changed strength as expressed in Eq. (2.8).

$$E^T = \frac{\Delta\sigma}{\Delta\varepsilon} = \frac{0.30 f_c^T - 0.15 f_c^T}{\Delta\varepsilon} \quad (2.8)$$

Where E^T = modulus of elasticity at temperature T (MPa)

f_c^T = compressive strength at temperature T (MPa)

$\Delta\sigma$ = stress increment (MPa)

$\Delta\varepsilon$ = strain increment

American society for testing and materials organization has also developed the ASTM C469/C469M – 10 "Standard Test Method for Static Modulus of Elasticity and Poisson's Ratio of Concrete in Compression" [15], a traditional methods for non – damaged concrete. As same as RILEM TC 129 – MHT, Secant modulus must be determined on the cylindrical specimens with different in slenderness ratio at room temperature and constant humidity. Loading head touched both top and bottom surface without any gap in order to prevent the unpredictable movement or other interruptions. Then, modulus of elasticity can be calculated as expressed in Eq. (2.9)

$$E = \frac{\sigma_1 - \sigma_2}{\varepsilon_2 - 0.000050} \quad (2.9)$$

Where E = modulus of elasticity (psi)

σ_1 = stress component at 50 x 10^6 longitudinal strain (psi)

σ_2 = stress component at 40% of ultimate load (psi)

ε_2 = longitudinal strain component produced by σ_2

Besides the effect of high temperature on changes in mechanical properties, some researchers [8, 9] have discovered that porosity plays a role in the relationship for

mechanical properties against porosity. It can be inferred from those two studies that the strength is direct proportional to density of concrete. The meaning is, if material density is low, strength is also low, vice versa.

2.3 Variation of concrete properties with respect to temperature

The variation of thermal, mechanical properties and mass transportation of cementitious material is required for better understanding of material performance and material behavior at elevated temperature.

2.3.1 Concrete under and after high temperature treatment

Under high temperature treatment, concrete normally changes its moisture content, chemical structure, physical appearance and mechanical properties which are apparently observed by color variation, changed microstructure or aggregates. Vaporization of free moisture started at around 100 °C due to its own boiling point introducing high internal pressure in the cement paste and surroundings, internal autoclaving. If introduced internal pressure is greater than material strength, concrete cracking or spalling is initiated at this stage. Moreover, it is conceivable that the chemical bonded water is also partially lost at 100 °C contributing the shrinkage and diminished capacity. At about 300 °C, concrete is further dehydrated from the expulsion of chemically bound water in hardened cement paste but the change of total pore volume affected by dehydration remains rather small. The primary changes in material properties initiate upon the disintegration of calcium hydroxide (CH) at 430 °C while CSH remains persistent up to 530 °C and starts decomposing at 560 °C. Heating to 600 °C leads to a substantial increase of the total pore space correlating with the dissociation of CSH becomes significant at only above 600 °C and extremely increasing with respect to temperature. The additional of total pore space after subjected to fire

exposure may be suspected that the loss of chemical compounds, break open the blockages to isolated pore or micro – cracking occurred.

A group of Chinese researchers, Chi – Sun Poon, Salman Azhar, Mike Anson and Yuk-Lung Wong [16], have reported that the temperature of greater than 300 °C and long exposure time lead to a significant drop of material strength. Moreover the types of aggregate, additives, shape and size of specimens also have an influence on the strength drop off of post – fire concrete.

Although the material properties are deteriorated under and after fire, some recovering behaviors have been introduced as reported in the previous literatures. Chi – Sun Poon, Salman Azhar, Mike Anson and Yuk-Lung Wong [16] have conducted the recovery in terms of strength and durability of fire – damaged concrete after post – fire curing. Their experimental results indicate that concrete can recover its own strength and durability depending on type of concrete, maximum temperature of exposure, cooling regimes and curing duration. The recovery phenomenon of post – fire concrete is a result of rehydration of unhydrated grains and new formation that regenerate CSH and CH, heal the internal crack or honey combs damaged during fire. However, the mechanism of calcium oxide rehydration that regenerates newly CH is rather complicated because of the instability of reaction [7].

2.3.2 Variation of thermal and mechanical properties at elevated temperature

Many researchers [13, 17] have focused on changes in thermal and mechanical properties and proposed the numerical model for determining the variation of material properties after high temperature treatment as shown in Table 2 – 1 to Table 2 – 3.

Table 2 – 1 Variation of thermal properties of concrete after high temperature [17]

Thermal properties	Variation with respect to temperature
Specific heat (J/kg · °C)	$C_{c,T} = 900$ $\quad 20°C \le T \le 100°C$ $C_{c,T} = 900 + (T - 100)$ $\quad 100°C < T \le 200°C$ $C_{c,T} = 900 + \frac{(T-200)}{2}$ $\quad 200°C < T \le 400°C$ $C_{c,T} = 1100$ $\quad 400°C < T \le 1200°C$
Thermal conductivity (W/m · °C)	For lower boundary: $k_{c,T} = 1.36 - 0.136(\frac{T}{100}) + 0.0057(\frac{T}{100})^2$ $\quad 20°C < T \le 1200°C$ For upper boundary: $k_{c,T} = 2 - 0.245(\frac{T}{100}) + 0.0107(\frac{T}{100})^2$ $\quad 20°C < T \le 1200°C$

Table 2 – 2 Variation of mechanical properties of concrete after high temperature [13, 17]

Mechanical properties	Variation with respect to temperature	Ref.
Elastic modulus (MPa)	$E_{c,20°C} = 22000(\frac{f_{c,20°C}}{10})^{0.3}$ $\frac{E_{c,T}}{E_{c,20°C}} = \frac{2f_{c,T} / \varepsilon_{c1,T}}{2f_{c,20} / \varepsilon_{c1,20}}$	[17]
	$\frac{E_{cr}}{E_c} = \begin{cases} -0.00165T + 1.033 & 20°C < T \le 125°C \\ \frac{1}{1.2 + 18 \times (0.0015T)^{4.5}} & 125°C < T \le 800°C \end{cases}$	[13]
Poisson's ratio	$\nu_c = 0$ for non – damaged concrete $\nu_c = 0.2$ for damaged concrete	[17]
Compressive strength (MPa)	$\frac{f_{cr}'}{f_c'} = \begin{cases} 1.01 - 0.00055T & 20°C < T \le 200°C \\ 1.15 - 0.00125T & 200°C \le T \le 800°C \end{cases}$	[13]

Table 2 – 2 Variation of mechanical properties of concrete after high temperature [13, 17] (cont.)

Mechanical properties	Variation with respect to temperature	Ref.
Tensile strength (MPa)	$f_{ct,20°C} = 0.3(f_{c,20°C})^{2/3}$ for strength $\leq C50/60$ $f_{ct,20°C} = 2.12\ln(1+\frac{f_{c,20°C}}{10})$ for strength $> C50/60$	[17]
	$\frac{f_{tr}'}{f_t'} = \begin{cases} 1.05 - 0.0025T & 20°C < T \leq 100°C \\ 0.80 & 100°C < T \leq 200°C \\ 1.02 - 0.0011T & 200°C < T \leq 800°C \end{cases}$	[13]
	$\frac{f_{ct,T}}{f_{ct,20°C}} = -0.000526T + 1.01052 \quad 20°C < T \leq 400°C$ $\frac{f_{ct,T}}{f_{ct,20°C}} = -0.0025T + 1.8 \quad 400°C < T \leq 600°C$	[18]

Where $\frac{f_{c,T}}{f_{c,20°C}}$ = normalized compressive strength shown in Table 2 – 3

$\varepsilon_{c1,T}$ = peak strain shown in Table 2 – 3

$\varepsilon_{cu,T}$ = ultimate strain shown in Table 2 – 3

Table 2 – 3 Variation of normalized compressive strength, peak strain and ultimate strain of concrete after high temperature [17]

Temperature T, (°C)	Siliceous aggregate			Calcareous aggregate		
	$\frac{f_{c,T}}{f_{c,20°C}}$	$\varepsilon_{c1,T}$	$\varepsilon_{cu,T}$	$\frac{f_{c,T}}{f_{c,20°C}}$	$\varepsilon_{c1,T}$	$\varepsilon_{cu,T}$
20	1.00	0.0025	0.0200	1.00	0.0025	0.0200
100	1.00	0.0040	0.0225	1.00	0.0040	0.0225
200	0.95	0.0055	0.0250	0.97	0.0055	0.0250
300	0.85	0.0070	0.0275	0.91	0.0070	0.0275
400	0.75	0.0100	0.0300	0.85	0.0100	0.0300
500	0.60	0.0150	0.0325	0.74	0.0150	0.0325
600	0.45	0.0250	0.0350	0.60	0.0250	0.0350

2.3.3 Variation of internal mass transportation at elevated temperature

Mass transportation through concrete has pros and cons. For example, compressive strength will be higher in the moist curing condition; however, reinforced concrete structure will be risk when chloride penetration through concrete exceed corrosion threshold. In non – saturated condition, the chloride penetration rate is directly proportional to moisture diffusion [19] so it can be concluded that moisture in concrete introduces almost failure mechanisms.

Franke L. and Julnipitawong P. [20] said the effective repairing technique associated with damages due to moisture will be appropriately proposed after damages characteristic are clarified when internal moisture amount is known. In addition, Xi Y. and Damrongwiriyanupap N. [19] explain the meaning of moisture as pore relative humidity which is a combination of liquid water and water vapor. Therefore, each phase of internal moisture amount should be determined by using different equations associated

with Fick's law and Darcy's law. In previous study, most of the simulations of water transportation in concrete are based on the principles of thermodynamics. Therefore, the effect of variation of temperature and pressure should be also considered.

1. Moisture transport without influence of temperature gradient [20]

   For experiments in isothermal condition, moisture diffusion will not be influenced by temperature gradient because they are assumed a constant temperature over specimens. Isothermal moisture transportation models for any temperature are shown in Table 2 – 4.

Table 2 – 4 Isothermal moisture transportation model

Properties	Variation with respect to temperature
Water vapor model based on Fick's law	$\dot{m}_{d,diff} \cong \frac{-D_d}{R_d \cdot T} \cdot \nabla(p_d \cdot \theta_d)$ $\dot{m}_{d,conv} = -\theta_d \cdot \rho_d \cdot K_g \cdot \nabla p_g$ $\dot{m}_d = \dot{m}_{d,diff} + \dot{m}_{d,conv}$
Where $\dot{m}_{d,diff}$ = water vapor diffusion $\dot{m}_{d,conv}$ = water vapor convection R_d = gas constant T = temperature (K) p_d = water vapor partial pressure (Pa) θ_d = water vapor amount (kg/m^3) ∇p_g = pressure gradient in gas phase K_g = permeability coefficient of material	
Liquid water model based on Darcy's law	$\dot{m}_{w.diff} = -D_w \cdot \nabla w$ $\dot{m}_{w,conv} = -\theta_w \cdot \rho \cdot \frac{K_w}{\eta_w} \cdot \nabla p_k$ $\dot{m}_w = \dot{m}_{w,diff} + \dot{m}_{w,conv}$
Where $\dot{m}_{w,diff}$ = liquid water diffusion $\dot{m}_{w,conv}$ = liquid water convection K_w = permeability (m^2) θ_w = water content (kg/m^3) η_w = water viscosity (Pa·s) ρ = water density (kg/m^3) p_k = capillary pressure (Pa)	

However, Xi Y. and Damrongwiriyanupap N. found that the increasing rate of moisture diffusion is influenced by heat flow in concrete at non – saturated condition. The specimen and moisture profile at 10 days and 50 days of exposure to 1 mol/dm^3 NaCl solution result are shown in Figure 2 – 6 to Figure 2 – 8, respectively.

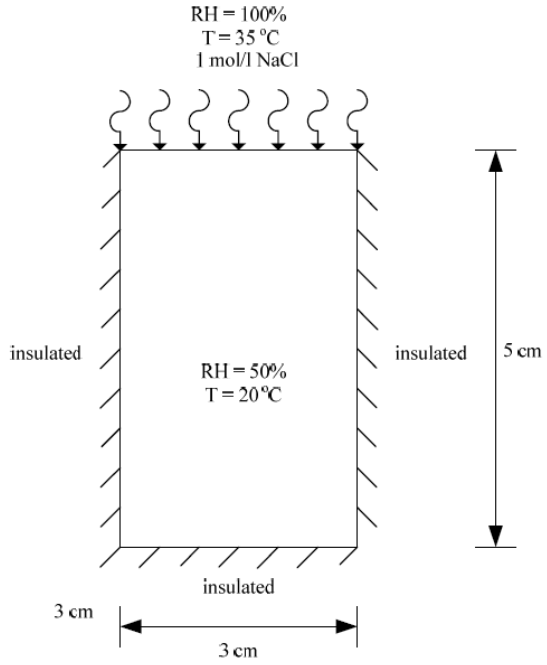

Fig. 2 – 6 Xi Y. and Damrongwiriyanupap N. specimen in analysis [19]

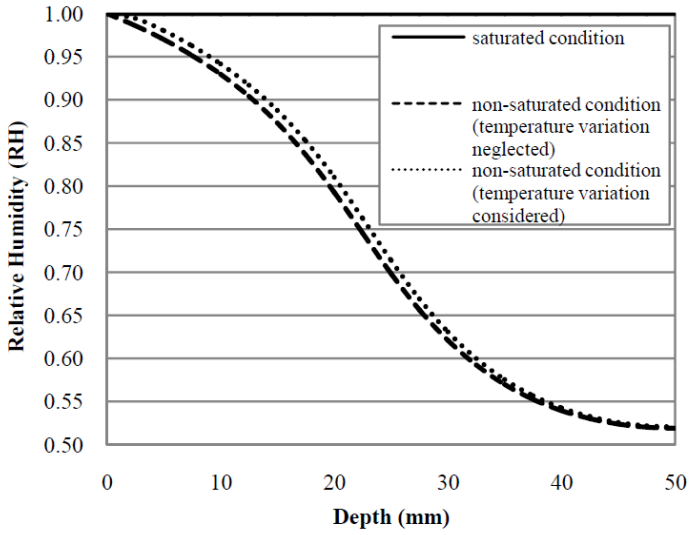

Fig. 2 – 7 Internal moisture profile changed after 10 days of exposure for temperature variation considered [19]

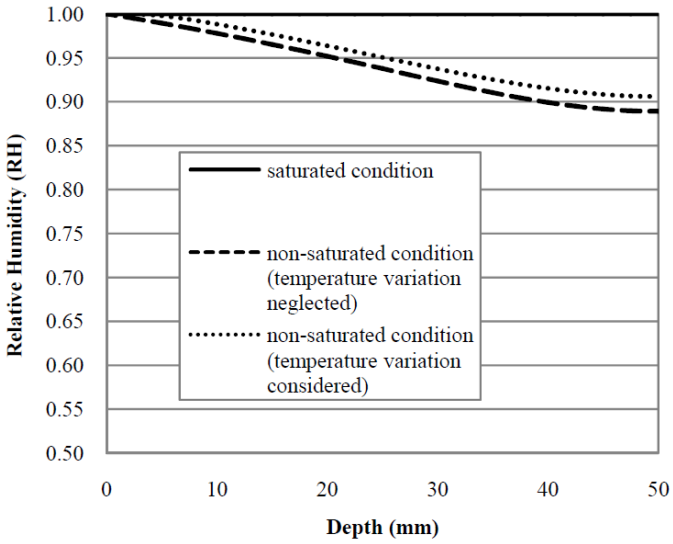

Fig. 2 – 8 Internal moisture profile changed after 50 days of exposure for temperature variation considered [19]

According to the changed moisture profile due to temperature variation considered, in non – saturated and non – isothermal condition, moisture transportation has to be affected by temperature variation. Therefore, the nature of moisture transportation should be changed at elevated temperature.

2. Moisture transport with influence of temperature gradient

At elevated temperature, internal water content will be boiled and evaporate because of temperature increasing. Driven by the boiling process, material can be divided into a dry and a wet part [21]. The interface between dry and wet part is called drying front which caused liquid water boiled to vapor since the heat exposure surface. At a sharp drying front, measured temperature is equal to 100 °C corresponding to the boiling point of water and the highest pressure will be found here. However, pressure should be equal to the atmospheric pressure at the surface and continuously increase until reaching the highest pressure at drying front. Actually, there is no exactly sharp drying front

while temperature increasing because liquid water will move into a wet part with a saturation and water vapor can escape outside. In fire exposure condition, drying front will recede far from surface of exposure due to water boiled as shown in Fig. 2 – 9 and vapor evaporated cause high pore pressure and spalling in final. According to a combination of dry and wet parts, a saturation in wet part implied that the moisture transport here can be ignored; therefore, only moisture transportation in dry part is considered at elevated temperature. At fire incident, the severest damage is surface spalling which can reduce the performance, e.g. strength, stability and serviceability of concrete structure. However, less than 3 percent by weight of moisture content of concrete material will not susceptible to spalling for non – dense concrete [22].

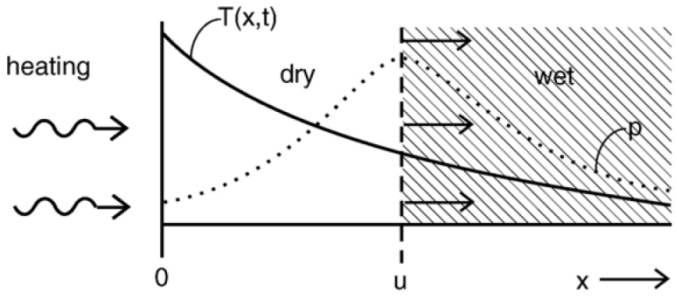

Fig. 2 – 9 Recession of drying front at elevated temperature [21]

According to the figure above, temperature profile is inversely proportional to distance from exposure surface that G. H. A. van der Heijden et al. proposed the temperature profile as shown in Equation (2.22).

$$T(x,t) = T_0 + \frac{2F_0}{K}\left(\sqrt{\frac{\kappa t}{\pi}}\exp\left(\frac{-x^2}{4\kappa t}\right) - \frac{x}{2}erf\left(\frac{x}{2\sqrt{\kappa t}}\right)\right) \quad (2.10)$$

Where F_0 = constant heat flux (W/m^2)

T_0 = temperature at t = 0

K = thermal conductivity of concrete (W/m · °C)

κ = thermal diffusivity (m^2/s)

As shown in Equation above, exponential function of distance causes temperature decreased into material and the drying front, 100 °C temperature, will recede as a function of time and temperature. In addition, water is not saturated in pore system but there is amount of water in hydration product called calcium silicate hydrate (CSH). That water will be boiled same as one in pore system introducing dehydration reaction in which the performance of material is significantly affected. However, its rate is very slow compared with the vaporization product because of the decomposition reaction [21].

2.4 Introduction to RBSM

Rigid Body Spring Model (RBSM), which was first developed by Kawai in 1977, is one of these discrete approaches using the principle of virtual work for analysis in 1988 by Ueda et al. [23]. Concrete is modeled as an assemblage of rigid elements consisting of mortar model, aggregate model, and zero – size springs and lattice element model or truss network model interconnected along their boundaries through flexible interfaces. The interfaces may be viewed as springs, whose initial properties can be set to approximate the overall elastic properties of the continuum. Fracture initiation and propagation are modeled by successfully introducing fracture criterion of concrete material into spring properties. The Kawai's spring model is attractive due to their simplicity, freedom in mesh generation, and providing a discrete representation of fracture. The Kawai's spring model is used for modeling concrete material with random geometry. The continuum material like concrete is modeled as an assemblage of rigid particles interconnected by springs along their boundaries. The RBSM places no special emphasis on contact modeling in contrast to the distinct element method and

the discontinuous deformation analysis method. The material is randomly generated by using Voronoi diagrams in order to prevent mesh bias on the failure conditions.

2.4.1 Material model

A material model is conducted with a random geometry called Voronoi diagram because of the independence of meshing and accurate interpretation when model reaches the failure criteria and represented both mortar and coarse aggregate. Moreover, there is a shape and size bias in discrete analytical model. So in 2D analysis, each particle should be around 2.0 – 2.5 mm [23] and contained the same size in all analyses, whilst the area of 3D elements is introduced appropriately.

To simulate a behavior of cementitious material, each Voronoi cell will be interconnected by zero – size spring at boundary surface with material properties of simulated concrete but there are some differences between 2 – dimensional RBSM and 3 – dimensional one as described followings:

1) 2 – dimensional RBSM [23]

2 – dimensional RBSM is a simple simulation and suitable for simple problems with a little concern about formation of failure. Since the shape and size effects have to be concerned, almost of Voronoi cells should be maintained at the same size. Each cell has three independent degrees of freedom consisting of two components of translation and an angle of rotation located at each cell's center of gravity. The two zero – size springs, one of normal and one of shear spring, must be installed at the boundary surface of each particle with their own specified material characteristics to represent bond behavior of cementitious material as shown in Fig. 2 – 10.

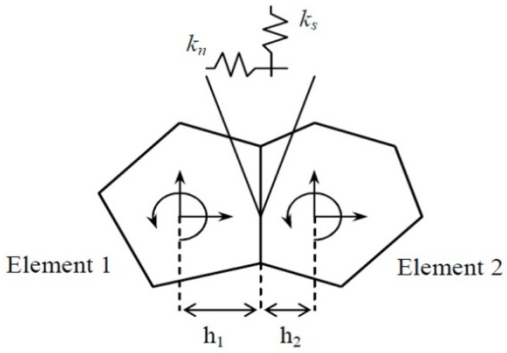

Fig. 2 – 10 Material model of 2D RBSM [23]

In previous study, the relationship between the mesoscopic material properties and the macroscopic level is assumed because the values at the mesoscopic level should be different from the macroscopic one. The input material characteristics are determined by experiments in macro scale as shown in Eq. (2.11) and Eq. (2.12).

$$\nu_{elem} = 20\nu^3 - 13.8\nu^2 + 3.8\nu \qquad 0 \le \nu \le 0.3 \tag{2.11}$$

$$E_{elem} = \left(-8\nu_{elem}{}^3 + 1.2\nu_{elem}{}^2 - 0.2\nu_{elem} + 1\right)E \tag{2.12}$$

Where E and ν are the value of elastic modulus and Poisson's ratio at macroscopic level, respectively. Then the coefficient of two zero – size springs interconnecting with the same type of Voronoi cell can be determined as expressed in Eq. (2.13) and Eq. (2.14).

$$k_n = \frac{E_{elem}}{1-\nu_{elem}{}^2} \tag{2.13}$$

$$k_s = \frac{E_{elem}}{1+\nu_{elem}} \tag{2.14}$$

However, the two equations above have to be adopted by weighted arithmetic mean if springs are installed at the boundary surface between the different types

of particle, e.g. the interface between mortar and coarse aggregate Voronoi cell. Then, the coefficient of two zero – size springs become:

$$k_n = \frac{k_{n1}h_1 + k_{n2}h_2}{h_1 + h_2} \tag{2.15}$$

$$ks = \frac{k_{s1}h_1 + k_{s2}h_2}{h_1 + h_2} \tag{2.16}$$

Where subscripts 1 and 2 are corresponding to elements at the interface.

Normal spring always acts elastically and automatically break when internal stresses of springs reach the failure criteria, e.g. tensile strength, shear strength of mortar at the meso scale. Whilst, Wang and Ueda [23, 24] and Nagai et al. [23] assumed the coarse aggregate is a linearly elastic inert material; therefore, it means the spring stiffness of both normal and shear springs are too much to be broken.

Constitutive model of normal spring is shown in Fig. 2 – 11. Cracks occur between Voronoi cells when stress reaches tensile strength and linearly decrease depending on crack width. In this study, maximum crack width is set to be 0.03 mm.

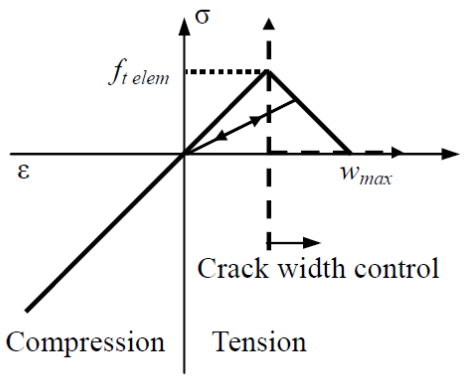

Fig. 2 – 11 Constitutive model of normal spring [23]

For same Voronoi type, shear springs are the elasto – plastic material and constitutive model is shown in Fig. 2 – 12 without damage in normal spring. The failure criteria for mortar are shown in Fig. 2 – 13 and Eq. (2.17).

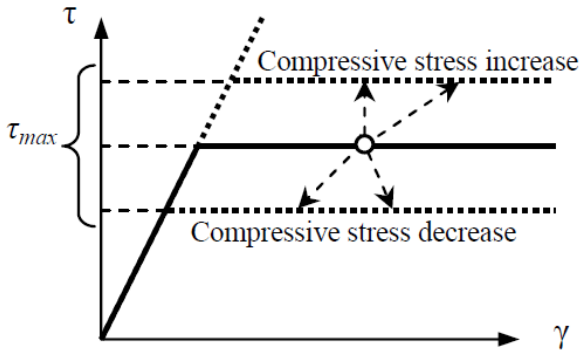

Fig. 2 – 12 Constitutive model of shear spring [23]

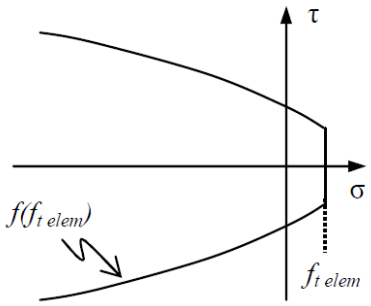

Fig. 2 – 13 Failure criteria for mortar [23]

$$\tau_{\max} = \pm(0.11 f_{t,elem}{}^{3.0}(-\sigma + f_{t,elem})^{0.6} + f_{t,elem}) \quad \sigma \le f_{t,elem} \tag{2.17}$$

At interface between different types of particle, the maximum crack width is set to be 0.01 mm and failure criterion is adopted as shown in Fig. 2 – 14 and Equation (2.18)

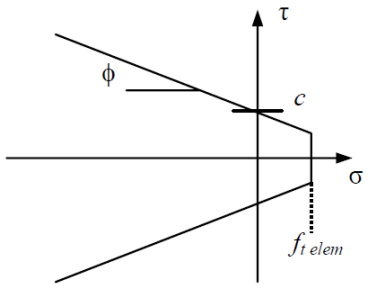

Fig. 2 – 14 Failure criteria for interface between different types of particles [23]

$$\tau_{\max} = \pm(-\sigma \tan\phi + c) \qquad \sigma \le f_{t,elem} \tag{2.18}$$

2) 3 – dimensional RBSM

The application of 3 – dimensional RBSM is similar to 2 – dimensional one but it is more appropriate to use as structural analysis for accidents such as fire incidents, earthquake and crack propagation due to rebar corrosion. Each Voronoi cell is conducted in 3 dimensions and the average size is about 5.0 mm [25] and maintained the same size in analysis. Each cell has six independent degrees of freedom consisting of three components of translation and three angles of rotation located at middle of each cell. The three zero – size springs, one of normal and two of shear springs, must be installed at the boundary surface of each 3D polyhedron particle which is divided by triangles to find a location of center of gravity with their own specified material characteristics to represent bond behavior of cementitious material as shown in Fig. 2 – 15.

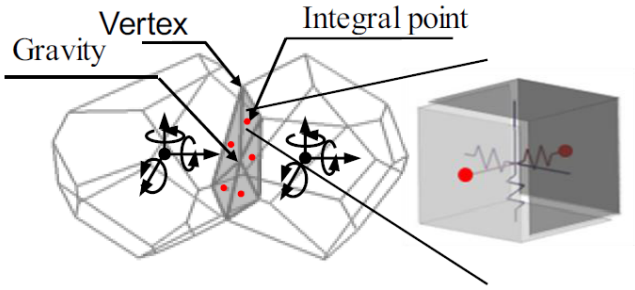

Fig. 2 – 15 Material model of 3D RBSM [26]

Kohei Nagai, Yasuhiko Sato and Tamon Ueda[27], the relationship between the meso scale material properties and the macroscopic level is assumed because the values at the mesoscopic level should be different from the macroscopic one. The input material characteristics are determined by experiments in macro scale as shown in Eq. (2.19) and Eq. (2.20).

$$\nu_{elem} = -24.8\nu^4 + 31.9\nu^3 - 16.4\nu^2 + 4.28\nu \tag{2.19}$$

$$E_{elem} = (-33.7{\nu_{elem}}^4 + 17.0{\nu_{elem}}^3 - 4.13{\nu_{elem}}^2 + 0.327\nu_{elem} + 1)E \tag{2.20}$$

Where E and ν are the value of elastic modulus and Poisson's ratio at macroscopic level, respectively. Then the coefficient of two zero – size springs interconnecting with the same type of Voronoi cell can be determined as expressed in Eq. (2.21) and Eq. (2.22).

$$k_n = \frac{(1-\nu_{elem})E_{elem}}{(1+\nu_{elem})(1-2\nu_{elem})} \tag{2.21}$$

$$k_s = \frac{E_{elem}}{1+\nu_{elem}} \tag{2.22}$$

Constitutive model of normal spring for 3D RBSM is same as 2D RBSM proposed by Kohei Nagai, Yasuhiko Sato and Tamon Ueda.[23] Cracks occur between

Voronoi cells when stress reaches tensile strength and linearly decrease depending on crack width. In this study, maximum crack width is set to be 0.03 mm.

For same Voronoi type, shear springs are the elasto – plastic material and constitutive model is shown in Fig. 2 – 16 without damage in normal spring. The failure criteria for mortar are shown in Fig. 2 – 17 and Eq. (2.23).

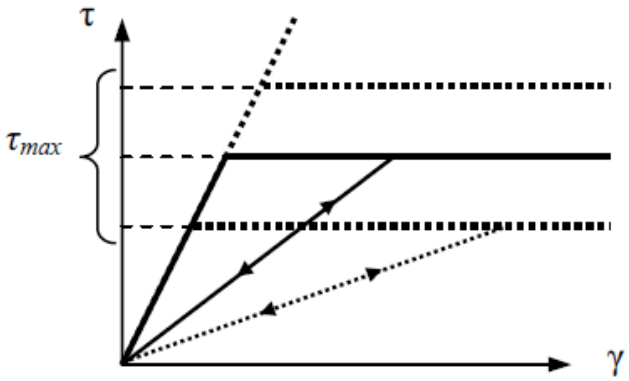

Fig. 2 – 16 Constitutive model of shear spring [27]

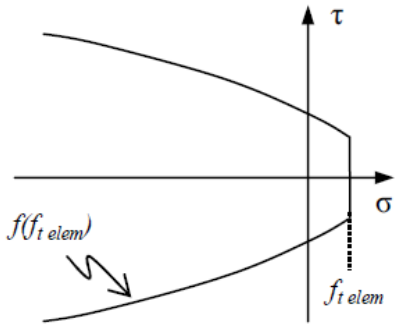

Fig. 2 – 17 Failure criteria for mortar [27]

$$\tau_{\max} = \pm\left(0.30 f_{t,elem}{}^{2.5}\left(-\sigma + f_{t,elem}\right)^{0.4} + 0.15 f_{t,elem}\right) \qquad (2.23)$$

$$\sigma \le f_{t,elem}$$

At interface between different types of particle, the maximum crack width and failure criteria are same as 2D RBSM.

Nakamura et al. simplified the material properties for initial input into a simulation is equal to the tested value at ambient condition; however, they should be changed while concrete is exposed to elevated temperature for both 2D and 3D analysis.

For all of 2 – dimensional and 3 – dimensional RBSM, tensile strength is always set to be a material strength in simulation and the concrete behavior is linearly elastic material but it depends on increasing stresses while specimens is loaded. The springs will elongate due to crack propagation and be broken when internal stress is upper than material strength at the meso level.

2.4.2 Lattice element model

Lattice element or truss network model, a pathway for mass transportation through concrete, is introduced in RBSM together with material model. It can have more than one lattice element system in some problems. For example in fire exposed analysis, there are two probable lattice element systems such as heat and vapor. The basic knowledge of this kind of element for all of 2D is quite same to 3D simulation. Each of them is similar to a pipe [24] and has their own cross – sectional area which is equal to the area of interface between Voronoi cells.

As shown in Figure 2 – 18, it is a comparison of lattice elements between 2D and 3D simulation. In the same type of Voronoi, lattice elements are used as link from one particle's centroid to another one besides; while they are installed at the boundary surface between different kinds of particle for 2D simulation. On the other hand, all

lattice elements for all types of Voronoi in 3D simulation are the links from one particle's centroid to center of gravity of interface.

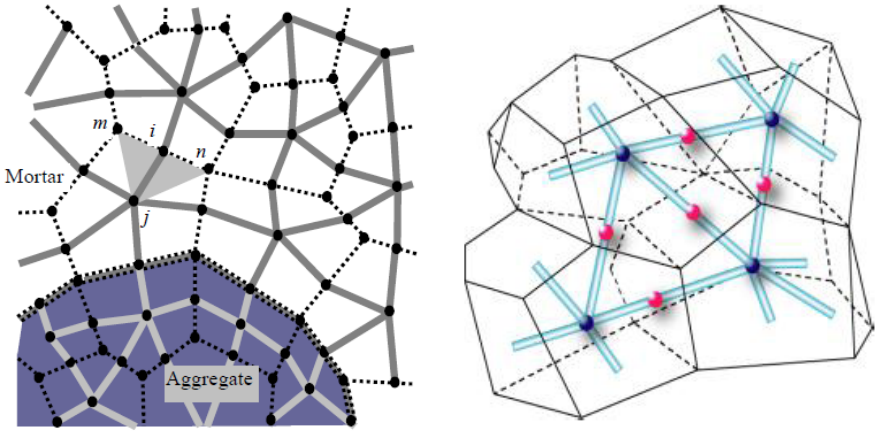

Fig. 2 – 18 Comparison of lattice elements between 2D and 3D simulation [24]

Actually, there is no ideal frictionless pathway for mass transportation through concrete; therefore, it should be corrected by some coefficients corresponding to the kind of lattice elements. For example, the coefficient of chloride diffusion for chloride penetration problem into mortar and concrete is equal to 2.392×10^{-2} mm^2/h and 1.971×10^{-2} mm^2/h, respectively (Oh and Jang 2004). Moreover, there are two probable lattice element systems in fire incident problem consisting of heat and moisture transfer. Therefore they should be the heat transfer coefficient and moisture conductivity which must be changed due to elevated temperature in fire incident problem [26].

2.5 Model installation and verification

Kohei Nagai, Yasuhiko Sato, and Tamon Ueda [23] constructed the RBSM simulation about relation of compressive and tensile strength of mortar specimens and verified by experiment. In experiment, there are three targets compressive strength consisting of 15, 35 and 55 MPa which can be shown a good agreement of model and experiments in Fig. 2 – 19.

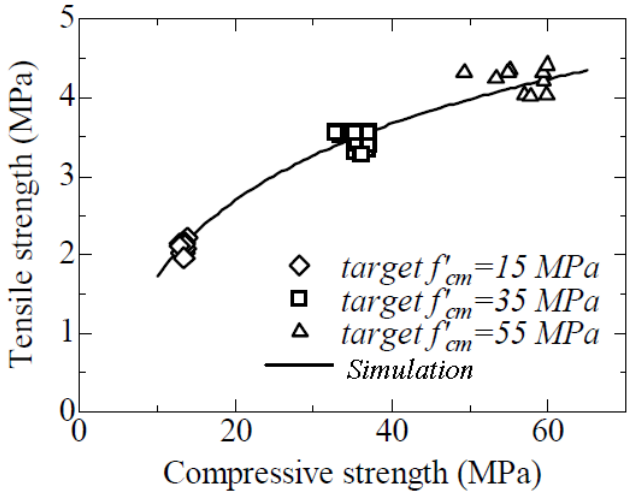

Fig. 2 – 19 Good agreement of compressive and tensile strength relation between simulation and experiments [23]

They have introduced the relationship between compressive and tensile strength as shown in Eq. (2.24).

$$f_{tp} = 1.4\ln(f_{cm}') - 1.5 \quad (2.24)$$

Where f_{tp} = mortar's pure tensile strength (MPa)

f_{cm}' = mortar's compressive strength (MPa)

In addition, they have simulated failure mode in compression and tension of 100 × 200 mm mortar specimen which also gives a good agreement of mode of failure in experiments and stress – strain relation as shown in Fig. 2 – 20 and Fig. 2 – 21.

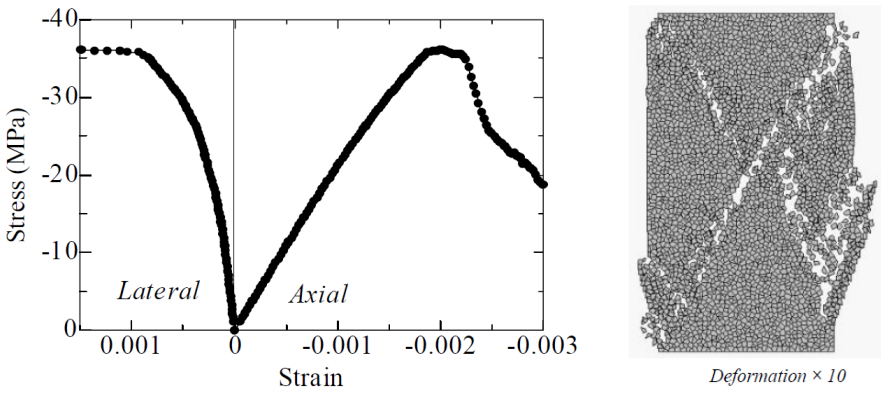

Fig. 2 – 20 Simulated stress – strain relation and mode of failure in compression test [23]

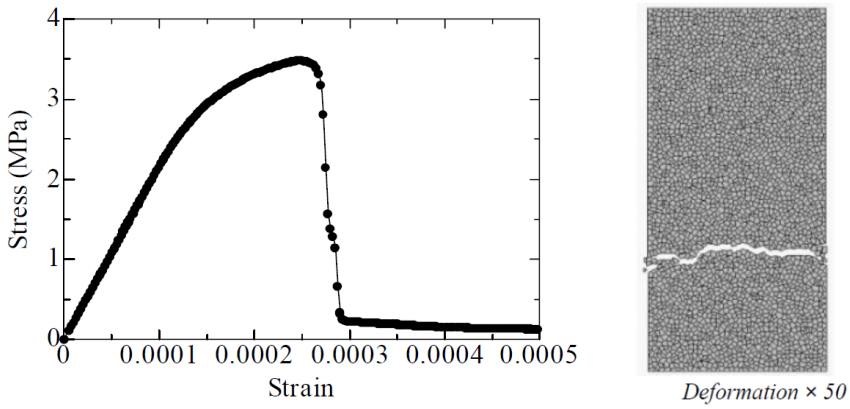

Fig. 2 – 21 Simulated stress – strain relation and mode of failure in tension test [23]

To explain from two figures above, it can be shown that the simulation introduced by Kohei Nagai, Yasuhiko Sato, and Tamon Ueda can represent the actual behavior of mortar specimen in compression and tension test. Columnar mode of failure in compression test and transverse cracks in tension test are similar to actual mode of failure in both kinds of test, simulated tensile strength is approximately 10% of compressive strength, and specimens fail at strain level reaching 0.0003.

H. Nakamura et al. [26] investigated the effect of thermal stress and vapor pressure for burnt concrete separately in order to clarify the effect of them on pattern of spalling. In fact, internal cracks due to internal constraint are growing as a function of elapsed time exposure until connecting with surface cracks. After that, explosive spalling occurs as shown in Fig. 2 – 22.

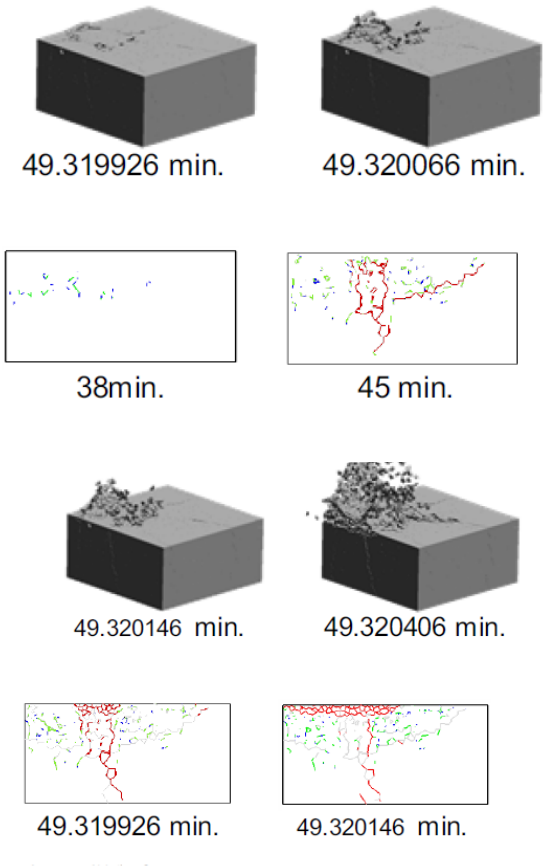

Fig. 2 – 22 Cracking propagation due to fire exposure [26]

Firstly, only effect of thermal stress was concerned. Crack pattern is not similar to explosive spalling in actual experiments, and cracks occur only inside specimens as shown in Fig. 2 – 23. Moreover, it found that stress at surface does not increase significantly.

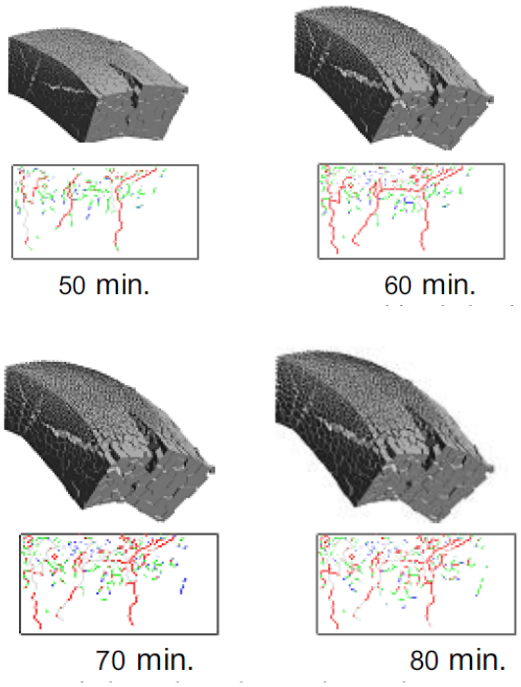

Fig. 2 – 23 Cracks pattern due to effect of thermal stress only [26]

Secondly, only effect of vapor pressure was concerned. Cracks do not develop inside specimen but it can be observed near the surface only, and crack pattern is closed to explosive spalling in actual experiments as shown in Fig. 2 – 24. Moreover, spalling will occur when vapor pressure reaching 8.0 MPa which is larger than tensile strength.

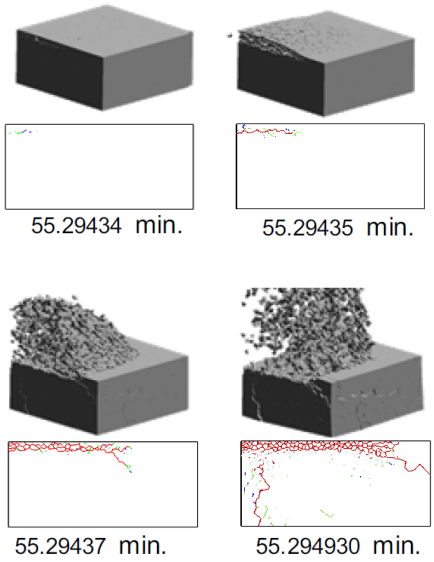

Fig. 2 – 24 Cracks pattern due to effect of vapor pressure only [26]

According to two cases above, They [26] concluded that vapor pressure plays an important role on explosive spalling during fire exposure while thermal expansion also give an effect on spalling at early time of exposure.

CHAPTER 3

RESEARCH METHODOLOGY

3.1 Introduction

In this chapter, research methodology will be explained step by step based on the following key points.

- Experimental setup consists of test specimens and test program for gathering the needed data for computational work.
- Computational work consists of inverted analysis and structural analysis.
- Material model for fire deteriorated oven – dried mortar after fire exposure consists of chemical – physical properties, physical – mechanical properties and integrated effect of chemical and physical properties on mechanical properties.

3.2 Experimental setup

3.2.1 Test specimens

A series of fire tests as shown in Table 3 – 1 were conducted using oven – dried mortar specimens. The dimensions of the samples are 50 mm x 20 mm and 50 mm x 40 mm in cross-section, and 400 mm in overall length. These beams were cast from a mortar mix conforming to JIS R5201 – Physical Testing Method for Cement [28]. The mix proportion is one part of cement to two parts of graded standard sand by weight and w/c is 0.65. Before casting, workability of mortar was checked by ASTM C230/C230M – 08 “Standard Specification for Flow Table for Use in Tests of Hydraulic Cement” [29]. And mixing sequence of mortar conform to ASTM C305 – 11 “Standard Practice for Mechanical Mixing of Hydraulic Cement Pastes and Mortars of Plastic Consistency” [30]. Each of these beam specimens was dried in the oven after age of 28 days old in

order to eliminate retaining free water stopping hydration. After that, the dry specimens were kept in a sealed box until test; therefore, the moisture content of samples was kept constant by atmospheric humidity. Then, compressive strength and tensile strength of mortar samples was tested under ASTM C109/C109M – 11b "Standard Test Method for Compressive Strength of Hydraulic Cement Mortars" [31] and ASTM C307 - 03(2008) "Standard Test Method for Tensile Strength of Chemical – Resistant Mortar, Grouts, and Monolithic Surfacing" [32], respectively.

Table 3 – 1 Details of all specimens varied by exposure time

Exposure time (min)	Piece (s)			
	50 mm – cube	Briquette	Prismatic shape	
			50 x 20 x 400	50 x 40 x 400
0	3	3	10	10
60	3	3	10	10
120	3	3	10	10
Total	9	9	30	30

3.2.2 Test program

The fire tests were conducted at the Fire Safety Research Center (FSRC) of Chulalongkorn University under ASTM E119 – 00a "Standard Test Methods for Fire Tests of Building Construction and Materials" [1] without ceramic fiber protection to simulate the unsealed boundary surface during fire incident as shown in Fig. 3 – 1. The specimen condition during the fire test in the furnace was simulated as unsealed and unstressed conditions. After burning process, some samples including control set of specimens were cut along the length of sample with 10 mm thick and 100 mm long for conducting

3 – point bending test. Other samples were brought to make a powder sample and 5 mm cube for chemical properties and physical properties, respectively.

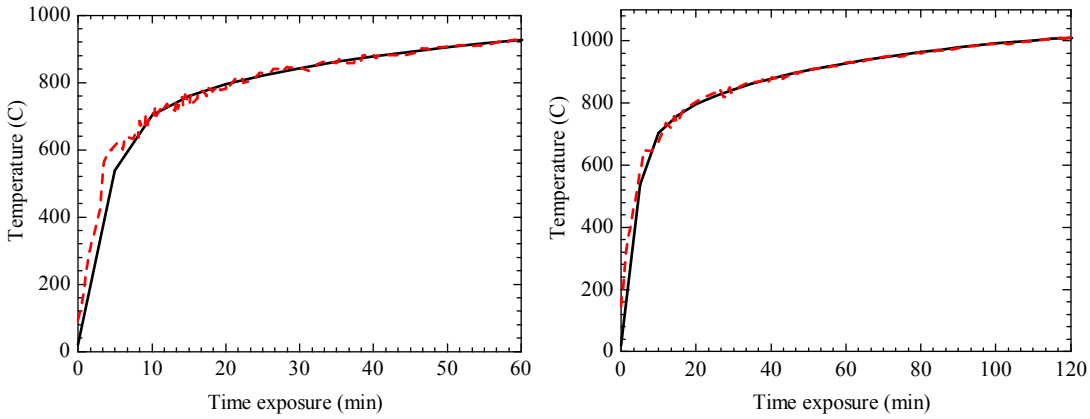

Fig. 3 – 1 Target temperature and actual temperature of ASTM E119 during test

1) Chemical analysis

The major cement hydrated products, CSH and CH are measured by using heavy liquid separation method and Thermo Gravimetric/Differential Thermal Analyzer (TG/DTA) technique, respectively. The CSH content was measured by Heavy Liquid Separation technique in which the sediment and supernatant containing aggregates and finer phases, respectively was separated. Then, the supernatant was used to determine the amount of CSH by Methanol – Salicylic acid technique. In this study, the specific gravity (S.G.) of heavy liquid solution was set to be 2.30. This method is quite popular in mineralogical laboratories to classify pure mineral or group of them by their concentration [33]. Thermo Gravimetric/Differential Thermal Analyzer (TG/DTA) technique was used to determine CH content in which chemical reaction expressed in Eq. (3.1) during the test. For the dissociation of CH, chemical compounds, lime and water, were newly formed.

$$Ca(OH)_2 \rightarrow CaO + H_2O \quad (3.1)$$

In addition, lime can be easily oxidized by CO_2 and formed new crystalline solid namely $CaCO_3$ as shown in Eq. (3.2).

$$CaO + CO_2 \rightarrow CaCO_3 \quad (3.2)$$

According to the law of conservation of mass, the amount of CH can be determined from the evaporated mass of water.

2) Physical analysis

By means of Archimedean approach, mortar samples were dried at 105 °C for 24 – hour in order to eliminate all evaporable water (also known as the capillary pore water), made a saturated condition by soaking in water for 24 – hour, measured a weight at each condition. A porosity value is then estimated as shown in Eq. (3.3).

$$Porosity = \frac{\rho_w (m_s - m_d)}{V_s} \times 100 \quad (3.3)$$

Where ρ_w = water density (g/mm^3)

m_s = mass of saturated sample (g)

m_d = mass of dry sample (g)

Also, Mercury intrusion porosimetry (MIP) is one of the most popular techniques which can determine porosity and pores size distribution of porous material based on threshold pressure and pore diameter relation. Mortar samples were introduced into a cell sample which was evacuated; then, samples were surrounded by mercury in low pressure analysis step. At high pressure state, pressure was applied on the surface of sample in order to force mercury penetrate into pore system. Owing to its own limitations, in continuous system, if larger pores can be filled by mercury through small

pore necks only, MIP may not provide the actual results; otherwise exceeding applied pressure may break the barriers in discontinuous system.

Once as hydration reaction proceeds, the pore space becomes entirely filled and let the isolated pore occurred. The porosity values obtained from MIP must differ from other methods because the pressure introduced to sample during the test can collapse the pore walls to the isolated one [3]. Therefore, it can be said that one obtained from MIP technique is closer to actual porosity value than other methods.

As exposing to fire incidents, the molecular structure of cement hydrated products were probably destroyed, pore space should be developed again. Generally, the cumulative volume of mercury intruded must be plotted with respect to pore diameter in order to know the integrated volume of pore per gram of freeze – dried samples.

3.3 Material model

The changed material properties after fire exposure consisting of chemical properties, physical properties and mechanical properties was proposed as the chemo – physical relation and the physical – chemical relation.

3.3.1 Relationship between chemical and physical properties

The properties of this binder are chemically disturbed. Since the binding ability upon cementitious material is diminished under fire exposure, any deterioration may easily occur throughout micro – cracking and pore – structure coarsening. Besides its chemical properties, the pore structure of fire – damaged mortar is also one of the fundamental properties that should be considered for post – high temperature treatment condition. In addition, conventional methods for clarifying the fire deterioration on mortar

are inadequate and do not allow to define the actual causes of changes in basic properties; therefore, to obtain the better understanding, the chemo – physical relation is strongly needed for evaluating a post – fire material performance.

3.3.2 Relationship between physical and mechanical properties

Due to the diminishing of chemical properties that influenced the physical properties, mechanical performance of material was also disturbed. A porosity of mortar sample was estimated by the residual quantity of CSH in whole sample. Also, mechanical properties would be diminished by the influence of variation of porosity value [4, 13, 16, 34]; therefore, the relationship between porosity against mechanical properties must be concerned in order to better understand the actual behavior of both non – damaged and fire – damaged mortar in this study.

3.4 Computational works

3.4.1 Inverted analysis

Inverted analysis or back analysis is a technique which can be used to obtain a pure tensile strength, elastic modulus, tensile softening branch, load – deflection curve and fracture energy which was calculated from area under load – deflection curve by means of trapezoidal rule. Half model meshing as shown in Fig. 3 – 2 was simulated with actual dimension measured by constant strain triangle and the elemental fineness was not constant along the specimens' axis.

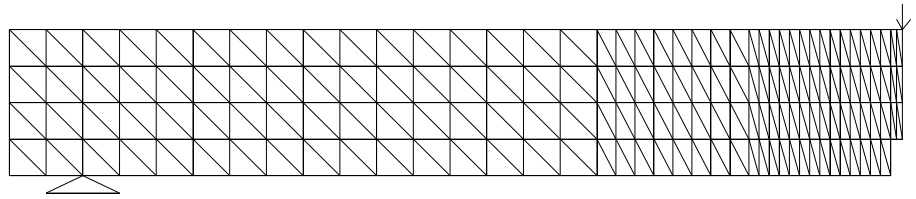

Fig. 3 – 2 Half model meshing with actual dimension for inverted analysis

There were 4 elemental sizes consisting of 2.5 mm, 1.25 mm, 0.625 mm and 0.25 mm width from end of specimens to loading point at mid – span. The reason is, with increasing deformation, the micro cracking coalesce, finally resulting in a single macro cracking; therefore, the meshing size near crack location should be finer than the meshing size near supporting point.

In calculation steps of inverted analysis, it was conforming to JCI – S – 001 – 2003: Method of test for fracture energy of concrete by use of notched beam [35] which is openly available free software in Japan for both a website version and downloaded version. For tested specimen's geometry which is appropriate for this calculation, it should be a rectangular cross section beam and artificial crack is made at the mid – span.

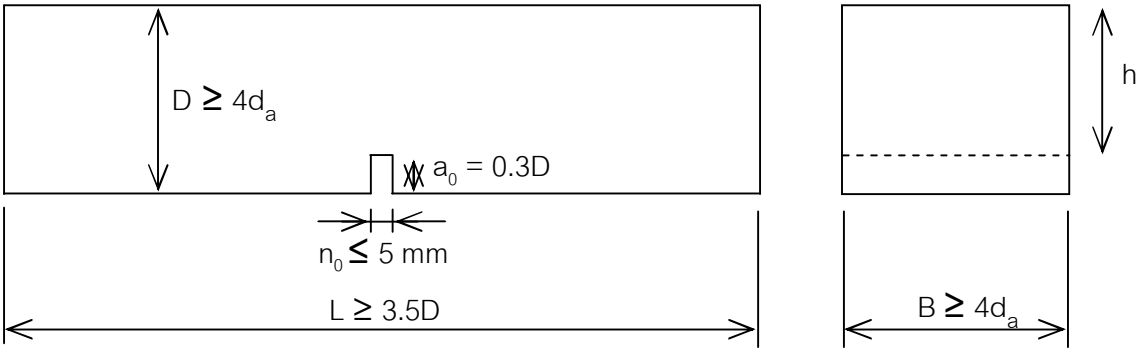

Fig. 3 – 3 Specimen dimensions

Fig. 3 – 3 shows the specimen's geometry. The depth (D) and width (B) of cross section should be greater than 4 times of maximum aggregate size (d_a). The total length of specimen (L) should be greater than 3.5 times of its depth while notch depth (a_0) and notch width (n_0) are probably equal to 0.3D and less than 5 mm, respectively.

The flow chart of calculation step in order to obtain the inverted analysis results is shown in Fig. 3 – 4.

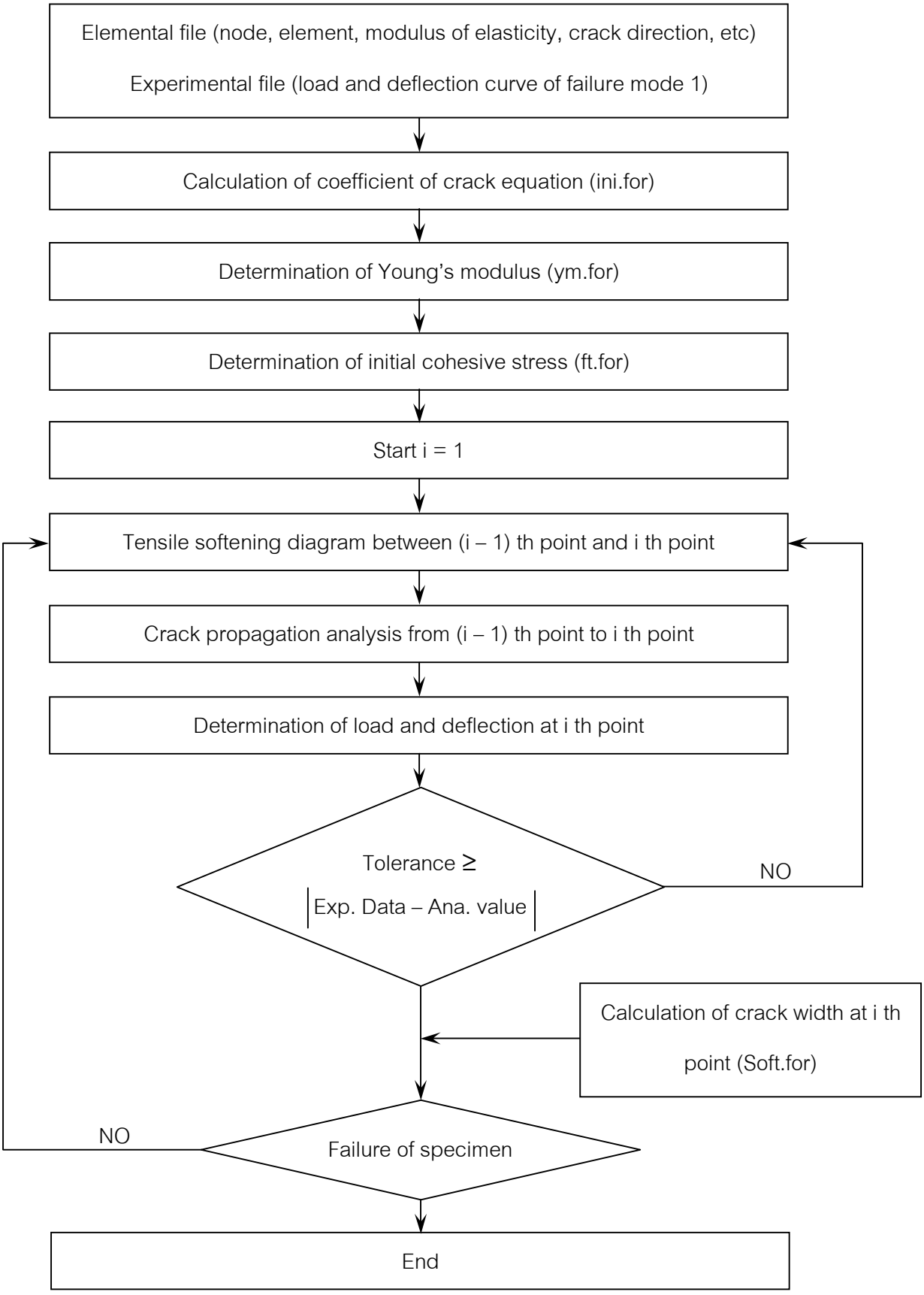

Fig. 3 – 4 A work flow of inverted analysis by using a free software of JCI

3.4.2 RSBM simulation

Both non – damaged and damaged material models proposed in meso – scale were verified by experimental results of 3 – point bending test in macroscopic samples with 50 x 20 mm in cross – section and total 400 mm long. The ultimate load of 3 – point bending test for experimental results were compared with the simulation by using RBSM.

3.5 Research schedule

Activities	Month																	
	2011			2012												2013		
	Oct	Nov	Dec	Jan	Feb	Mar	Apr	May	Jun	Jul	Aug	Sep	Oct	Nov	Dec	Jan	Feb	Mar
1. Literature reviews																		
2. Proposal																		
3. Casting specimens																		
4. Burning process																		
5. Experimental setup																		

Activities	Month																	
	2011			2012												2013		
	Oct	Nov	Dec	Jan	Feb	Mar	Apr	May	Jun	Jul	Aug	Sep	Oct	Nov	Dec	Jan	Feb	Mar
6. Chemical properties investigation																		
7. Physical properties investigation																		
8. Mesoscopic 3 – point bending test																		
9. Analytical study																		
10. Discussion and conclusion																		
11. Thesis defense and submission																		

3.6 Flow chart of research methodology

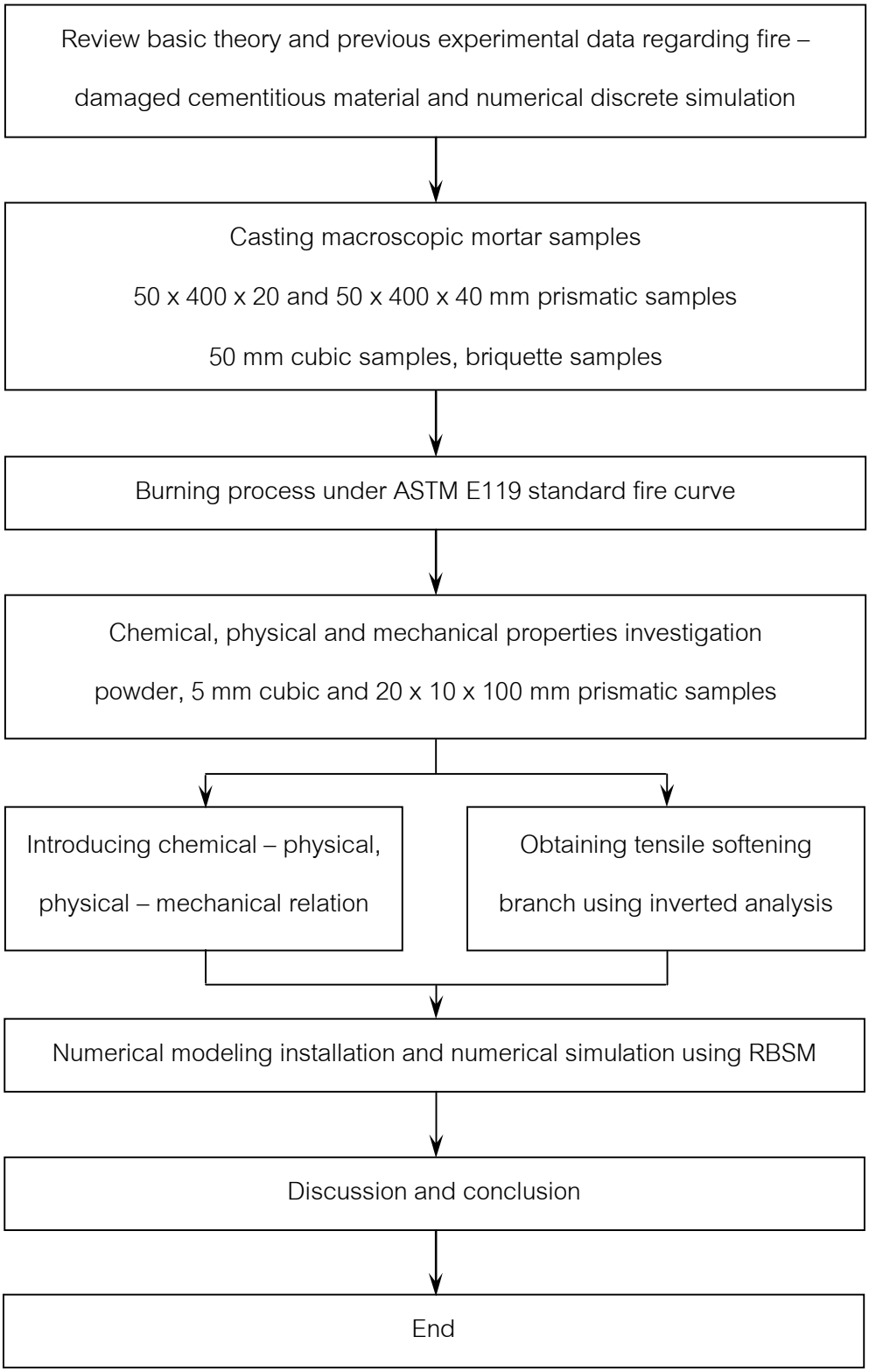

CHAPTER 4

EXPERIMENTAL RESULTS AND DISCUSSION

The experiments are divided into two categories consisting of preliminary test to find the appropriate thickness of specimens and final results as shown followings:

4.1 Preliminary test

The proportion of materials for the standard mortar shall be one part of cement to two parts of graded standard sand by weight and w/c is 0.65 which conform to JIS R5201 – Physical Testing Method for Cement [28].

To clarify the appropriate thickness of specimens for preventing an explosive spalling while exposing to fire and how damage distribute, there are two series of mortar specimens such as air – dried and oven – dried condition after one day in – mold curing and six days moist curing – totally seven – day age before test.

4.1.1 Experimental setup

Beam shape and cubic specimens have burnt for 55 minutes under standard fire curve conforming to ASTM E119 – 12 “Standard Test Methods for Fire Tests of Building Construction and Materials” [1] without ceramic fiber protection to simulate the unsealed boundary surface during fire incident. The layout of specimens in oven is shown in Fig. 4 – 1.

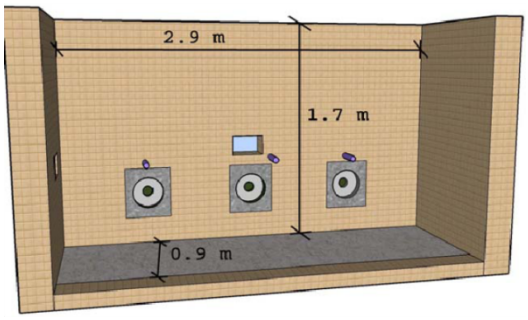

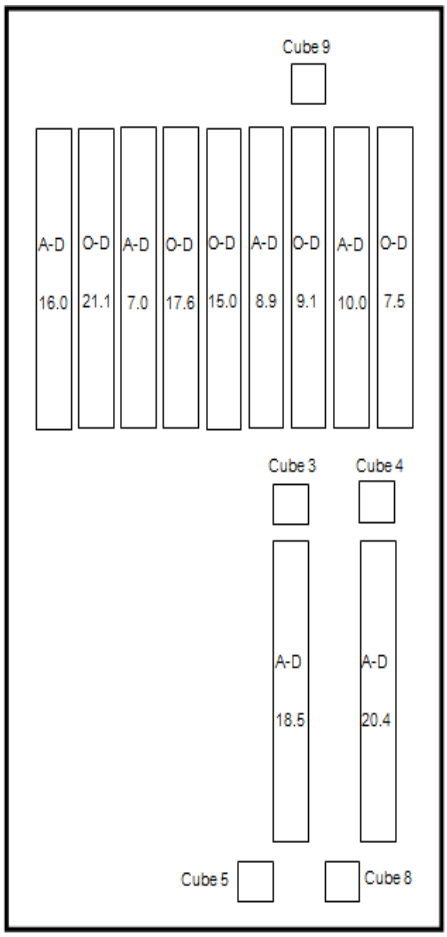

Fig. 4 – 1 Location of specimen in furnace

4.1.2 Comparison between air – dried and oven – dried mortar

1. Air – dried condition

Six specimens consisting of 7.0, 8.9, 10.0, 16.0, 18.5 and 20.4 mm thick for before burning and post – fire were shown in Fig. 4 – 2 and Fig. 4 – 3, respectively.

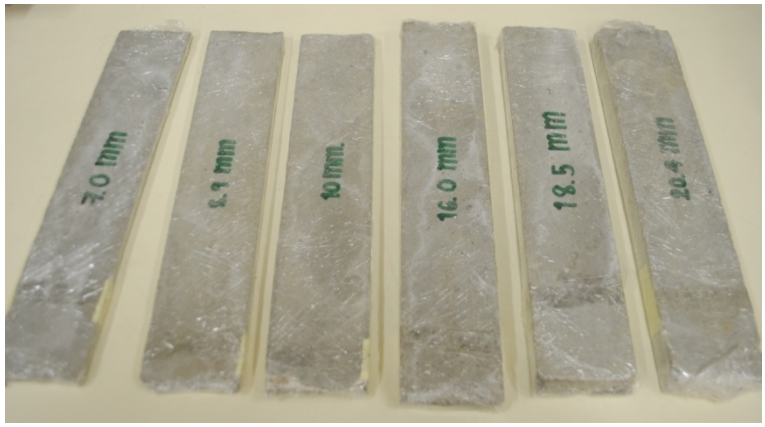

Fig. 4 – 2 Air – dried condition specimens before test

Fig. 4 – 3 Air – dried condition specimens after test

After subjected to fire, damages were seen to be uniform along deteriorated cross sectional area while some specimens were totally disappeared due to explosive spalling. Each deteriorated specimen is shown in Fig. 4 – 4 to 4 – 8, respectively.

Fig. 4 – 4 Deterioration of air – dried condition specimen 7.0 mm thick

Fig. 4 – 5 Deterioration of air – dried condition specimen 16.0 mm thick

Fig. 4 – 6 Deterioration of air – dried condition specimen 18.5 mm thick

Fig. 4 – 7 Deterioration of air – dried condition specimen 20.4 mm thick

Fig. 4 – 8 Deterioration of air – dried condition standard cube specimens

Remark Specimen 8.9 mm and 10.0 mm thick were totally disappearing.

2. Oven – dried condition

Five specimens consisting of 7.5, 9.1, 15.0, 17.6, and 21.1 mm thick for before burning and post – fire were shown in Fig. 4 – 9 and Fig. 4 – 10, respectively.

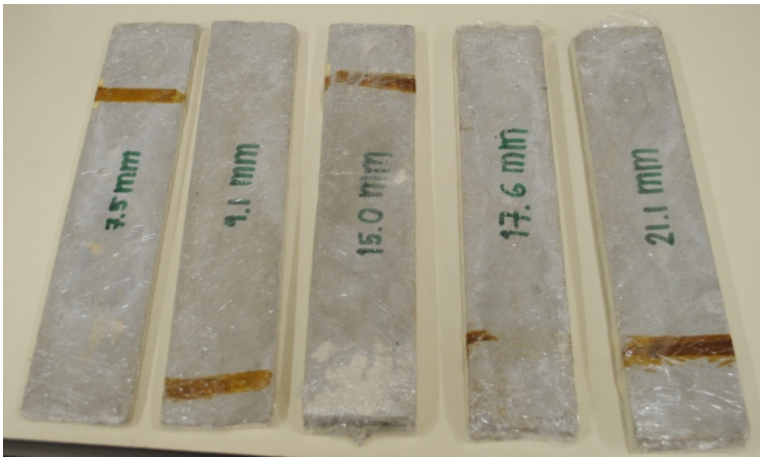

Fig. 4 – 9 Oven – dried condition specimens before test

Fig. 4 – 10 Oven – dried condition specimens after test

After subjected to fire, damages were seen to be uniform along deteriorated cross sectional area while only 9.1 mm thick specimen was totally disappeared due to explosive spalling. Each deteriorated specimen is shown in Fig. 4 – 11 to 4 – 15 respectively.

Fig. 4 – 11 Deterioration of oven – dried condition specimen 7.5 mm thick

Fig. 4 – 12 Deterioration of oven – dried condition specimen 15.0 mm thick

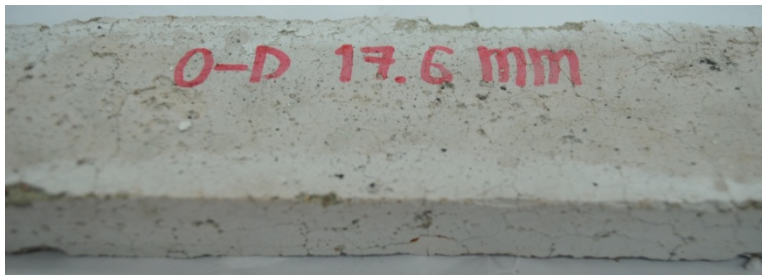

Fig. 4 – 13 Deterioration of oven – dried condition specimen 17.6 mm thick

Fig. 4 – 14 Deterioration of oven – dried condition specimen 21.1 mm thick

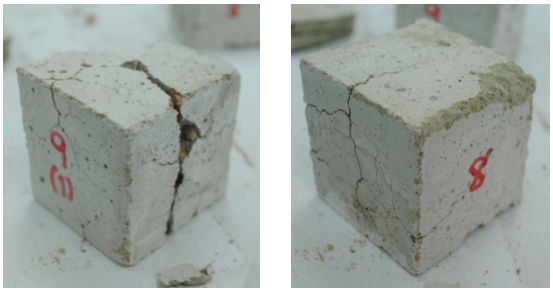

Fig. 4 – 15 Deterioration of oven – dried condition standard cube specimens

Remark Specimen 9.1 mm thick was totally disappearing.

The summary of deteriorated specimens for both air – dried and oven – dried specimens is shown in Table 4 – 1.

Table 4 – 1 Summary of deteriorated beam shape specimens

No.	Thickness (mm)	Weight		Water Loss		Remarks	
		Wet (g)	Dry (g)	(g)	(%)	1	2
1	7.0	215	206	9	4.37	Air dried	
2	8.9	278	263	15	5.70	Air dried	Disappeared
3	10.0	309	292	17	5.82	Air dried	Disappeared
4	16.0	617	603	14	2.32	Air dried	
5	18.5	619	605	14	2.31	Air dried	Disappeared
6	20.4	688	670	18	2.69	Air dried	Disappeared
7	7.5	254	225	29	12.89	Oven dried	
8	9.1	292	253	39	15.42	Oven dried	Disappeared
9	15.0	508	450	58	12.89	Oven dried	
10	17.6	567	502	65	12.95	Oven dried	
11	21.1	717	631	86	13.63	Oven dried	

The comparison between air – dried and oven – dried condition was also extended to the comparison of compressive strength of mortar by ASTM C109/C109M - 11b “Standard Test Method for Compressive Strength of Hydraulic Cement Mortars” [31] for all specimens. The results were shown in Table 4 – 2.

According to the both physical characteristics of specimens after burning process and preliminary results, it can summarize that the appropriate thickness of specimens should be thicker than 20.0 mm to let uniformly damaged and prevent an explosion in oven. Moreover, internal vapor pressure plays an important role on explosive spalling while concrete (or mortar) is exposed to fire [21, 26]; therefore, there are two series of oven – dried specimen consisting of a series of 20.0 mm and a series of 40.0 mm thickness specimens to be able to change degree of deterioration in this study.

Table 4 – 2 Compressive strength results for air – dried and oven – dried specimens in ambient and exposing to fire condition

No.	Weight		Water Loss		Dimension		Area	Load	Compressive Strength	Remarks	
	Wet (g)	Dry (g)	(g)	(%)	Width 1 (cm)	Width 2 (cm)	(cm^2)	(kg)	(ksc)	1	2
1	292	257	35	13.62	5.18	5.16	26.73	7500	280.60	Oven dried	Non - damage
2	299	264	35	13.26	5.22	5.16	26.94	7400	274.73	Oven dried	Non - damage
3	302	266	36	13.53	5.22	5.21	27.20	-	-	Oven dried	Damaged
4	292	255	37	14.51	5.20	5.27	27.40	-	-	Oven dried	Damaged
5	295	260	35	13.46	5.23	5.22	27.30	-	-	Oven dried	Damaged
6	288	283	5	1.77	5.18	5.18	26.83	7100	264.61	Air dried	Non - damage
7	292	287	5	1.74	5.23	5.09	26.62	7250	272.34	Air dried	Non - damage
8	291	286	5	1.75	5.20	5.23	27.20	-	-	Air dried	Damaged
9	296	292	4	1.37	5.13	5.21	26.73	-	-	Air dried	Damaged

4.2 Experimental results

All samples consisting of 50 x 400 x 20 and 50 x 400 x 40 mm prismatic samples 50 mm cubic samples, briquette samples were burnt under ASTM E119 with two different time exposure and control set of specimen; therefore, there were three set of specimens. After 28 – day old, all of them were dried at 105 °C in the oven in order to eliminate the retaining free water; then some of them were burnt. After burning process, both invisible and visible cracks have been developed on the surface and inside specimens as shown in Fig. 4 – 16, Fig. 4 – 17 and Fig. 4 – 18 for control samples, 60 and 120 minutes of exposure, respectively.

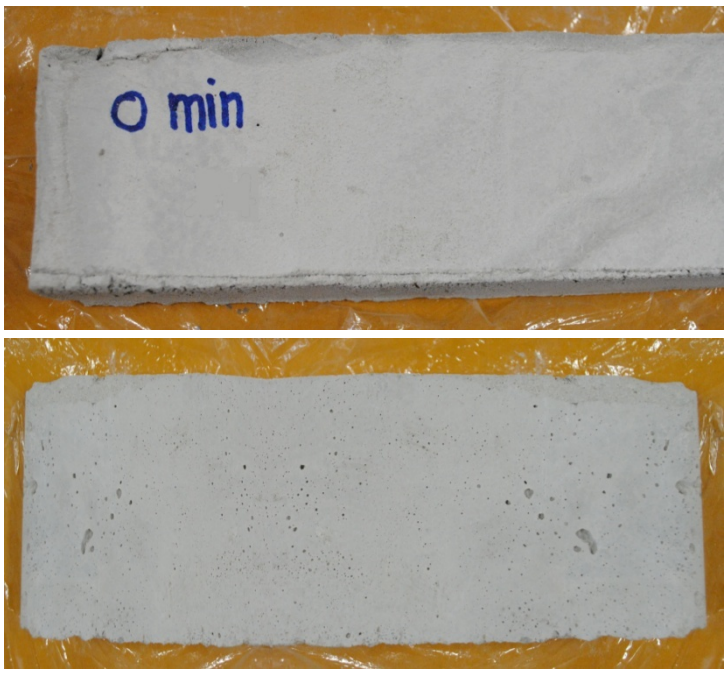

Fig. 4 – 16 Control specimens

Fig. 4 – 17 Cracked samples after 60 minutes of exposure

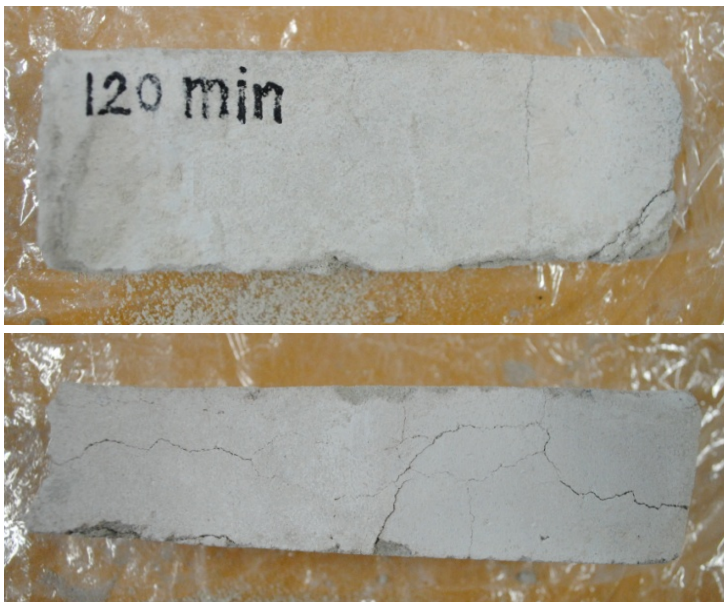

Fig. 4 – 18 Cracked samples after 120 minutes of exposure

For deteriorated samples, visible cracks were obviously seen on the surface of samples. Moreover, the minor invisible cracks were probably propagated after subjected to high temperature treatment together with major cracks.

After subjected to fire exposure and cooled down to temperature, all fire – damaged specimens were kept in the vacuum desiccators until test date. Some of them were chosen to be specimens for chemical and physical properties test while the others were chosen to be samples for mechanical properties test. The location of picked area of original specimens for each property is shown in Fig. 4 – 19 to Fig. 4 – 20.

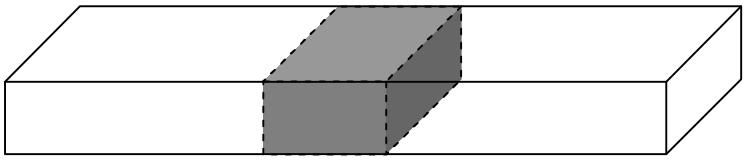

Fig. 4 – 19 Chosen location of original prismatic samples for chemical and physical properties test

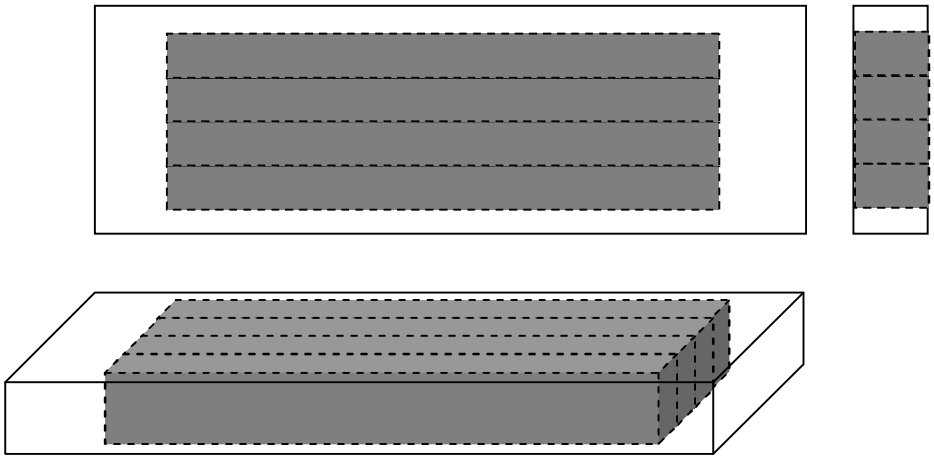

Fig. 4 – 20 Chosen location of original prismatic samples for mechanical properties test

A powder sample and 5 mm cubic samples were made from the center of original specimen as shown in Fig. 4 – 19 because it could represent the properties of whole sample without any bias of two directions of fire exposure near the edge. The specimens for mechanical properties test were made from the original prismatic specimen avoiding

major cracks; therefore, the outer surface was cut and testing specimens were picked inside.

4.2.1 Chemical properties

After hydration between cement grains against water, the strength compounds were produced and material strength depends on a content of strength compounds such as CSH and CH. However, fire accident brings the extremely serious deterioration to concrete structure. The overall performance of structural concrete was significantly diminished starting with an interference of chemical structure, changes in physical and mechanical properties. Generally, mechanical properties can represent the behavior of local or whole structure but it can describe only the difference of strength with respect to time exposure not including primary reasons of this phenomenon. Therefore, the explanation of fire deterioration of oven – dried mortar in this study involved the integration of chemical – physical properties on mechanical properties. For both under fire and post – fire cementitious material, the changes in chemical and physical properties such as loss of free moisture or decomposition of cement hydrated products might bring a drop – off of mechanical properties [4, 13, 16, 34]. Furthermore, porosity in term of pore – structure coarsening and both visible and invisible crack formation for fire – damaged cementitious material is critical to a reduction in overall performance of concrete structure [3, 5, 8, 9].

1. Calcium silicate hydrate content (CSH)

   Calcium silicate hydrate, $(CaO)_3(SiO_2)_2 \cdot 4(H_2O)$, (CSH) is the largest volume containing 70 – 80 percent by volume after hydration and the most important chemical compound of cement hydration product because it is a

strength compound. After subjected to high temperature treatment, CSH was decomposed due to the vaporization of free moisture water in molecular structure became non – strength compound; therefore, the strength capacity of structure was obviously reduced after subjected to high temperature up to 500 °C. Normally, CSH content in sample was determined by heavy liquid separation method by separating sediment and supernatant. By means of the methanol – salicylic acid technique, the CSH content in sample was determined. Fig. 4 – 21 and Fig. 4 – 22 show the process of heavy liquid separation and methanol – salicylic acid techniques, respectively.

Fig. 4 – 21 Heavy liquid separation method

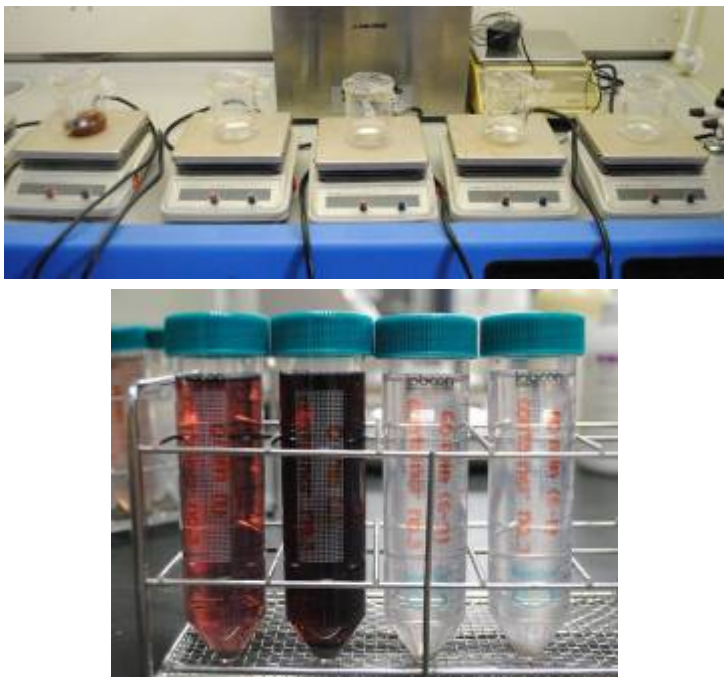

Fig. 4 – 22 Methanol – Salicylic acid method

The powder samples were divided into two parts consisting of sediment and supernatant by centrifuging in heavy liquid solution made from the solution of bromoform and ethanol in order to separate finer particle, namely supernatant containing the cement hydrated product from coarser particle called sediment containing the aggregate. Supernatant was dried in vacuum desiccators for a day and shook in solution made from the solution of methanol and salicylic acid which can dissolve CSH by magnetic force without motion for 2 hours. If CSH still remained in the sample, color of shook sample would be purple. After that, shook samples were washed in methanol until clear of color and dried in vacuum desiccators for a day. Weighing and calculating for the amount of calcium silicate hydrate were done. The result can be shown in Table 4 – 3 and Fig. 4 – 23.

Table 4 – 3 CSH content in powder sample

Specimen		Weight of samples	CSH content in sample	
Time exposure (min)	Specimen no.	(g)	(g)	% by weight
0	1	2.9789	0.0838	2.8131
	2	2.9472	0.1112	3.7731
60	1	2.9425	0.0418	1.4206
	2	2.9484	0.0037	0.1255
	3	2.9211	0.0048	0.1643
	4	3.0470	0.0061	0.2002
120	1	3.0397	0.0180	0.5922
	2	2.9611	0.0159	0.5370
	3	3.0442	0.0104	0.3416
	4	2.8603	0.0141	0.4930

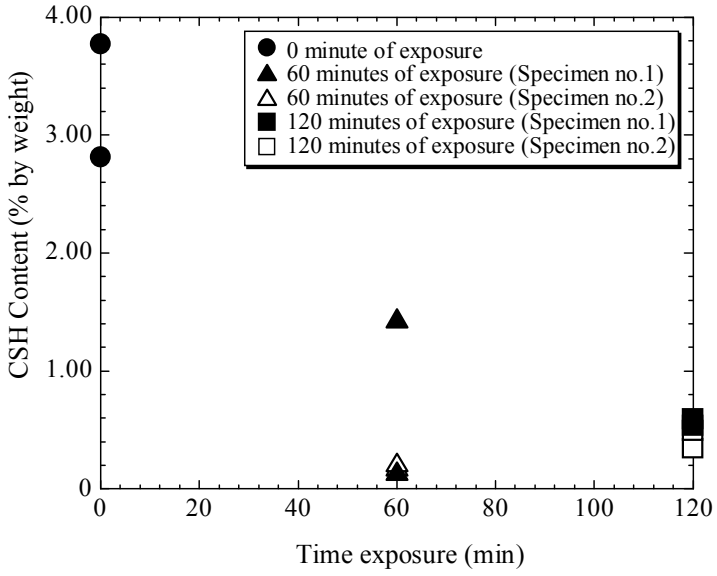

Fig. 4 – 23 Amount of CSH in whole sample by weight percentage

As shown in Fig. 4 – 23, there are four numbers of results for each deteriorated specimens. Normally, there are two original samples which were chosen to evaluate the content of CSH but the reliability of results depends on the experience of researcher; therefore, there are four number of results in total after repetition. According to the tendency of CSH reduction shown in Fig. 4 – 23, it can be found that the CSH content was obviously diminished after 60 minutes of exposure. However, no significant difference between 60 and 120 minutes of exposure time was observed. The reason is because CSH was substantially decomposed after 60 minutes under elevated temperature [5]. Since subjected to high temperature treatment, the molecular water was escaped out from the chemical compound. Therefore, the molecular structure of CSH was disturbed and had an influence on the reduction of material strength. In addition, the diminishing of CSH did not only affect material strength, but the porosity value was also disturbed. Based on the hydration of cement powder, hydration products were generated and expanded to the free space [3], it is logical that the pore connectivity was diminished. Therefore, if the decomposition process of hydrated products occurs, pore – structure must be disturbed.

2. Calcium hydroxide content (CH) and calcium carbonate content (CC)

Calcium Hydroxide (CH), one of major cement hydrate, is known as passivation layer of steel reinforcement in reinforced concrete structure; therefore, its decomposition may affect the durability of reinforced concrete. After exposed to elevated temperature, CH started to decompose and formed new carbonate chemical compound.

Thermo Gravimetric/Differential Thermal Analyzer (TG/DTA) technique was used to determine CH content in which chemical reaction expressed in Eq. (4.1) during the test. For the dissociation of CH, chemical compounds, lime and water, were newly formed.

$$Ca(OH)_2 \rightarrow CaO + H_2O \quad (4.1)$$

In addition, lime can be easily oxidized by CO_2 and formed new crystalline solid namely $CaCO_3$ as shown in Eq. (4.2).

$$CaO + CO_2 \rightarrow CaCO_3 \quad (4.2)$$

According to the law of conservation of mass, the amount of CH can be determined from the evaporated mass of water. The residual CH content after subjected to fire exposure is shown in Table 4 – 4 and Fig. 4 – 24.

Table 4 – 4 CH content in powder sample

Specimens		Weight of samples	CH content	
Time exposure (min)	Specimen no.	(g)	% by weight	Average
0	1	20.247	3.8513	3.8513
60	1	14.948	1.3585	1.9698
	2	27.753	2.5810	
120	1	29.328	0.2527	0.1264
	2	35.831	0.0000	

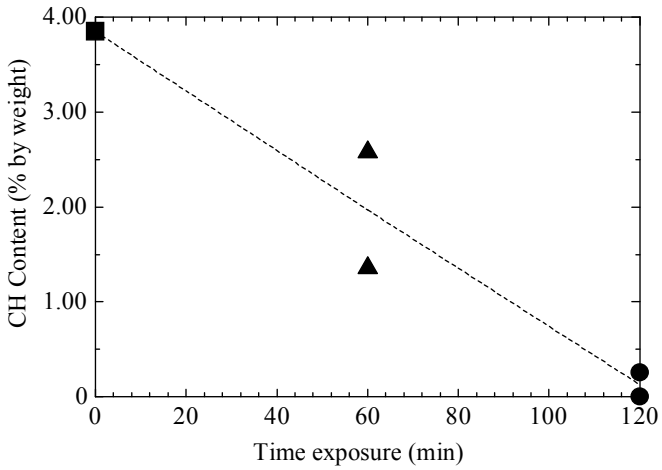

Fig. 4 – 24 Amount of CH in whole sample by weight percentage

The molecular of water in CH was gradually liberated from cement paste especially in the range of 450 - 500 °C [6]. Therefore, it was also reduced significantly after 60 minutes and 120 minutes of exposure. However, the decomposition of CH was not so significant on strength loss compared with both invisible and visible cracks due to expansion and shrinkage of new compound during the formation process [7].

By means of thermal analysis, there were not only CH in sample can be determined, but CC were also quantitatively measured. The result was shown in Table 4 – 5 and Fig. 4 – 25.

Even the quantity of calcite should be increased because of additional product which follows Eq. (4.2), the results from TG/DTA still confirm the reduction of calcite. The reason is because calcite could exist for a short time and be rapidly decomposed from temperature greater than 600 °C [6] as same as other chemical compounds decomposition under high temperature.

Table 4 – 5 CC content in powder sample

Specimens		Weight of samples	CC content	
Time exposure (min)	Specimen no.	(g)	% by weight	Average
0	1	20.247	3.031	3.031
60	1	14.948	2.368	2.104
	2	27.753	1.840	
120	1	29.328	1.378	1.681
	2	35.831	1.984	

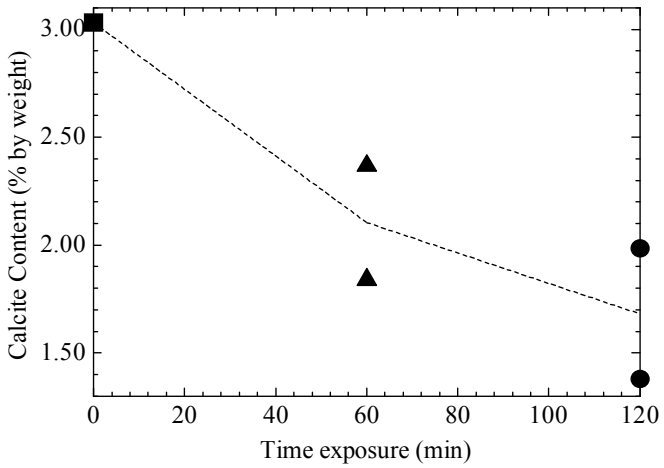

Fig. 4 – 25 Amount of CC in whole sample by weight percentage

3. X – ray diffraction (XRD) technique for Identifying unknown compound

An X – ray beam is an electromagnetic wave characterized by an electric field vibrating at constant frequency, perpendicular to the direction of movement. X – ray is scattered by electron and diffracted as a function of atomic position. When an X – Ray beam encounters a crystal, the intensity count of diffracted X – Ray depends on both the atomic arrangement and atomic

species. For identifying unknown samples by X – ray diffraction (XRD) technique, we can confirm the existing of unknown compounds for only crystalline solid by measuring the diffraction angle which is equal to 2θ due to an angle of incidence and an angle of reflection. Each compound has its own characteristic peak of intensity and the d value; however, they are known to be affected by several factors because of the phases of matter, e.g., amorphous solid and crystalline solid. It leads to be the erroneous identification of sample when X – Ray beam encounters an amorphous solid. Therefore, XRD test is satisfied only for crystalline solid and the characteristic peak of intensity is shown in Table 4 – 6.

However, the main chemical compounds considered are only Gypsum, Ettringite, and Calcite. The first two chemical compounds can affect the long – term durability of concrete (or mortar). The chemical reaction between gypsum and sulphate ion (SO_4^{2-}) produces ettringite with very large expansion leads to cracks. In addition, Calcite ($CaCO_3$) was formed by the decomposition of CH while it also expands and shrinkage during the decomposition and formation; therefore, it should be considered the amount changed.

Table 4 – 6 Characteristic peaks of crystalline solid in powder sample

Type	Mineral	Diffraction angle (2θ)
Cement mineral	Alite	51.6, 51.9
	Belite	31.0
		41.2, 41.7
	Aluminate phase	33.2
	Ferrite phase	12.2
		33.8
	$CaSO_4 \cdot 2H_2O$	11.7
	$CaSO_4$	25 ~ 26
Cement hydrate	Ettringite	9.1
	Mono – sulphate	9.9
	Mono – carbonate	11.6
	Hemi – carbonate	10.7
	C_3AH_6	17.3
	Salt (Solid state)	11.3
Admixture	$CaCO_3$ (Calcite)	48.5
Fly ash	Quartz	21.8
	Mullite	16.4
Control phase in standard sample	α - Al_2O_3	52.5
	MgO	42.9
	CaF_2	28.3

The result of XRD test is shown Fig. 4 – 26.

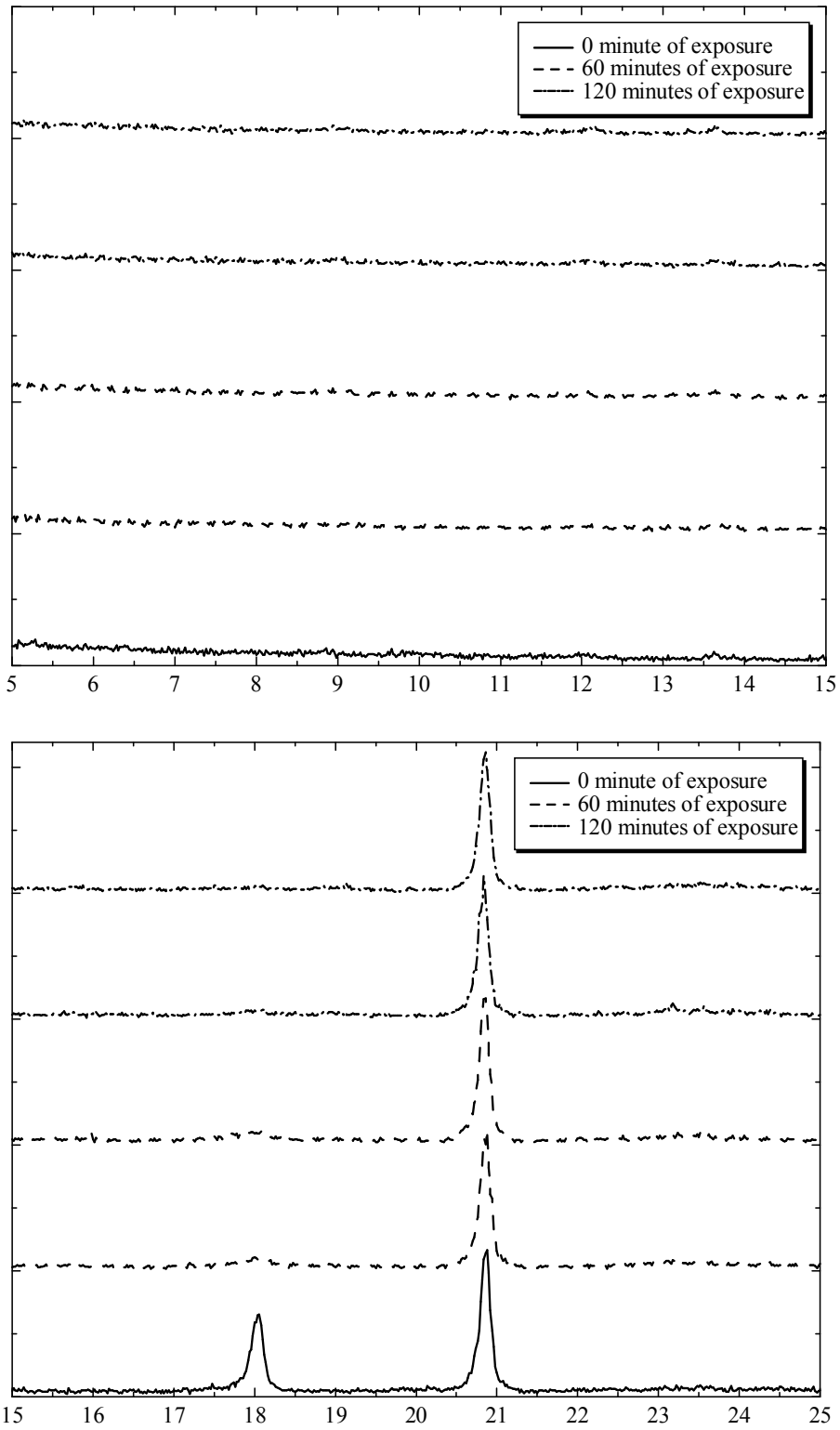

Fig. 4 – 26 Identification of unknown compound by XRD technique

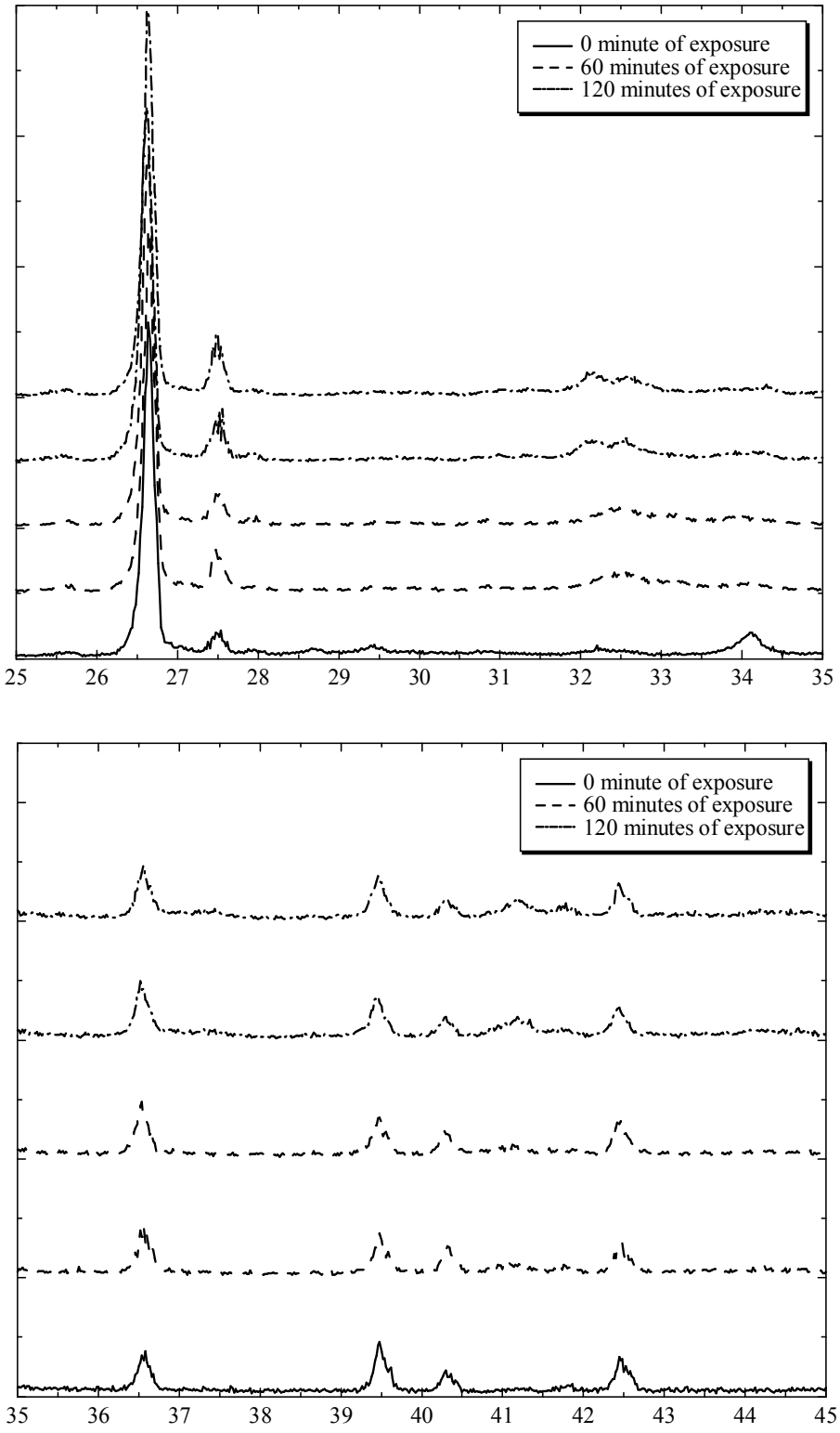

Fig. 4 – 26 Identification of unknown compound by XRD technique

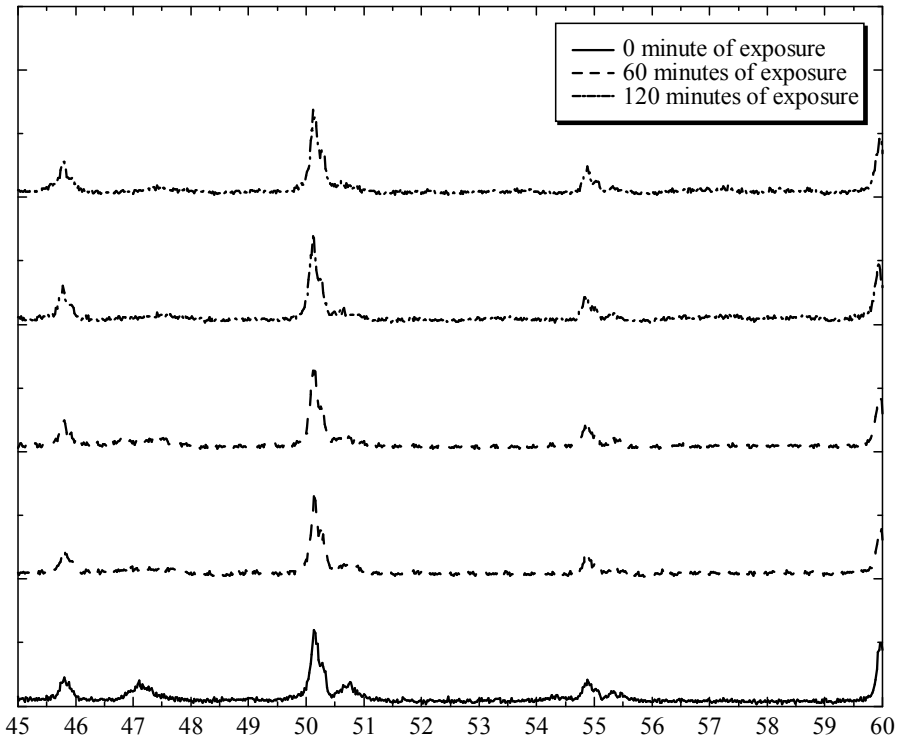

Fig. 4 – 26 Identification of unknown compound by XRD technique

According to figures above, we could not find the characteristic peaks related with the main chemical compounds considered. In control set of specimens, the characteristic peak of gypsum should be found because the manufacturing process of cement powder in Thailand always adds a few amounts of gypsum as a retarder of cement hydration reaction but the result may be affected by several factors as mentioned above; therefore, its characteristic peak was disappeared. For Calcite, it might be totally decomposed which was initiated at 530 °C after subjecting to elevated temperature; therefore, the characteristic peak was also disappeared.

However, as mentioned above, the scattering and diffraction of X – Ray beam are known to be affected by several factors so the existence of some chemical compound cannot be detected accurately; for example, $CaCO_3$ can be

detected by TG/DTA at the second peak. The reproducibility among the replicates should be done in order to ensure.

4.2.2 Physical properties

1. Porosity assessments by Archimedean technique

By means of Archimedean approach, mortar samples were dried at 105 °C for 24 – hour in order to eliminate all evaporable water (also known as the capillary pore water), made a saturated condition by soaking in water for 24 – hour, measured a weight at each condition. A porosity value is then estimated as shown in Eq. (4.3).

$$Porosity = \frac{\rho_w (m_s - m_d)}{V_s} \times 100 \quad (4.3)$$

Where ρ_w = water density (g/mm^3)

m_s = mass of saturated sample (g)

m_d = mass of dry sample (g)

The result is shown in Table 4 – 6. From the result of Archimedean technique, it can be seen that the porosity of mortar after subjecting to elevated temperature were significantly increased. The increment of porosity might be because of the decomposition of some chemical compounds such as CH, CSH or $CaCO_3$ which let arbitrary space occurred; therefore, the porosity increased.

2. Porosimetric analysis

Mercury intrusion porosimetry (MIP) is one of the most popular techniques which can determine porosity and pores size distribution of porous material based on threshold pressure and pore diameter relation. Mortar samples were introduced into a cell sample which was evacuated; then,

samples were surrounded by mercury in low pressure analysis step. At high pressure state, pressure was applied on the surface of sample in order to force mercury penetrate into pore system. Owing to its own limitations, in continuous system, if larger pores can be filled by mercury through small pore necks only, MIP may not provide the actual results; otherwise exceeding applied pressure may break the barriers in discontinuous system.

Once as hydration reaction proceeds, the pore space becomes entirely filled and let the isolated pore occurred. The porosity values obtained from MIP must differ from other methods because the pressure introduced to sample during the test can collapse the pore walls to the isolated one [3]. Therefore, it can be said that one obtained from MIP technique is closer to actual porosity value than other methods.

As exposing to fire incidents, the molecular structure of cement hydrated products were probably destroyed, pore space should be developed again. Generally, the cumulative volume of mercury intruded must be plotted with respect to pore diameter in order to know the integrated volume of pore per gram of freeze – dried samples. The result is shown in Fig. 4 – 27.

It can be observed that the total volume of mercury intruded which represent the total pore volume for deteriorated samples is greater than a control specimen. As shown in Table 4 – 7, the porosity values by Archimedean approach are less than those of MIP since the applied pressure did break the blockages through the existing isolated pore.

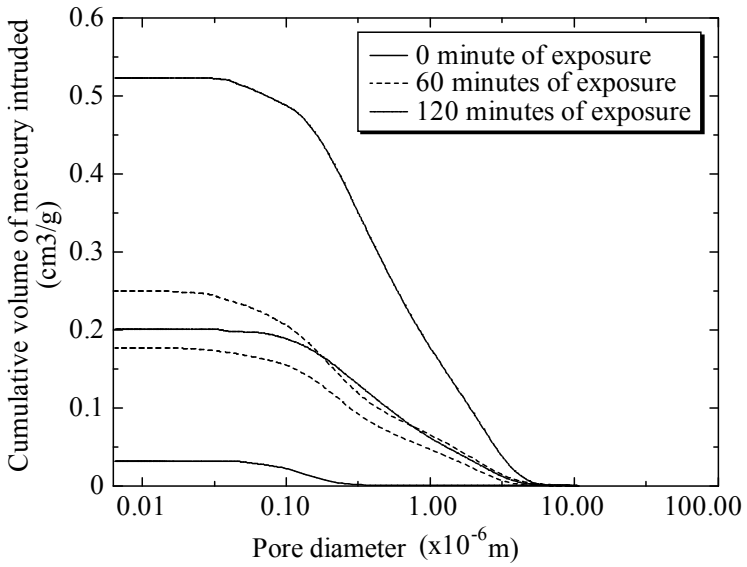

Fig. 4 – 27 Cumulative volume of mercury intruded into samples

Table 4 – 7 A comparison of porosity value between Archimedean and MIP techniques

Time exposure (min)	Porosity (Archimedean) (cm^3/g)	Total pore volume (MIP) (cm^3/g)
0	0.0307	0.0321
60	0.1824	0.2136
120	0.2062	0.3622

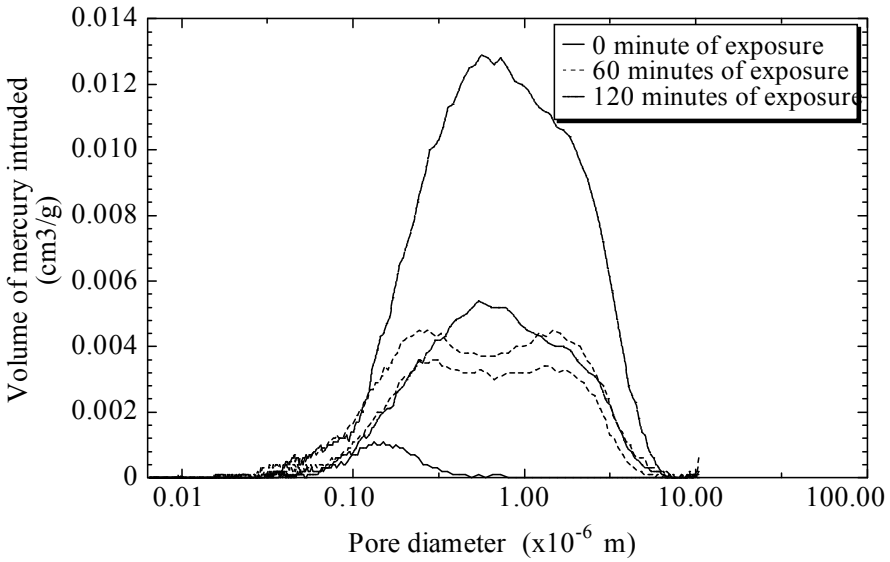

Fig. 4 – 28 Differential curve of mercury intruded into samples

Fig. 4 – 28 shows the relationships between pore diameter and volume of mercury intruded at any pore size. The pore diameter at characteristic peak for deteriorated specimens is larger than a control one because of the decomposition of chemical compounds after fire exposure. In addition, two characteristics peaks were observed in burnt samples. One possibility of the occurrence of the second peak is to crush on hydrated products which impede the intrusion path; therefore, the neck size at a given peak may not correspond to the pore diameter.

To focus on deteriorated samples, two characteristic peaks are clearly appeared for after 60 minutes of exposure while there is only one peak for another set of samples. It can be explained that the surface and the blockages were almost broken for 120 minutes of exposure because of deterioration. Furthermore, due to the variability of material strength after fire exposure, pressure at the second peak is reasonable to say that can be varied by size of pore necks or thickness of framework [3].

Since an unpredictable crack phenomenon during the test, the total pore volume sometime represents the porosity value including broken pore walls to a distinct network. Therefore, a porosity value from Archimedean technique may be preferable way for deteriorated samples.

4.2.3 Mechanical properties

1. Compressive strength and tensile strength

Although compressive strength and tensile strength are the basic properties for cementitious material likely concrete and mortar which have to be tested, the main purpose of this test is to predict how material performance change after subjected to fire exposure and the approximate value of maximum point load applied at mid – span for 3 – point bending test was determined by using elastic theory as shown in Eq. (4.4).

$$P_{\max} = \frac{2 f_t b h^2}{3L} \tag{4.4}$$

Where $P_{\max}$ = maximum applied load (N)

f_t = tensile strength (MPa)

b = width of specimen (mm)

h = height of specimen (mm)

L = span length (mm)

The approximate value of compressive strength and tensile strength were shown in Table 4 – 8, Fig. 4 – 29 and Fig. 4 – 30.

Table 4 – 8 Compressive strength and tensile strength of mortar samples

Specimens		f_c'		f_t	
Time exposure (min)	Specimen no.	N/mm^2	Avg.	N/mm^2	Avg.
0	1	41.09	37.17	3.75	3.94
	2	36.79		4.03	
	3	33.65		4.04	
60	1	6.06	6.23	0.15	0.14
	2	6.65		0.13	
	3	5.98		0.14	
120	1	7.09	6.16	0.27	0.16
	2	5.91		0.11	
	3	5.48		0.10	

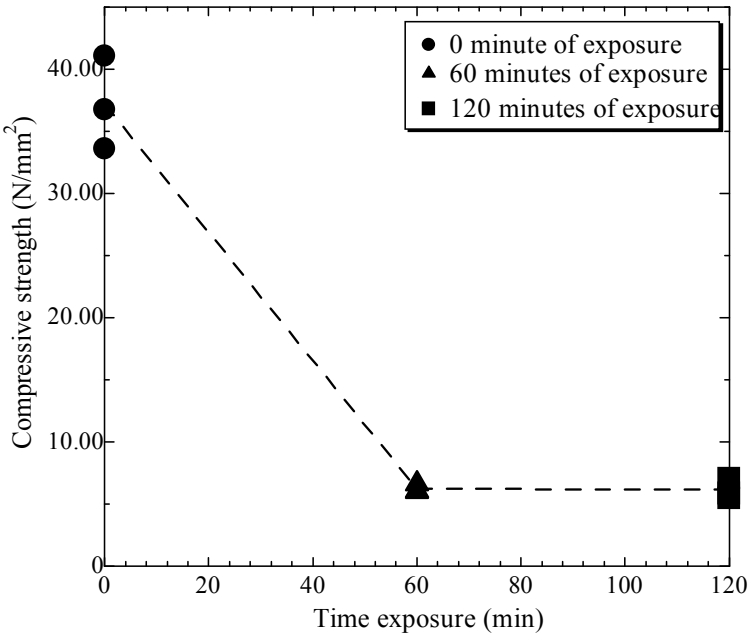

Fig. 4 – 29 Reduction in compressive strength for post – fire samples

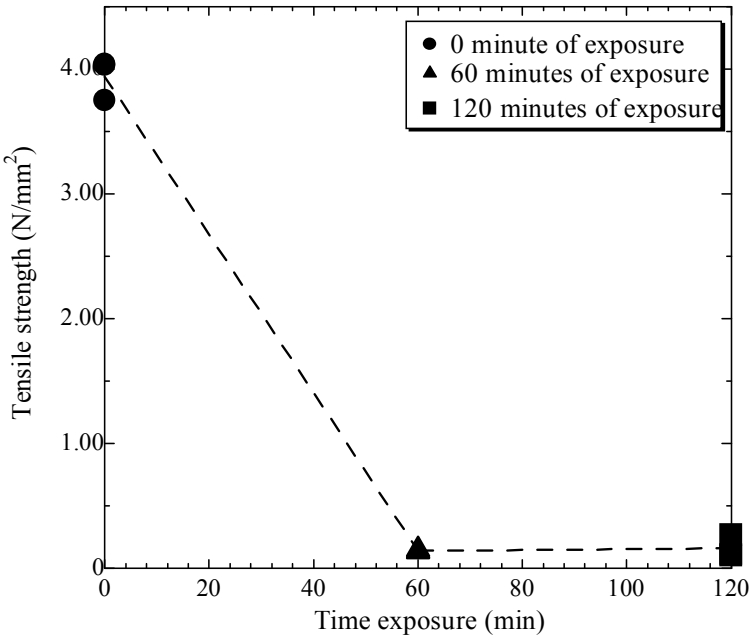

Fig. 4 – 30 Reduction in tensile strength for post – fire samples

Fig. 4 – 29 and Fig. 4 – 30 show the same tendency in reduction of basic strength for post – fire mortar samples. The influence of changes in chemical and physical properties leads to this reduction in material strength. It was substantially diminished in the range between 0 and 60 minute of exposure and both residual compressive strength and tensile strength of fire – damaged mortar after one hour of exposure is not significantly different. One possibility to explain this kind of situation is material strength was extremely destroyed since less than one hour of exposure. Therefore, other mechanical properties may not be significantly reduced after 60 minutes exposed to high temperature treatment.

An Indian researcher, Kumar A. [36] has proposed his experimental study for tensile strength against compressive strength of non – damaged mortar samples. To compare with the experimental result of this study at the same compressive strength, it is reasonable to see from the comparison as shown in

Fig. 4 – 31 that tensile strength of fire – damaged samples were smaller than non – damaged one.

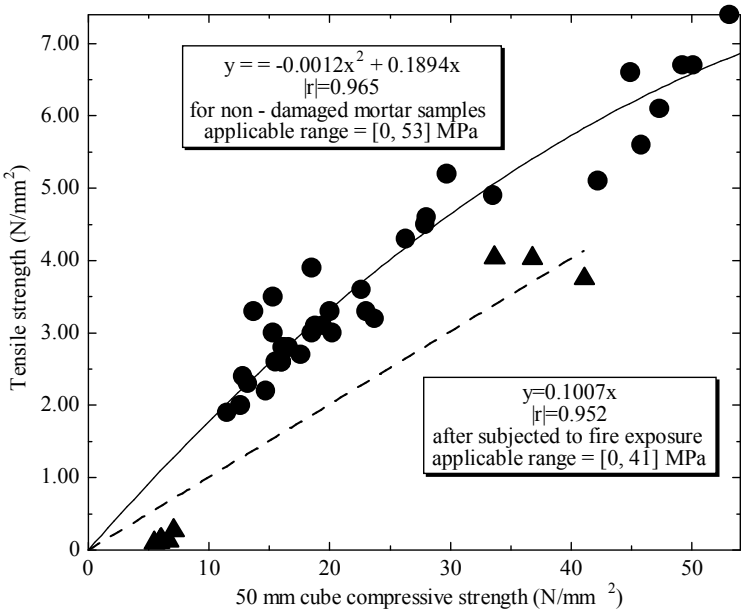

Fig. 4 – 31 A relationship between compressive and tensile strength

However, the number of experimental result for compressive strength and tensile strength in this study is only 3 samples for each time exposure; therefore, the experimental relation for compressive strength against tensile strength was a linear equation. Furthermore, the applicable range of these relationships was scoped only for less than 53 N/mm^2 and 41 N/mm^2 for non – damaged and fire – damaged mortar, respectively.

2. 3 – point mesoscopic bending test

A load – deflection curve was gathered from 3 – point bending test with roller support at both ends. The reason is to prevent the axial force along member axis during the test. All samples controlled the crack location at mid – span by setting a notch were done on the mesoscopic samples with 10 x 20 mm in cross section and 90 mm in span length. As shown in Fig 4 – 32, there were 3

LVDTs set at both ends and mid – span to measure support settlements and deflection at mid – span, respectively.

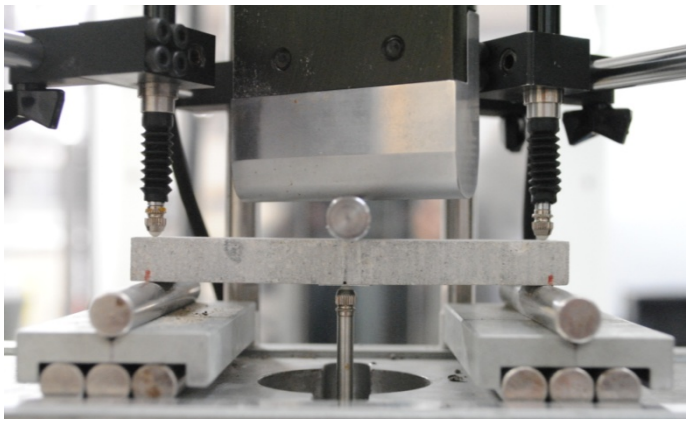

Fig. 4 – 32 3 – point mesoscopic bending test

The average displacement measured at both ends during the test was eliminated after test for neglecting the effect of support settlement; therefore, load – deflection curve represents the relationship between load and relative displacement.

For deteriorated specimens consisting of 60 minutes and 120 minutes of exposure, they were divided into two groups of results. The first group of results is for the specimens whose failure occurred at artificial cracks while another group is for the specimens which fail at unexpected location because fire deterioration is random.

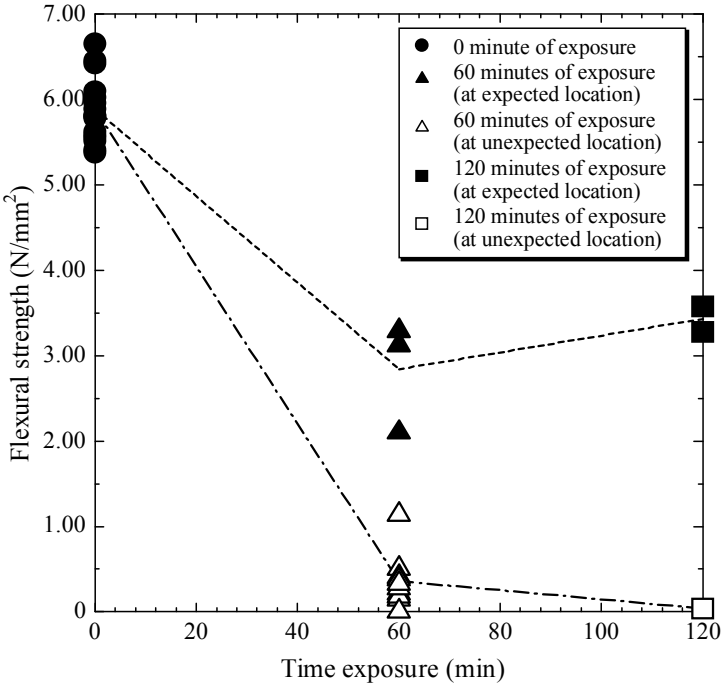

Fig. 4 – 33 Reduction in flexural strength for post – fire samples

Fig. 4 – 33 shows the tendency of reduction in flexural strength for damaged samples. It can be roughly seen that flexural strength would be diminished with the increment of exposure time; however, the results were divided into two groups as mentioned above. The shaded spots represent the test results whose specimens failed at artificial crack after applying point load at mid – span. The flexural strength was significantly reduced in the range between 0 and 60 minutes of exposure but there was a slightly recovered for the one in the range between 60 and 120 minutes of exposure. The reason is fire deteriorations in mortar samples were extremely random in nature. Sometimes, the tested specimens were probably made from the zone without major cracks of burnt original samples; however, the difference between the results of two different time exposure were not so significant and the modulus of rupture for all damaged mortar samples were less than the value of control group. Another spots represent the residual flexural strength whose location of failure was

unpredictable due to the behavior of fire damages. Although the reduction in flexural strength was obviously observed with an increment of time exposure as same as the shaded spots, the residual flexural strength in this group was so small compared with another group. One possibility to explain this kind of situation is, a severe damaged zone might be chosen to be testing specimens.

3. Shear test

A mesoscopic shear strength was experimentally measured by using double direct shear technique on the same samples and testing machine with 3 – point bending test. Fig. 4 – 34 shows the two pieces of devices for double direct shear test. The upper one was the loading head with 11 mm span length and the lower one was the simply support with 12 mm span length. The testing specimens as shown in Fig. 4 – 35 from both end of bending one were set the 4 of 0.5 mm artificial cracks in order to control the crack location and test setup was shown in Fig. 4 – 36. The results were shown in Fig. 4 – 37.

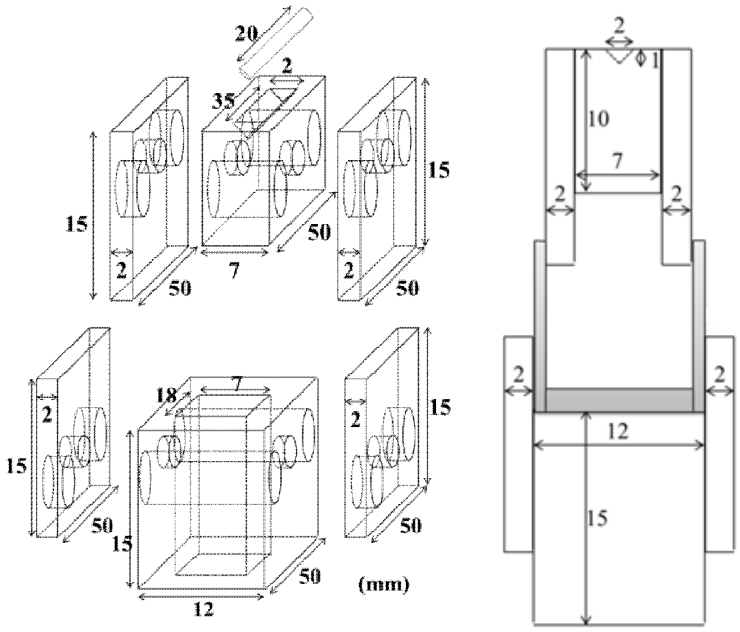

Fig. 4 – 34 Drawings of double direct shear devices (drawn by Miura T.)

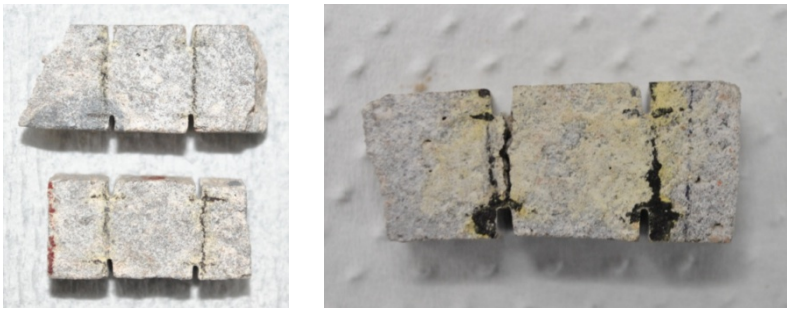

Fig. 4 – 35 Specimens for double direct shear test

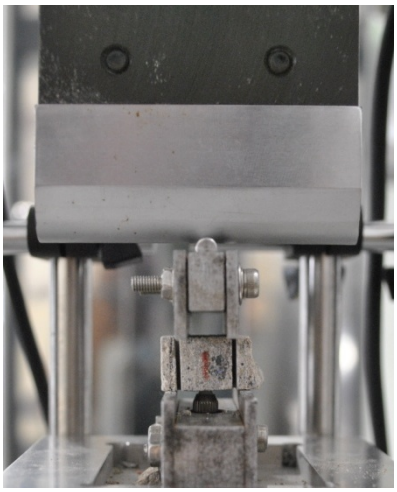

Fig. 4 – 36 Test setup for mesoscopic shear strength measurement

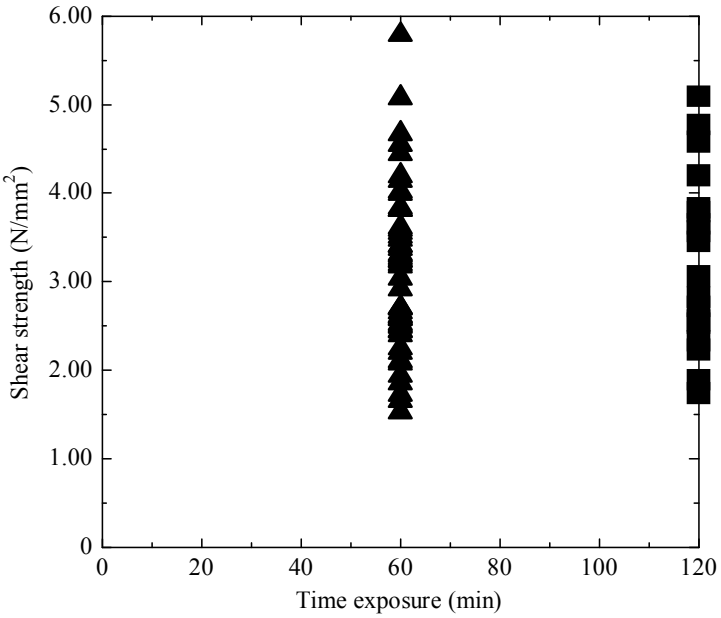

Fig. 4 – 37 Experimental results of double direct shear test

However, the testing results were inclined to be a compressive strength due to inappropriate size of specimen. Also, the control samples could not be tested because of the maximum capacity of testing machine. Therefore, the preferable way to estimate the shear strength is to be calculated from their own actual flexural strength by numerical equation proposed by Japanese researchers as shown in Eq. (4.5).

$$\tau_{\max} = 1.083 f_b + 1.11 \qquad (4.5)$$

Where $\tau_{\max}$ = shear strength (N/mm^2)

f_b = flexural strength (N/mm^2)

Miura T. and Sato Y. have proposed this linear equation to predict shear strength from tested flexural strength which was suitable for non – damaged and damaged mortar samples. Therefore, it may be more suitable way for predicting the shear strength of both control and fire – damaged samples. The results were shown in Fig. 4 – 38.

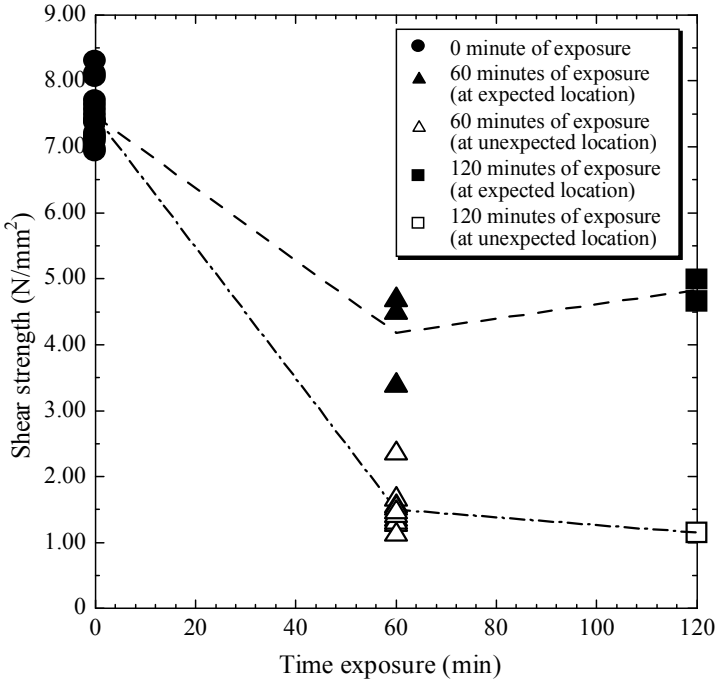

Fig. 4 – 38 Reduction in shear strength for post – fire samples

Because the shear strength as shown in Fig. 4 – 38 was calculated from tested flexural strength; therefore, it had the same reduction tendency as flexural strength results. The shaded spots represent the test results whose specimens for bending test failed at artificial crack after applying point load at mid – span. The calculated shear strength was significantly reduced in the range between 0 and 60 minutes of exposure but there was a slightly recovered for the one in the range between 60 and 120 minutes of exposure. Another spots represent the residual shear strength whose location of failure during flexural test was unpredictable due to the behavior of fire damages. Although the reduction in shear strength was obviously observed with an increment of time exposure as same as the shaded spots, the residual shear strength in this group was so small compared with another group.

4.3 Proposed material model

4.3.1 Relationship between chemical and physical properties

1. Relationship between CSH against porosity

With respect to two different time exposure in this study, the numerical model for predicted the porosity value by the quantity of CSH in sample was proposed in term of maximum temperature in furnace as shown in Fig. 4 – 39. It shows relationships between porosity and CSH. The regression lines were obtained for different exposure times.

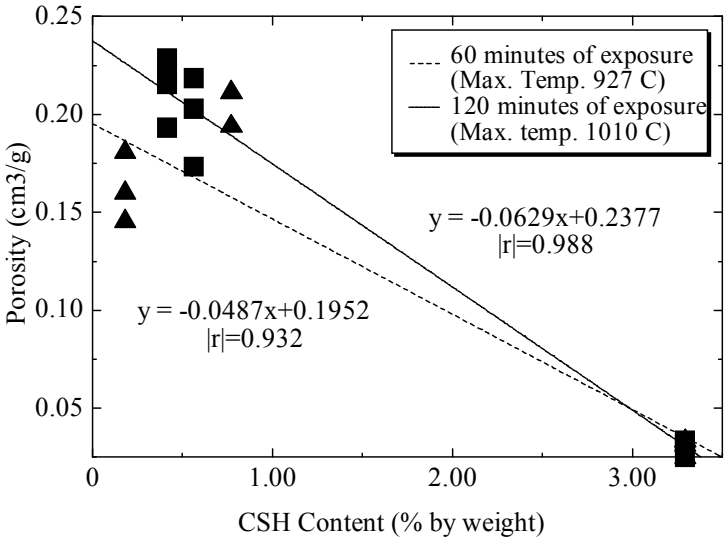

Fig. 4 – 39 Relationship between CSH and porosity

Since the volatilization of CSH was initiated at 560 °C, the non – evaporable water was gradually escaped out so a cohesive force between CSH layers was demolished. The porosity in samples exposed to higher temperature is greater than the samples exposed to a lower one because in case of high temperature the molecular structure of CSH might be substantially destroyed. Those two linear regression equations stated in figure can be used to estimate the porosity value at any amount of residual CSH after fire exposure with the same tendency while maximum temperature is different. With respect to the increment of maximum temperature from 60 minutes to 120 minutes during fire exposure, pore – structure coarsening was intensified because of the CSH decomposition phenomenon.

2. Relationship between CH against porosity

Figure 4 – 40 shows relationship between porosity and CH. The regression lines were obtained for different exposure times.

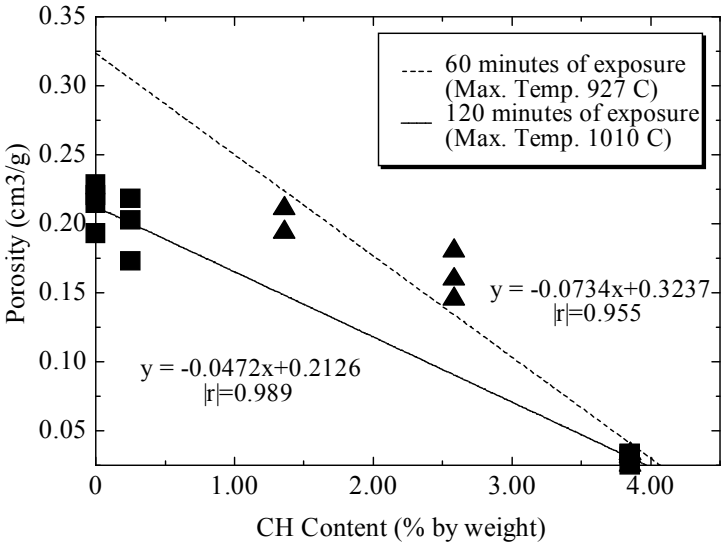

Fig. 4 – 40 Relationship between CH and porosity

The tendency of this relationship should be the same tendency as the relationship between CSH and porosity because the molecular structure of CH is also dissociated. However, a mechanism for the rehydration of CH may be able to happen but it is so complicated and not easy to expect because of the uncertainty of rehydration process shown in Ref. [7]. One possibility of this relationship is to say that the rehydration for post - fire samples; therefore, the pore space may be refilled by new formation of CH.

During hydration, it is well – known that the growth of hydration products expand into pore space; then, the clear interconnections between pores may become CSH strictly frameworks and increase the permeability of those porous materials.

Under fire exposure conforming to ASTM E119 [1], the cement hydrated products namely CSH and CH were decomposed as time exposure increased. The residual CSH and CH after exposed to fire for both two different time exposure are less than the control specimens, even though the further hydration process of residue unhydrated grains can proceed at the beginning of high temperature treatment. In the

case of CSH, the rate of dehydration reaction is so high at first time range 0 minute to 60 minutes under elevated temperature while it is very low in the range between 60 minutes to 120 minutes of exposure. The existence of CSH remained until 5 minutes of exposure and started to dissociate from 5 minutes upward but is not suddenly disappear; therefore, the volatilization of non – evaporable water from gel is gradually developed and become measurable after 10 minutes under fire. It is reasonable to say that it is significantly decomposed which affect the inequitable rate of dehydration. For CH case, it has the same tendency with CSH but the rate of decomposition reaction is almost the same in both two ranges because the rehydration of calcium oxide may occur and cause the new formation of CH.

Again, there is not only chemical property of fire – damaged mortar changed, but the physical property is also disturbed through the effect of changed chemical property. As widely known about the location of cement hydrated products in hardened mortar, those decomposition process always generates a more porous material. An increased porosity value is not only caused by the disappearance of hydration products, a very low crushing material strength is also one possibility to develop cracks during the porosity test by means of Mercury intrusion porosimetry test because of an exceeding applied pressure on the samples' surface.

In addition, the physical property of mortar samples after heating and subsequent cooling down is governed by the changed of molecular structure of cement hydrated products with respect to maximum temperature in the furnace in term of time exposure. The relationship between cohesive material and porosity, and the relationship between CH and porosity do not have the same tendency as previously mentioned in relationship between CSH against porosity and CH against porosity. In general, calcium oxide which is a product in carbonation reaction can provide the rehydration process

and new formation can refill the existing pore spaces; therefore, the permeability of fire – deteriorated mortar may recover and the chemo – physical relation of residual CSH after fire and porosity plays a dominant role on pore structure coarsening rather than CH.

4.3.2 Relationship between physical and mechanical properties

As mentioned above, a porosity of mortar sample was estimated by the residual quantity of CSH in whole sample. Also, mechanical properties would be diminished by the influence of variation of porosity value [4, 13, 16, 34]; therefore, the relationship between porosity against mechanical properties must be concerned in order to better understand the actual behavior of both non – damaged and fire – damaged mortar in this study.

Regarding two different time of subjecting to high temperature treatment in this study, the residual flexural strength has been interpreted in terms of its porosity which was predicted by the retained amount of CSH in sample after deterioration. The regression lines as shown in Fig. 4 – 41 were obtained for different exposure times and maximum temperature in furnace.

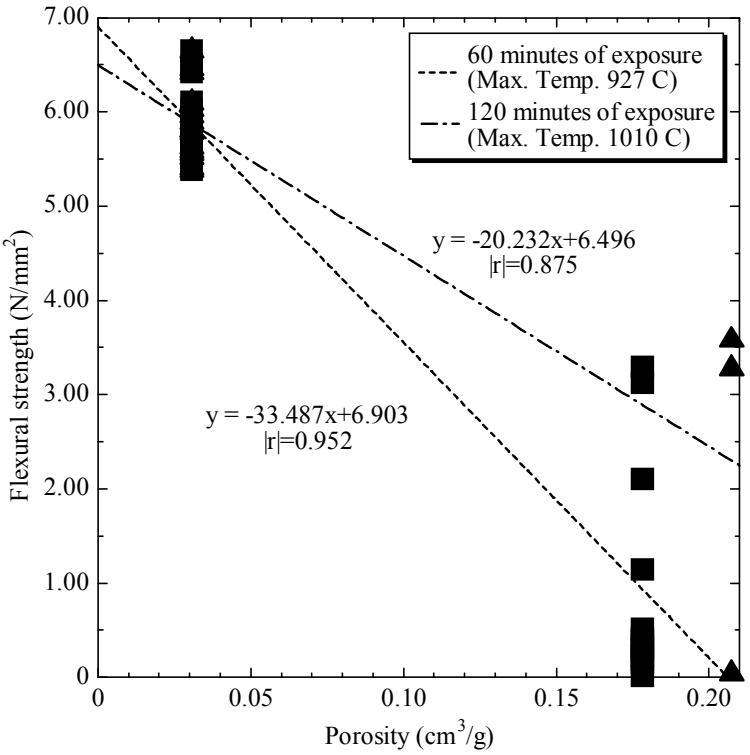

Fig. 4 – 41 Effect of porosity on the flexural strength

Also, shear strength was calculated from flexural strength because shear strength was converted from flexural strength as expressed in Eq. (4.5). Therefore, the regression lines as shown in Fig. 4 – 42 must have the same tendency as the relationship between porosity and flexural strength.

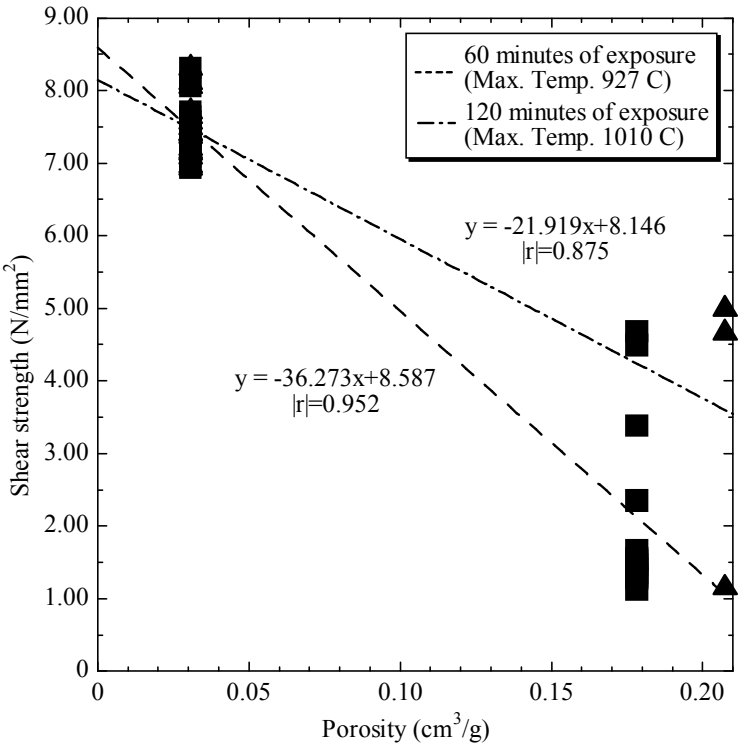

Fig. 4 – 42 Effect of porosity on the shear strength

Since the changes in porosity value after subjected to high temperature treatment up to the target temperature of ASTM E119 [1], mesoscopic flexural and shear strength has been diminished due to the decomposition of strength compounds and Van der Waal forces between CSH layers. Fig. 4 – 41 and Fig. 4 – 42 show the influence of porosity on the residual strength in which a higher maximum temperature in furnace which has a higher strength rather than the lower temperature. In fact, mortar samples with same porosity value should have the same material strength; however, it was probably recovered depending on several factors such as rehydration process, post – fire cooling regimes or atmospheric humidity [7, 16].

In this study, it can be obviously seen that the decomposition of cement hydrated products was a primary reason of the changes in other material properties, i.e.

physical properties and mechanical properties. After subjected to fire exposure, the decomposition of chemical compounds was initiated; therefore, mortar became more porous compared with the non – damaged one. In addition, the pore structure of cement based material likely mortar plays a dominant role on the material strength such as compressive strength, tensile strength, flexural strength and shear strength [9]. Sometimes, material performance may recover due to several factors.

4.4 Inverted analysis results

Inverted analysis was appropriate for only specimens in which 3 – point bending test were done and specimens were fail at expected location only because elemental meshing were generated as a half model. Also, the calculation process for inverted analysis can consider only half model.

4.4.1 Tensile strength and modulus of elasticity

From inverted analysis, tensile strength value was calculated regardless of the other effects such as shear effect; therefore, it was a pure tensile strength. The way to calculate the tensile strength value was started with doing iteration between elastic modulus and obtained a tensile strength with various probabilities. The highest possibility was chosen and used as an input in next iteration, the range of lower limit and upper limit in iteration would be gradually narrow down. Iteration process was stopped when input tensile strength for renew elastic modulus was equal to tensile strength which was obtained from iteration. On the process of inverted analysis to obtain the pure tensile strength, corrected modulus of elasticity was also obtained.

Fig. 4 – 43 and Fig. 4 – 44 show the tendency of reduction in properties gathered from inverted analysis.

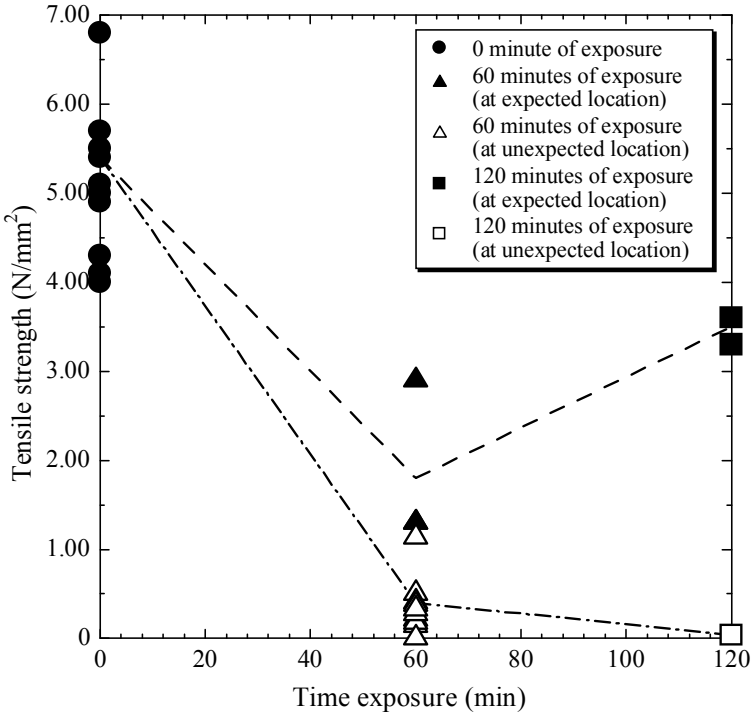

Fig. 4 – 43 Reduction in inverted analysis tensile strength for post – fire samples

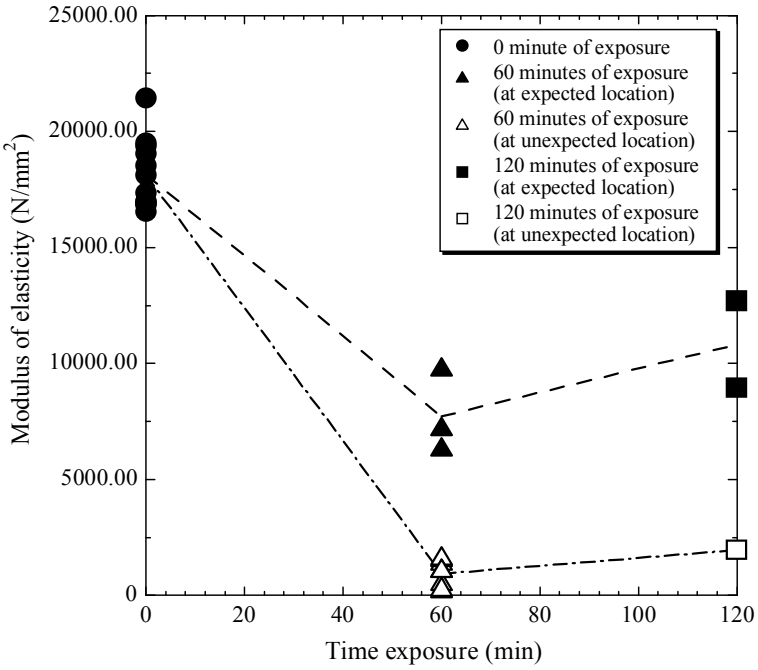

Fig. 4 – 44 Reduction in inverted analysis modulus of elasticity for post – fire samples

Compared with flexural strength results, pure tensile strength value using inverted analysis was almost similar to flexural strength; therefore, although an inverted analysis is appropriate for only specimens in which 3 – point bending test were done and specimens were fail at expected location, there were two groups of results as same as flexural and shear strength results. In case of fail at expected location samples, a tensile strength value was obtained from inverted analysis directly while flexural strength was written down as representative of tensile strength. For modulus of elasticity, the one – third technique was brought to calculate elastic modulus for a group of sample which was not fail at artificial crack during flexural test. To glance over the overall tendency, tensile strength and modulus of elasticity had been reduced after high temperature treatment. However, both of them could recover after an hour of exposure as same as other material strength, i.e. flexural strength, shear strength. One possibility to explain this kind of situation is material performance may recover due to several factors [16].

In spite of being the pure tensile strength, the inverted analysis tensile strength was still greater than briquette samples. To explain this, it might be because calculated tensile strength was measured from the specimens picked from zone without any major cracks while it had a lot of major crack existing in briquette samples before test; therefore, the lower strength happened.

4.4.2 Tensile softening branch and fracture energy

After actual pure tensile strength has been calculated as mentioned in 4.4.1, the calculation of tensile softening branch was started because the corrected tensile strength from previous step was an initial value of tensile softening branch. Then, a relationship between crack width at bottom fiber during 3 – point bending simulation and tensile stress was generated. Tensile strength was decreased with an increment of

crack width at bottom fiber because a section capacity would be gradually decreased. A fracture energy (G_f) was calculated by the area under tensile softening curve by using trapezoidal rule.

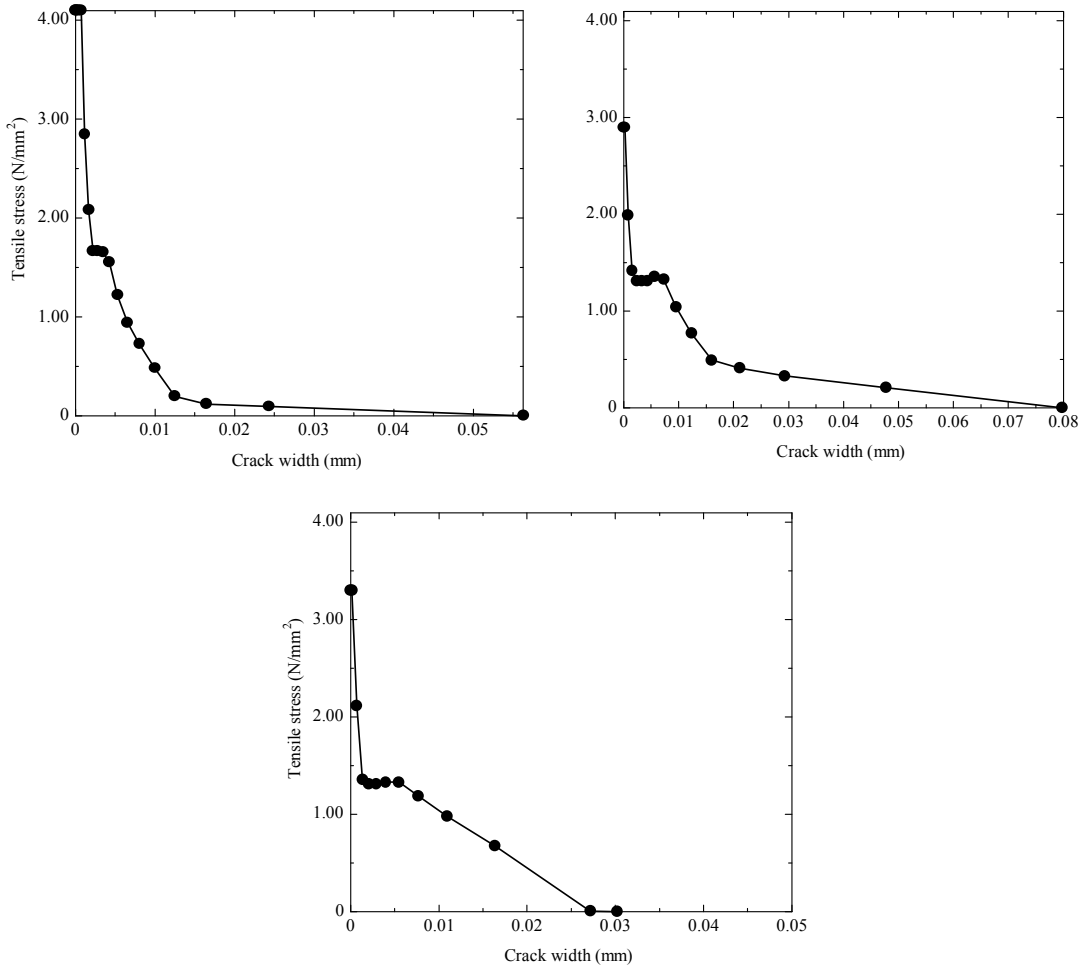

Fig. 4 – 45 A comparison of tensile softening branch for 3 different exposure times

As shown in Fig. 4 – 45, the top left, top right and bottom graphs show the tensile softening branch of non – damaged, 60 minutes of exposure and 120 minutes of exposure samples, respectively. It could be obviously seen that the initial value of tensile strength for damaged samples were less than the one in control sample. In case of damaged samples, a shape of damaged samples was relatively flat but fracture energy

was not significantly reduced compared with control specimens. The result of fracture energy was shown in Fig. 4 – 46.

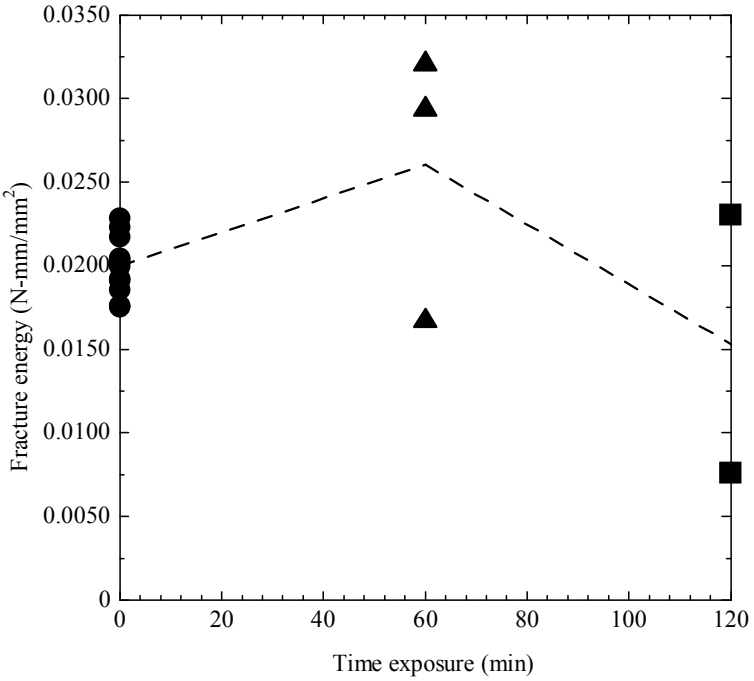

Fig. 4 – 46 Fracture energy calculated by area under tensile softening curve

Since the crack opening could not be measured directly, it had to be derived from the total deformation that was found for the applied measuring length. A procedure which has been used to derive a relationship between tensile stress and crack width was shown in Fig. 4 – 47. In this approach, the crack opening was assumed to be equal to the total deformation minus the elastic deformation and an irreversible deformation which accounted for non – elastic effects during unloading of the material adjacent to the crack faces.

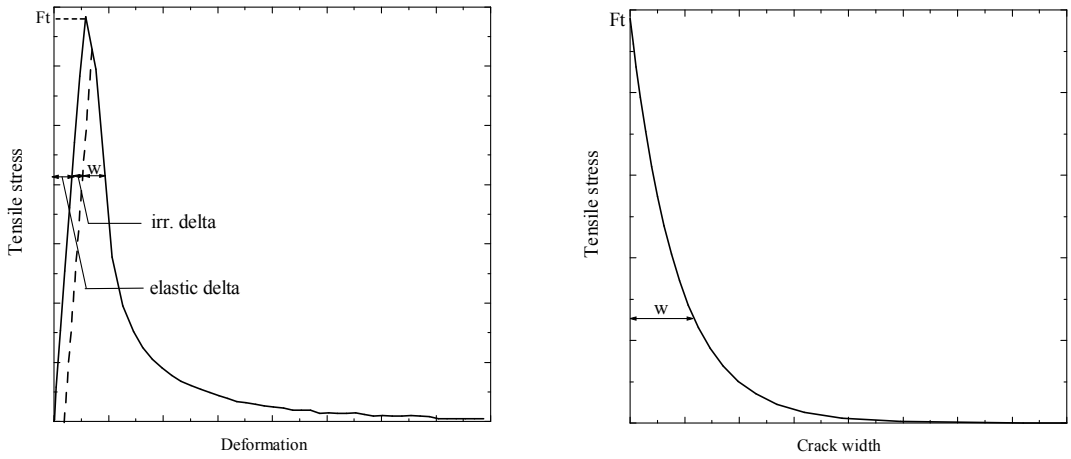

Fig. 4 – 47 Procedure to derive a relationship between tensile stress and crack width

The most important input parameter for non – linear fracture mechanics calculations of cementitious material is undoubtedly the stress – crack opening relation. A single crack is the leading factor and crack evolution is determined by the relation between crack opening and crack normal stress.

Cornelissen et al. has found from their experimental details that the most direct way to obtain the relationship between crack normal stress and crack width for mortar was still the determination by means of a deformation – controlled uniaxial tensile test. In addition, it could be noted that the pre – peak nonlinearities were rather small; therefore, a numerical equation as expressed in Eq. (4.6) was proposed in order to generate the tensile softening curve.

$$\frac{\sigma}{f_t} = \left(1 + \left(c_1 \frac{w}{w_c}\right)^3\right) \exp\left(-c_2 \frac{w}{w_c}\right) - \frac{w}{w_c}\left(1 + c_1^{\,3}\right) \exp(-c_2) \qquad (4.6)$$

Where σ = crack normal stress

f_t = tensile strength

w = crack width

w_c = maximum crack width

c_1, c_2 = coefficient

The best fit of each time exposure was obtained for different value of c_1 and c_2 because of its own behavior. The value of c_1, c_2 and relationship between porosity and c_1, c_2 were shown in Table 4 – 9 and Fig. 4 – 48, respectively.

Table 4 – 9 Coefficient c_1 and c_2 for each different time exposure

Time exposure (min)	c_1	c_2	Porosity (cm^3/g)
0	2.03	10.01	0.0307
60	3.17	10.93	0.1783
120	3.49	12.03	0.2074

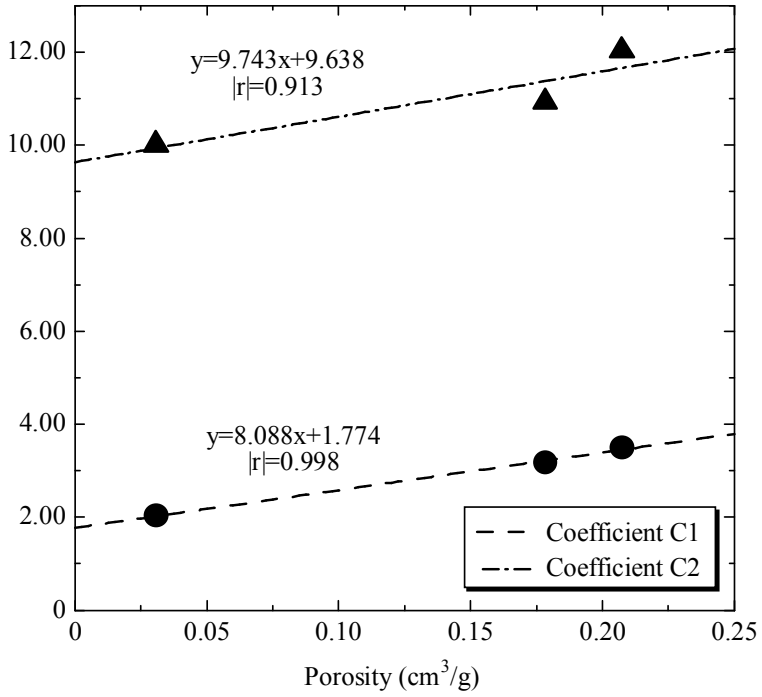

Fig. 4 – 48 Relationship between porosity and coefficient c_1 and c_2

From this relation, a tensile softening curve for sample with any values of porosity could be generated accurately. To ensure that, a good agreement of simulation by Eq. (4.6) was shown comparing with the actual tensile softening curve gathered from inverted analysis as shown in Fig. 4 – 49.

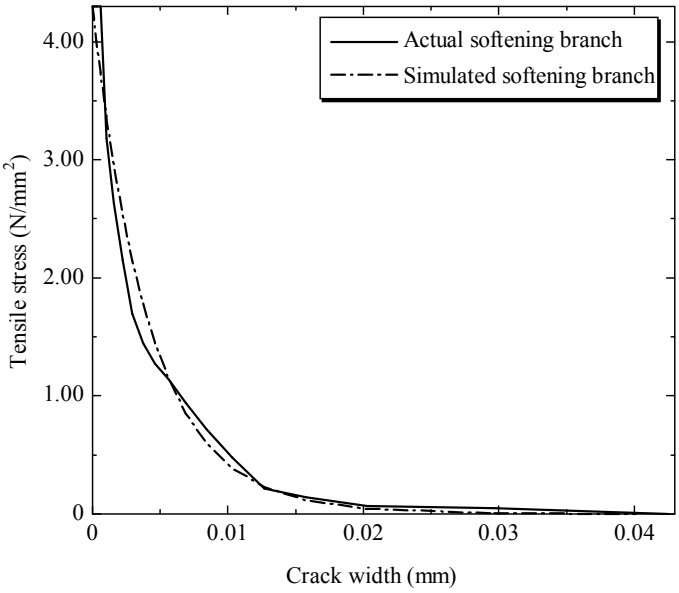

Fig. 4 – 49 Good agreements of actual and simulated tensile softening branch

Thus, it was undoubtedly said that the numerical simulation together with coefficient c_1 and c_2 as a function of porosity as expressed in Eq. (4.6) was valid for any time exposure.

4.5 Model verification

Until now, all the test results were done on mesoscopic samples but, in practical, the performance of structural concrete was evaluated in full – scale structure. Therefore, the purpose of this task is to compare only the maximum load of actual 3 – point bending test in macro scale with the simulation result using the mesoscopic experimental data, i.e. tensile strength, modulus of elasticity, fracture energy and maximum crack width which were obtained from inverted analysis. For 2D – RBSM

simulation, there were 4 steps consisting of model construction, boundary condition setting, material information setting, and analysis and result presentation.

1. Model construction

In this step, model was constructed with only actual height and length of specimen because it was simulated by 2 – dimensional simulation. The size of random geometry depended on the number of Voronoi, means its size was very fine for a greater number of element along the length of specimen. In this study, an average Voronoi size was set to be 2.5 mm corresponding to the meshing size of mesoscopic sample in back analysis. Then, Voronoi elements were randomly generate in order to reduce mesh bias and crack direction as shown in Fig. 4 – 50. Table 4 – 10 shows the model information used in this simulation.

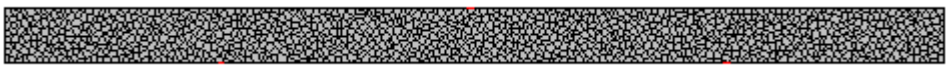

Fig. 4 – 50 Model construction with random geometry

Table 4 – 10 Model information used in this simulation

Time exposure (min)	Dimension			Total number of element	
	Height (mm)	Length (mm)	Thickness (mm)	Model	Mortar
0	23.7	400.0	69.2	1200	1200
60	23.8	400.0	46.9	1200	1200
120	24.7	400.0	65.5	1350	1350

Because all of samples in this study were mortar, there was not coarse aggregate in simulation.

2. Boundary condition

In this step, vertical movement was constraint at both supporting point in order to eliminate the effect of support settlement while both vertical and horizontal movement were constraint at loading point as shown in Fig. 4 – 51. A displacement in one step at loading point was set to be 0.001 mm downward.

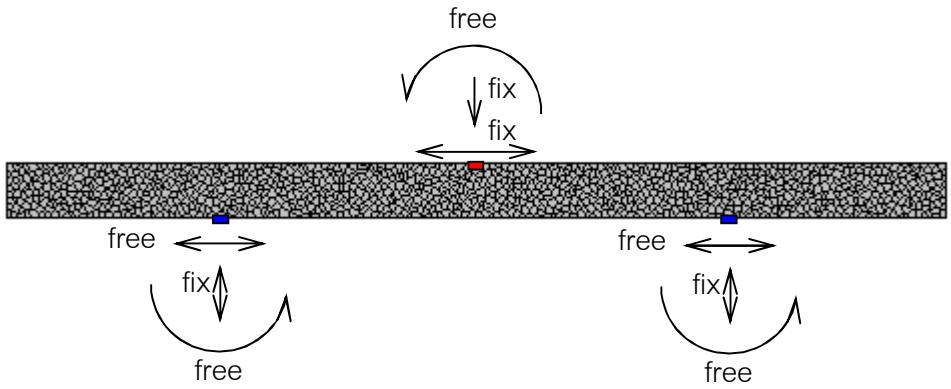

Fig. 4 – 51 Boundary condition for each sample

Actually, the supporting points shown in Fig. 4 – 51 were not exactly supporting point in the test because the model was assembled from Voronoi which is not just a point. However, the supporting points in simulation were located on the element in the nearly actual point; therefore, the chosen supporting points were reasonable.

3. Material information

In this step, material properties such as modulus of elasticity, Poisson's ratio, tensile strength, fracture energy and maximum crack width need to be set. Also, the amount of CSH and CH which influenced the mechanical properties were set. There were two groups of material properties consisting of initial and temporal value in which temporal value was used as actual material properties in

analysis. Table 4 – 11 and Table 4 – 12 show the material information from inverted analysis and the chemical compounds content used in this simulation, respectively.

Table 4 – 11 Material information used in this simulation

Time exposure (min)	Type	E (N/mm^2)	ν	f_t (N/mm^2)	G_f (N/mm)	w_c (mm)
0	Ini.	18123.5	0.18	5.4	0.01998	0.03669
	Temp.	18123.5	0.18	5.4	0.01998	0.03669
60	Ini.	18123.5	0.18	5.4	0.01998	0.03669
	Temp.	7721.6	0.18	1.8	0.02605	0.07745
120	Ini.	18123.5	0.18	5.4	0.01998	0.03669
	Temp.	10818.1	0.18	3.5	0.01531	0.07313

Table 4 – 12 Chemical compound content used in this simulation

Time exposure (min)	Type	CSH (%W/W)	CH (%W/W)
0	Ini.	3.2931	3.8513
	Temp.	3.2931	3.8513
60	Ini.	3.2931	3.8513
	Temp.	0.4776	1.9698
120	Ini.	3.2931	3.8513
	Temp.	0.4910	0.1264

4. Analysis and result presentation

In this step, 3 – point bending test of defined model was started. After peak load, analysis was suddenly stopped at 70 percent of maximum load.

Then, the load – deflection of 2D samples were automatically generated. To be converted from 2D to 3D load – deflection curve, loading data was multiplied by thickness of each specimen. The good agreement of non – damaged and after an hour of exposure samples between experimental results and simulation were shown in Fig. 4 – 52 to Fig. 4 – 54, respectively. Table 4 – 13 shows the peak load and peak deformation.

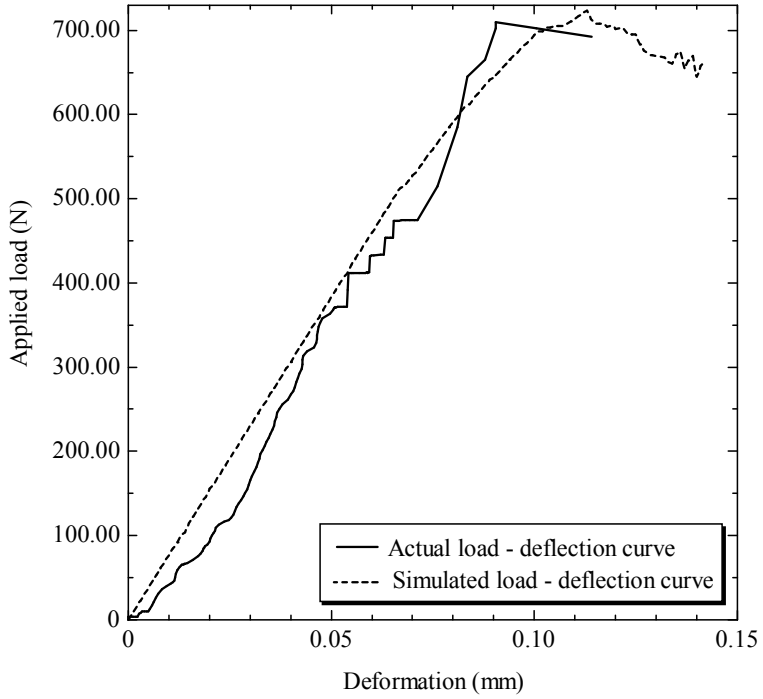

Fig. 4 – 52 Experimental data and RBSM simulation of non – damaged samples

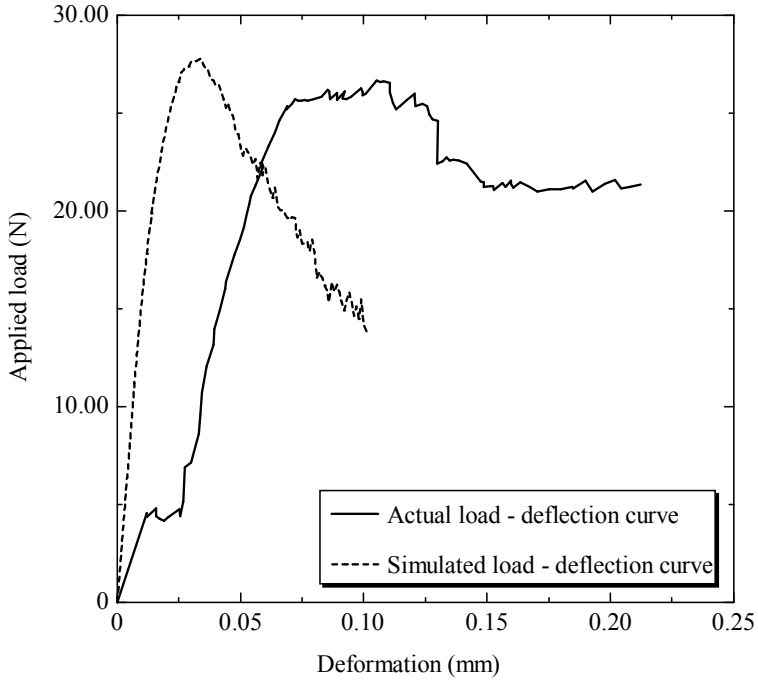

Fig. 4 – 53 Experimental data and RBSM simulation of 60 minutes after fire

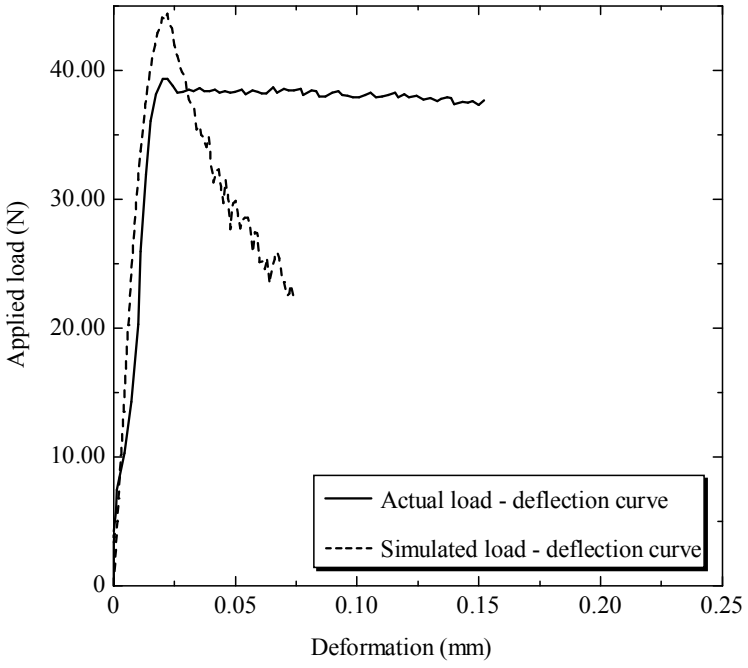

Fig. 4 – 54 Experimental data and RBSM simulation of 120 minutes after fire

Table 4 – 13 Peak load and peak deformation

Time exposure (min)	Peak load (N)		Peak deformation (mm)	
	Experiment	Simulated	Experiment	Simulated
0	709.66	723.55	0.091	0.113
60	22.73	27.78	0.134	0.034
120	39.33	44.41	0.022	0.022

In case of non – damaged sample, there was not only a similar shape of experimental data and those one which was simulated by RBSM with material properties tested in meso – scale, but the actual maximum load was not significantly differ. Despite there was some defect made non – smooth graph in damaged sample during the test, both the load – deflection shape and maximum load were almost the same with considering the diminishing of material properties and residual chemical compounds in sample after subjected to fire exposure. In addition, another possibility to explain a small difference between experimental data and simulation is the size effect. Material properties of small and macro specimens may not be exactly the same because the overall performance of full – scale structure is probably influenced by several factors. Based on the results of the current study, it can be said that RBSM can be used to predict the maximum applied load for 3 – point macroscopic bending test accurately with material properties in meso – scale and considering the effect of chemical compounds content in whole sample; however, the simulation of tensile softening branch need to be modified in the future prospects.

CHAPTER 5

GENERAL CONCLUSIONS AND FUTURE PROSPECTS

5.1 General conclusions

In this study, efforts had been given to investigate the changes in material properties, i.e. chemical properties, physical properties and mechanical properties, of fire – damaged mortar which was made from standard mix proportion of JIS R5201 – Physical Testing Method for Cement[28] with numerical study of those properties and numerical simulation. To perform this task, 2D non – linear numerical simulation was developed. For post – fire cementitious material, the decomposition of chemical compounds was firstly initiated. Since it is well – known that the growth of hydration products expand into pore space; then, material became more porous compared with non – fired mortar which was confirmed by experimental results. In addition, the integration effect of chemical and physical properties has influenced on mechanical properties of material.

Based on afore mentioned, it can be concluded as follows:

1. The volatilization of water during high temperature treatment affect the stability of cement hydrated products. Hence, the so – called phenomena for chemical compounds decomposition are initiated. The time exposure range 0 – 60 minutes is most favorable for the degradation of cement hydrated products. By rehydration of Calcium Oxide, the additional amount of CH can be introduced but its mechanism is rather complicated; therefore, the chemo – physical properties relation of CSH and CH are not the same tendency.

2. Porosity as measured by Archimedean technique and Porosimetric analysis are almost the same; however, the former technique is quite better because there is no additional failure happened during experimental investigations. Pore – structure is intensified with respect to the increment of time exposure as examined by means of the appearance and disappearance of the second peak and the shift of observed characteristics peak in a differential curve of mercury intruded.
3. The residual quantity of cement hydrated products can be used as a damage index for fire – deteriorated mortar on physical property because of the growth and expansion into the pore space during the course of hydration reaction.
4. Experimentally tested mechanical properties, i.e. compressive strength, tensile strength, flexural strength and shear strength, were significantly diminished for post – fire concrete. However, strength recovery might happen but it was rather complicated depending on several factors.
5. The reduction of chemical compounds is a primary parameter for any proposed model because of its own behavior after high temperature treatment.
6. The chemical – physical properties in each case can be used to examine the porosity value affected by each parameter of post – fire mortar by using the residual hydration products for two different maximum temperatures in furnace.
7. The chemical – physical relation of residual CSH after fire and porosity plays a dominant role on pore structure coarsening rather than CH.
8. The physical – mechanical relation in each case can be used to examine how porosity value influenced each kind of strength for post – fire mortar.
9. The constitutive model is proposed based on the principle of deformation – controlled and valid for both non – damaged and fire – damaged samples by adjusting coefficient value only.

10. The proposed model in the current study is limited only for 28 – day old oven – dried mortar after subjected to less than 120 minutes of fire exposure.

5.2 Future prospects

The following points are recommended for future study:

1. The age of specimen at test date should be varied in order to better understand how fire accidents influence material properties at any ages.
2. The temperature history along cross section of macroscopic sample should be considered in order to study the temperature gradient affected the level of deterioration.
3. The rehydration of CH process should be clarified in order to know how it affects other material properties.
4. Upgrading the developed simulation to the 3D simulation to be able to simulate the actual specimens in flexural test.

REFERENCES

[1] ASTM Designations: E119 - 00a, Standard Test Methods for Fire Tests of Building Construction and Materials, 2000.

[2] RILEM TC 129 - MHT: 'Test methods for mechanical properties of concrete at high temperatures', Modulus of elasticity for service and accident conditions.

[3] Raymond A. Cook, Kenneth C. Hover, Mercury porosimetry of hardened cement pastes, Cement and Concrete Research 29 (1999):933-43.

[4] Omer Arioz, Effects of elevated temperature on properties of concrete, Fire Safety Journal 42 (2007):516-22.

[5] Gai-Fei Peng, Zhi-Shan Huang, Change in microstructure of hardened cement paste subjected to elevated temperatures, Construction and Building Materials 22 (2008):593-99.

[6] J. Piasta, Z. Sawicz, L. Rudzinski, Changes in the structure of hardened cement paste due to high temperature, Material Construction 17 (1984):291-6.

[7] Wei-Ming Lin, T. D. Lin, L. J. Powers-Couche, Microstructures of Fire-Damaged Concrete, ACI Materials Journal (1996):199-205.

[8] F. S. Rostasy, R. WeiB, G. Weidemann, Changes of pore structure of cement mortars due to temperature, Cement and Concrete Research 10 (1980):157-64.

[9] Xudong Chen, Shengxing Wu, Jikai Zhou, Influence of porosity on compressive and tensile strength of cement mortar, Construction and Building Materials 40 (2013):869-74.

[10] Ingberg S. H. et al., Combustible Content in Buildings, Washington, DC, National Bureau of Standard (1957).

[11] Prinya Chindaprasirt and Chai Jaturapitakkul, Cement, Pozzolan and Cement, Cement and Application, SCG Cement, ISBN 974 – 92536 – 7 – 1 (2009).

[12] Qi Zhang, G. Ye, E. A. B. Koenders, A simulation model for microstructure of portland cement paste at high temperature, 2nd International RILEM Workshop on Concrete Spalling due to Fire Exposure (2011):361-8.

[13] Y. F. Chang, Y. H. Chen, M. S. Sheu, et al, Residual stress-strain relationship for concrete after exposure to high temperatures, Cement and Concrete Research 36 (2006):1999-2005.

[14] K. D. Hertz, Limits of spalling of fire-exposed concrete, Fire Safety Journal 38 (2003):103-16.

[15] ASTM Designation: C469 – 10, Standard Test Method for Static Modulus of Elasticity and Poisson's Ratio of Concrete in Compression.

[16] Chi-Sun Poon, Salman Azhar, Mike Anson, et al., Strength and durability recovery of fire-damaged concrete after post-fire-curing, Cement and Concrete Research 31 (2001):1307-18.

[17] EC2 (2004), Eurocode 2: design of concrete structures - part 1.2: general rules structural fire design, London (UK), British standards Institution.

[18] Bazant P., J. C. Chern, Stress-induced thermal and shrinkage strains in concrete, ASCE Journal of Engineering Mechanics 113 No. 10 (1987):1493-511.

[19] Nattapong Damrongwiriyanupap and Yunping Xi, Modeling Chloride Penetration into Concrete Structures, Annual Concrete Conference 7.

[20] Parnthep Julnipitawong and Lutz Franke, Experiment investigations and models of water transport in concrete, Annual Concrete Conference 7.

[21] G. H. A. van der Heijden, R. M. W. van Bijnen, L. Pel, et al., Moisture transport in heated concrete, as studied by NMR, and its consequences for fire spalling, Cement and Concrete Research 37 (2007):894 – 901

[22] K. D. Hertz, L. S. Sorensen, Test method for spalling of fire exposed concrete, Fire Safety Journal 40 (2005):466-76.

[23] Kohei Nagai, Yasuhiko Sato, Tamon Ueda, Mesoscopic Simulation of Failure of Mortar and Concrete by 2D RBSM, Journal of Advanced Concrete Technology 2 No. 3 (2004):359-74.

[24] Licheng Wang, Tamon Ueda, Mesoscale Modelling of the Chloride Diffusion in Cracks and Cracked Concrete, Journal of Advanced Concrete Technology 9 No. 3 (2011):241-9.

[25] K. Nakashima, H. Nakamura, M. Kunieda, Fundamental analysis on evaluation for fire-proof performance of concrete, Creep, Shrinkage and Durability Mechanics of Concrete and Concrete Structures (2009):1029-35.

[26] H. Nakamura, K. Yoshida, M. Kunieda, et al., Simulation about effect on explosion spalling of thermal stress and vapor pressure, 2nd International RILEM Workshop on Concrete Spalling due to Fire Exposure (2011):213-9.

[27] Kohei Nagai, Yasuhiko Sato, Tamon Ueda, Mesoscopic Simulation of Failure of Mortar and Concrete by 3D RBSM, Journal of Advanced Concrete Technology 3 No. 3 (2005):385-402.

[28] Japanese Industrial Standard: JIS R 5201: 1997, Physical testing methods for cement.

[29] ASTM Designation: C230/C230M – 08, Standard Specification for Flow Table for Use in Tests of Hydraulic Cement.

[30] ASTM Designation: C305 – 11, Standard Practice for Mechanical Mixing of Hydraulic Cement Pastes and Mortars of Plastic Consistency.

[31] ASTM Designation: C109/C109M – 11b, Standard Test Method for Compressive Strength of Hydraulic Cement Mortars (Using 2-in. or [50-mm] Cube Specimens).

[32] ASTM Designation: C307 – 03 (2008), Standard Test Method for Tensile Strength of Chemical-Resistant Mortar, Grouts, and Monolithic Surfacings.

[33] Keith J. Henley, Improved heavy – liquid separation at fine particle sizes, American Mineralogist 62 (1977):377 – 381.

[34] S. Djaknoun, E. Ouedraogo, A. Ahmed Benyahia, Characterisation of the behavior of high performance mortar subjected to high temperatures, Construction and Building Materials 28 (2012):176-86.

[35] JCI - S - 001 - 2003, Method of test for fracture energy of concrete by use of notched beam, 2003.

[36] A. Kumar, A realistic evaluation of permeability and tensile strength from compressive strength in cement sand mixes, Asian Journal of Civil Engineering (Building and Housing) 8 No. 2 (2007):159-74.

VITA

Ms. Onnicha Rongviriyapanich was born in Bangkok, Thailand in July 23, 1987. She has graduated primary and high school certificate at Assumption Suksa School in 2006, and Bachelor's degree in Civil Engineering at Chulalongkorn University in 2010. She has been granted the scholarship for Chulalongkorn University Alumni Students by Faculty of Engineering and Department of Civil Engineering, Chulalongkorn University to do a Master's degree in the field of Structural Engineering, Department of Civil Engineering, Chulalongkorn University, Thailand since 2011.